FIBER BRAGG GRATINGS IN POLYMER OPTICAL FIBERS

THÈSE N^O 4021 (2008)

PRÉSENTÉE LE 15 FÉVRIER 2008
À LA FACULTÉ DES SCIENCES ET TECHNIQUES DE L'INGÉNIEUR
LABORATOIRE D'OPTIQUE APPLIQUÉE
PROGRAMME DOCTORAL EN PHOTONIQUE

ÉCOLE POLYTECHNIQUE FÉDÉRALE DE LAUSANNE

POUR L'OBTENTION DU GRADE DE DOCTEUR ÈS SCIENCES

PAR

Nico Gérard HARBACH

ingénieur mécanicien diplômé EPF
de nationalité suisse et originaire de Diessenhofen (TG)

acceptée sur proposition du jury:

Prof. P. Jacquot, président du jury
Prof. R. Salathé, directeur de thèse
Dr V. Michaud, rapporteur
Dr U. Sennhauser, rapporteur
Dr D. Webb, rapporteur

EPFL

ÉCOLE POLYTECHNIQUE
FÉDÉRALE DE LAUSANNE

Suisse
2008

Abstract

Polymer optical fibers (POF) have received increased attention in recent years in the fields of data communication and sensing applications. The lower cost and higher flexibility are the main advantages of POF compared to silica fibers and make them intersting candidates for Fiber Bragg grating (FBG) sensor applications. FBG are convenient measurement devices for strain and temperature measurements, as they can be multiplexed within one fiber yielding a sensor array and the fiber can be embedded in structures.

This work investigated the possibility of producing FBG in polymer fibers and their use as sensor units. It could be shown that using excimer laser irradiation at 308 nm, it is possible to write FBG in single-mode POF employing a standard phase mask, side writing technique. Index changes of up to 1.7×10^{-4} and reflectivies of up to 87% could be reached. The induced refractive index change due to pulsed UV irradiation was shown to be negative. The polymer material of the core (Polystyrene (PS) / Polymethyl methacrylate (PMMA)) was not sensitized prior to irradiation. During the grating formation an irradiation induced insertion loss of up to 11 dB/cm was observed. Excimer laser written FBG showed stability of over 9 months for approximately 40% of written FBG. Results of FBG writing using femto second laser irradiation showed FBG with reflectivities of up to 1.2×10^{-4}, however these POFBG were not stable.

The POFBG were characterized using optical low coherence reflectometry (OLCR) which enables to calculate the FBG location and length as well as the induced amplitude Δn_{ac} and mean refractive index change Δn_{dc}. Taking into account fiber and insertion losses, good agreement of these calculations and measurements were found. The results show that large variations of the induced index change result from irradiation. Local index change peaks of up to 4 times the mean value were observed, indicating inhomogeneity of the fiber material.

Birefringence in the core of the POF ($\approx 1.2 \times 10^{-3}$) is up to a factor 3 higher than in the cladding which is due to the PS content within the core. The birefringence is due to inelastic strain and stress induced in the drawing process. Annealing, uniform irradiation and FBG writing using 308 nm excimer laser light induces a decrease of the absolute birefringence value. The changes upon irradiation are confined to the core of the fiber. Large variations in the initial and final birefringence before and after irradiation supports the findings of the OLCR measurements indicating material inhomogeneities in the fiber.

POFBG were found to be sensitive to relative humidity, temperature and strain. This is in contrast to glass fiber FBG which do not show humidity sensitivity. POFBG relative humidity sensitivity is non-linear with a change of up to 8 nm for a RH change of $\approx 100\%$. The non-linearity is introduced by a non-linear water sorption process. The POF grating response to temperature changes under dry conditions (1.5 ± 1 % RH) is -10 ± 0.5 pm/°C. The temperature response of the FBG submerged in water is -36 ± 2 pm /° C due to an increased thermal expansion coefficient and a change in polarizability. Under ambient conditions the grating response to heating is typically ≈ -138 pm/°C, predominantly due to a change in POF swelling, i.e changes in relative humidity and POF water content.

The diffusion coefficient of water in this POF at 23.5°C is 6.7×10^{-9}cm^2/s for sorption and 10×10^{-9}cm^2/s for desorption. Equilibrium of water content within the fiber and the surrounding air is typically reached after approximately one hour. Calculation showed, that a reduction of the fiber diameter can increase this humidity sensitivity response time down to approximately 5 minutes for a fiber diameter of 25 μm.

Key words: Polymer optical fiber, fiber Bragg grating, photosensitivity, refractive index, birefringence, humidity, diffusion, temperature, strain, fiber sensor

Kurzfassung

Polymer optische Fasern (POF) für Datenkommunikation und Sensoranwendungen haben in den letzten Jahren vermehrt Beachtung gefunden. Die Vorteile des tieferen Preises und der höheren mechanischen Flexibilität im Vergleich zu Glasfasern machen sie zu interessanten Kandidaten für Faserbragggitter (FBG). Faserbragggitter als Temperatur- und Dehnungssensoren in Glasfasern finden heute verbreitet Anwendung da sie einfach zu integrieren sind und mehrere Sensoren in einer Faser realisiert werden können.

Diese Arbeit untersuchte die Möglichkeiten FBG in POF herzustellen und sie als Sensoren zu verwenden. Es konnte gezeigt werden, dass FBG in mono-mode POF durch Bestrahlung mit Excimer-Laser Licht bei 308 nm geschrieben werden können. Dazu wurde eine standard Phasenmaskentechnik angewendet. Brechungsindex-änderungen bis zu 1.7×10^{-4} bei einer Reflektivität von 87% konnte erreicht werden. Die UV-bestrahlung induziert eine negative Indexänderung. Während der Bestrahlung wird ein Verlust von bis zu 11 dB/cm im Gitter induziert. Von den produzierten Bragggittern waren ungefähr 40% während mindestens 9 monaten stabil. Als alternative zu Excimer-laser Bestrahlung wurden Experimente mit einem Femtosekundenlaser bei 400 nm Wellenlänge durchgeführt. Brechungsindex-änderungen bis zu 1.2×10^{-4} wurden erreicht, allerdings waren die so produzierten Gitter nicht stabil.

Optische Niderkohärenzreflektometrie (OLCR) ermöglicht die Berechnung von FBG-Eigenschaften wie Position, Länge, induzierte Brechungsindexamplitude Δn_{ac} und Durchschnittsindexänderung Δn_{dc}. Wenn die bestrahlungsinduzierten Verluste berücksichtigt werden, zeigen Berechnungen und Messungen gute Übereinstimmung. Starke Brechungsindexvariationen von bis zu vier mal grösseren Maximalwerten als dem Durchschnittswert entlang des FBG wurden sichtbar, was auf Inhomogenitäten im Fasermaterial rückschlissen lässt.

Die Doppelbrechung im Kern der POF ($\approx 1.2 \times 10^{-3}$) ist bis zu 3 mal grösser als im Mantel, was durch den Polystyrene (PS) Anteil im Kern beeinflusst wird. Die Ursachen für Doppelbrechung in POF ist inelastische Dehnung und elastische Spannung. Tempern der Faser, uniforme Bestrahlung und Produktion von Bragggittern mit 308 nm Laserlicht führten zu einer Reduktion des Betrags der Doppelbrechung. Die Änderungen durch Bestrahlung beeinflussen allerdings nur die Doppelbrechung im Kern der Faser. Starke Variationen der Doppelbrechungswerte sowohl vor als auch nach der Bestrahlung bestätigen OLCR Messungen und die gefundenen Inhomogenitäten des Fasermaterials.

POFBG zeigen eine Braggwellenlängenabhängigkeit von Feuchtigkeit, Temperatur und Dehnung, im Unterschied zu Glasfaser-FBG die keine Feuchtigkeitsabhängigkeit zeigen. Der Verlauf der Braggwellenlänge mit relativer Umgebungsluftfeuchte ist nicht-linear und die Änderung ist bis zu 8 nm für eine RH-änderung von 100%. Die nicht-linearität wird durch den nicht-linearen

Wasseraufnahmeprozess bestimmt. Die Temperaturabhängigkeit für trockene FBG ist -10 ± 0.5 pm/°C. Im Fall von nassen POFBG (unter Wasser) ist die Abhängigkeit auf Grund des grösseren thermischen Ausdehnungskoeffizienten und einer Änderung der Polarisierbarkeit ungefähr 3 mal grösser, -36 ± 2 pm $/° C$. Heizen unter Umgebungsbedingungen führt zu einer typischen Bragggratingantwort von ≈ -138 pm/°C, überwiegend auf Grund des wasserinduzierten Schwellens der POF.

Der Diffusionskoeffizient von Wasser in dieser POF ist 6.7×10^{-9}cm^2/s für Wasseraufnahme und 10×10^{-9}cm^2/s für Wasserabgabe bei 23.5°C.

Das Feuchtigkeitsgleichgewicht zwischen der Faser und der Umgebungsluft ist nach ca. einer Stunde erreicht. Berechnungen haben gezeigt, dass diese Zeit für Feuchtigkeitsmessungen bis auf ca. 5 Minuten reduziert werden kann, wenn man den Durchmesser der Faser auf 25 μm reduziert.

Schlüsselworte: Polymeroptischefaser (POF), Faserbragggitter, Photosensitivität, Brechungsindex, Doppelbrechung, Feuchtigkeit, Diffusion, Temperatur, Dehnung, Fasersensor

Contents

List of abbreviations

a	Core radius
α	Thermal expansion coefficient
atanh	Arcus tangens hyperbolicus
b	Caldding radius
β	Swelling coefficient
BzMA	Benzyl methacrylate
CW	Continous wave
C	Concentration
C_0	Initial concentration
C	Carbon
c	Normalized concentration
cm	Centimeter
Cl	Chlorid
°C	Degree celsius
CYTOP	Cyclic transparent optical polymer
dB	Dezibel
D	Diffusion coefficient
E	Young's modulus
ϵ	Strain
ϵ_{ax}	Axial strain
ϵ_z	Strain in z-direction
ϵ_r	Radial Strain
η	Core mode power confinment
eV	Electron Volt
FBG	Fiber Bragg Grating

fs	Femto second
γ	Humidity-optic coefficient
g	Gramms
GeO_2	Germanium oxid
GPa	Giga pascale
GOF	Glass Optical Fiber
GI	Graded Index
Hz	Hertz
H_2	Hydrogen
j	Flux
J	Joule
J_0	Bessel function of the first kind of order 0
J_1	Bessel function of the first kind of order 1
kg	Kilogramms
k	Gas-phase mass-transfer
k	Heat conductivity
km	Kilometer
kV	Kilo volt
λ_B	Bragg wavelength
λ	Wavelength
L	Length
Λ	Grating pitch
μm	Micro meter
mol	Mol
MHz	Mega hertz
MF	MonoFilaments
MM	Multi Mode
MMA	Methylmethacrylate
NA	Numerical aperture
nm	Nano meter
n_{core}	Core refractive index
n_{clad}	Caldding refractive index

n_{eff}	Effective refractive index
n_{ac}	Induced refractive index amplitude
n_{dc}	Mean induced refractive index
ν	Poisson's ratio
n_g	Group refractive index
OLCR	Optical low coherence reflectometry
POF	Polymer Optical Fiber
PC	Polycarbonate
POFBG	Polymer optical fiber Bragg grating
PD	Photo diode
π	Pi
p_e	Effective strain constant
p_{11}	Pockels coefficient
p_{12}	Pockels coefficient
PMMA	Poly methyl methacrylate
PS	Polystyrene
P	Pressure
pm	Pico meter
Q_D	Activation engergy
R	Universal gas constant
rms	Root mean square
ρ	Density
RH	Relative humidity
r	Radius
r_{core}	Core radius
R_{max}	Maximum reflectivity
SMF-28E	Single Mode glass optical fiber from Corning
S	Relative humidity
σ	Stress
σ_{zz}	Stress in zz-direction
SiO_2	Silica
Sh	Sherwood number
SI	Step Index
SM	Single Mode

T	Temperatur
TL	Tunable Laser
t	Time
τ	Normalized time
T	Transmission
tanh	Tangens hyperbolicus
T_g	Glass transition temperature
TOPAS $^{\circledR}$ COC	TOPAS cyclic olefin copolymer
UV	Ultra violet
V	V- number
mW	Milli watt
w	Gaussion mode field diameter
wt%	Weight percent
W	Watt
ξ	Thermo-optic coefficient
Xe	Xenon
Z	Normalized fiber separation distance

Chapter 1

Introduction

1.1 State of the art

1.1.1 Polymer optical fibers

Polymer optical fibers (POF) were first fabricated by Du Pont [1] in the 1960s. But only in the last 20 years POFs have received increasing attention, predominantly as they are very well suited for short distance data and communication networks which are used in cars [2–4], 'the-last-mile' [5], home networks [6,7] and in office and factory applications [8]. Other fields of use include lighting [1] and biomedical applications [9,10], the later also due to very good biocompatibility of Poly methyl methacrylate (PMMA) which is the most common used polymer for POFs [11]. A wide variety of sensors have been proposed, most of them using intensity modulation techniques [12–15] but only a few exploiting photoinduced structures [16,17]. With this increased interest in POF several companies evolved producing polymer optical fibres (Appendix D). In the 90s several groups reported on the production of single-mode polymer optical fibers [18–20] but the interest shifted fast to large core multi mode fibers. The high elasticity and ductility of polymers allows for large fiber sizes, still showing acceptable flexibility. This is in contrast to glass optical fibers (GOF) which have a low elastic limit and are brittle. Therefore GOF are made with smaller over all diameter and a surface protective polymer coating is applied which limits growth of cracks. Light weight and low cost further add to the advantages of POF. The larger core diameter compared to silica fibers paired with a high numerical aperture (NA) allow for easy and efficient coupling and therefore the use of cheap coupling equipment such as connectors and sockets. The type of polymer fiber most commonly used, is a multi mode, graded index or step index, large core fiber [21,22]. Advantages owing to the large core size are the reason why single mode POF are given less attention. Probably this is also the reason why SM POF are not commercially available. Up to date only one of the companies still produces Single Mode Polymer Optical Fibres but only on a custom order basis.

1.1.2   Photoinduced index structures

Since Hill [23] discovered the photosensitivity of germano-silicate optical fibers, such fibers and induced structures in such fibers have seen more and more applications for optical communication and sensing. The photosensitivity to UV light enables waveguide writing [24] as well as Bragg grating inscription [25]. The UV-induced refractive index change is related to two different mechanisms. Refractive index change due to the color center model [26] or due to densification [27]. Further hydrogen loading (i.e. diffusion of H_2 into the core of a fiber) can increase the maximum index change achieved [28, 29]. The Bragg gratings written, exploiting the photosensitive fiber, can than be used as wavelength multiplexing filters, band stops or for sensing purposes.

Polymers do not exhibit the same kind of photosensitivity as glass fibers. However polymers doped with photosensitive dies [30], or that have residual monomer contents which is then photo-cured are used for several applications like waveguide writing [31,32], data storage [33] or grating recording [30, 34–36]. Since the introduction of polymer optical fibers several attempts have been undertaken to create photoinduced Bragg gratings in these fibers, and Peng et al. [30] showed first FBGs in POF in 1999. Most of the POF gratings up to date were written in polymer fibers containing dopants or in fibers which were not fully polymerized. Using such fibers the photosensitivity is either due to the dopant, e.g. trans-cis isomerization of trans-4-stilbenemethanol [37], or to UV-induced polymerization of the fiber core material [38].

1.1.3   Sensing with Fiber Bragg gratings

Optical waveguides have the property of being immune to electro magnetic interference (EMI), which promotes the application in fields where this is of advantage like in power plant applications [39] or in order to reduce the need of specially shielded electrical cables like in cars' cable harness. Using fiber Bragg gratings as sensors has further advantages. The 'wavelength encoded' sensing signal makes the sensing independent of intensity variations of the interrogation light source. Several FBG can be multiplexed in one fiber by using different Bragg wavelengths thus reducing cost per sensing unit and increasing installation possibilities. One very important application is the embedding of FBGs in structures for the strain or structural health monitoring [40, 41]. Strain and temperature measurements are the main fields in which FBGs are used today, however many other sensing applications have been shown to be possible with FBGs, such as pressure [42], ultrasound [43] and acceleration [44]. Polymer fibers have three major advantages when compared to glass optical fibers (GOF). Their higher elasticity [1], their lower costs [2] and their biocompatibility. The higher ultimate elastic strain (i.e. up to 13% for PMMA [45] compared to 4% for silica) of the polymer fibers enables to increase the sensing

---

[1]$E_{POF} = 2 \div 3\ GPa$, $E_{SiO_2} = 72.5\ GPa$
[2]$10 \div 20\ \$/km$ for large core POF, $120\ \$/km$ for Corning SMF 28

range and the lower elastic modulus (Young's modulus) could lead to an increased sensitivity of stress measurements. These are the main reasons why POF are interesting candidates for fiber optical sensors, especially FBG sensors.

1.1.4   POF for sensing purposes

POF have seen many applications in the sensing field such as vibration [12] and environmental sensing [13]. O'Keeffe et al. [46] showed that the change in transmission spectrum of a PMMA fibre due to gamma irradiation can be used as a dosimeter. PMMA fibers with removed cladding have been shown as refractive index-change sensors in liquids [47,48] and was used by Philip-Chandy et al. as biofilm sensor [49]. The evanescent field of the POF fiber core was also used for pressure sensing [14]. A variety of sensors that rely on the light coupled into the cleaved end of a POF fiber have been presented [12,50] to measure vibration or displacement. Also the segmentation of a POF results in partial loss of guided light dependent on flexion of the fiber. This was used by Kuang et al. [51,52] to monitor vibration. Replacement of the cladding of POF has been demonstrated for relative humidity measurement purposes [15, 53,54]. The fabrication of such humidity sensors require removal of the cladding of POF and replacement with a humidity sensitive layer, which increases production time and cost of such sensors. Predominantly intensity based sensing schemes are employed where bending losses, evanescent field [14] or reflection dynamics are exploited. Recently also Optical time domain reflectometry (OTDR) based strain sensors have been demonstrated [55,56] and reported to be suited for strain measurements up to 40%. Fiber Bragg Gratings (FBG) in POF have lately emerged and showed several application fields. For example a very large thermal tuning could be demonstrated [17] due to a large Bragg wavelength shift. Our work shows that POFBG can not only be used for strain and temperature measurements, but an intrinsic humidity sensitivity of PMMA enables them to be used as humidity sensors.

1.2   Motivation and thesis outline

The main objective of this thesis was to study the possibility of POFBG production and application in the field of sensing. POF fibers are generally made of PMMA which is a polymer that exhibits good biocompatibility and much higher flexibility compared to silica fibers. With POFBG in such fibers, sensing applications can be envisaged on the human body, that are not possible using silica fibers due to risk of injury. For the production of such sensors the photosensitivity of polymer optical fibers (POFs) was to be studied. So far only specifically tailored POF were used for FBG inscription. The possibility to write FBG in POF produced from standard POF materials would be a big advantage because one would not need specially tailored photosensitive fibers. This was the motivation to work with fully polymerized PMMA/PS core fibers. In order to create photoinduced sturctures in this fiber, the limiting process parameters

and formation had to be studied. Excimer and femto second laser sources were selected as possible candidates for FBG writing and the feasibility for FBG writing had to be investigated. Finally, the feasibility of photoinduced fiber Bragg gratings, and their use as sensors had to be evaluated. Further objectives included the characterization of written FBG and their sensing properties and specifications.

Chapter 2 gives a general introduction on polymer optical fibers. Different polymers used in POF are presented and several aspects like the attenuation levels and the UV and IR absorption spectra for PMMA and PS are shown.

Chapter 3 reviews the different photosensitivity mechanisms found in polymers. It will be viewed in the aim of identifying strategies and promising techniques for FBG inscription in POF. Special emphasis will be given to the SM POF which will be used for this work.

Chapter 4 presents the developed technique for FBG writing in POF. An introduction on FBG theory is given and the state of the art of FBG in POF is discussed. The formation process of FBG is presented. The characterization of the mean and amplitude refractive index change are calculated from these results and analyzed. The majority of the POFBG are written using a XeCl excimer laser and some preliminary results for fs-laser written POFBG are presented as well. Different initial fiber conditions lead to a change in the formation mechanism of FBG which will be explained. Birefringence measurement of the POF were performed. It shows the superposed molecular alignment and stresses in the fiber. Comparing the birefringence before and after irradiation leads to indications where the changes in the fiber cross section take place which will be explained. FBG which were written in the frame of this work and which are used in this document to illustrate their characteristics are numbered as FBG1 through FBG21. A detailed list can be found in the Appendix.

Chapter 5 shows the possible sensing applications of POFBG. During this work the humidity sensitivity of POFBG was discovered and investigated. A discussion of the experiments on the humidity sensitivity and on the humidity driven Bragg reflection dynamics will be presented. It was possible to measure the diffusion coefficient of water into the POF through the response of the POFBG. Subsections will treat the POFBG humidity sensitivity at constant temperature, temperature sensitivity at constant humidity and sensitivity on both effects in combination. The temperature sensitivity of the FBG under different conditions such as dry, wet and ambient will be presented. In order to give the complete characterization of the POFBG sensitivity also the strain sensitivity is presented.

Chapter 6 summarizes and concludes the work. An outlook on future work will be given and questions that remain to be answered.

Bibliography

[1] Werner Daum, Jürgen Krauser, Peter E. Zamzow, and Olaf Ziemann. *POF - Polymer Optical Fibers for Data Communication*. Springer, 2002.

[2] Thomas Kibler, Stefan Poferl, Gotthard Böck, Hans-Peter Huber, and Eberhard Zeeb. Optical data buses for automotive application. *Journal of Lightwave Technology*, 22(9):2184–2199, 2004.

[3] D. Seidl, P. Merget, J. Schneider, R. Weniger, and E. Zeeb. Applications of POF's in data links of mobile systems. In *Proc. 7th Int. Polymer Optical Fiber (POF) Conf., Berlin, Germany*, 1998.

[4] Byteflight . Official Homepage, http://www.byteflight.com.

[5] Hirscher. Triple play realization of Swisscom with POF. In *POF 2007 Torino*, 2007.

[6] T. Koonen, H. van den Boom, I. T. Monroy, and G.-D. Khoe. Broadband data communication techniques in POF-based networks. In *27th European Conference on Optical Communication ECOC '01.*, 2001.

[7] Shuntaro Yamazaki and Minoru Shikada. POF for high-speed PC and home networks. In *Optical Fiber Communication Conference and Exhibit, 1998. OFC '98., Technical Digest*, 1998.

[8] T. Ono. Plastic optical fiber: The missing link for factory, office equipment. *Photonics Spectra*, Nov.:88–91, 1995.

[9] Alexandre Dupuis, Ning Guo, Nicolas Godbout, Suzanne Lacroix, Charles Dubois, and Maksim Skorobogatty. Prospective for biodegradable microstructured optical fibers. *Optics Letters*, 32(2):109, 2007.

[10] Theodore L. Parker and G. Robert Collins. Plastic optical fiber for in vivo use having a bio-compatible Polyurethane-siloxane copolymer, or polyurethaneureasiloxane copolymer cladding. US Patent No 4836646, 1989.

[11] M. Jager and A. Wilke. Comprehensive biocompatibility testing of a new PMMA-HA bone cement versus conventional PMMA cement in vitro. *Journal of Biomaterials, Science-Polymer Edition*, 14(11):1283–1298, 2003.

[12] K. S. C. Kuang and W. J. Cantwell. The use of plastic optical fibre sensors for monitoring the dynamic response of fibre composite beams. *Measurement Science and Technology*, 14:736–745, 2003.

[13] Y. M. Wong, P. J. Scully, R. J. Bartlett, K. S. C. Kuang, and W. J. Cantwell. Plastic Optical Fibre Sensors for Environmental Monitoring: Biofouling and Strain Applications. *Strain*, 39:115–119, 2003.

[14] G. Kodl. A New Optical Waveguide Pressure Sensor Using Evanescent Field. *Electronic Components and Technology Conference*, page 1943, 2004.

[15] Osamu Suzuki, Masahiro Miura, Masayuki Morisawa, and Shinzo Muto. POF-Type Optic Humidity Sensor and its Application. In *Optical Fiber Sensors Conference Technical Digest*, page 447, Tokyo, 2002.

[16] H. B. Liu, H. Y. Liu, G. D. Peng, and P. L. Chu. Strain and temperature sensor using a combination of polymer and silica fiber Bragg gratings. *Optics Communications*, 219:139–142, 2003.

[17] H. Y. Liu, G. D. Peng, and P. L. Chu. Thermal Tuning of Polymer Optical Fiber Bragg Gratings. *IEEE Photonics Technology Letters*, 13(8):824–826, 2001.

[18] D. Bosc and C. Toinen. Full Polymer Single-Mode Optical Fiber. *IEEE Photonics Technology Letters*, 4(7):749–750, 1992.

[19] D. W. Garvey, K. Zimmerman, P. Young, J. Tostenrude, Z. Zhou, M. Lobel, M. Dayton, R. Wittorf, and M. G. Kuzyk. Single-mode nonlinear-optical polymer fibers. *Journal of the Optical Society of America B*, 13(9):2017–2023, 1996.

[20] S. R. Vigil, Z. Zhou, B. K. Canfield, J. Tostenrude, and M. G. Kuzyk. Dual-core single-mode polymer fiber coupler. *Journal of the Optical Society of America B*, 15(2):895–900, 1998.

[21] T. Ishigure, E. Nihei, S. Yamazaki, K. Kobayashi, and Y. Koike. 2.5 gbit/s 100 m data transmission using graded-index polymeroptical fibre and high-speed laser diode at 650 nm wavelength. *Electronics Letters*, 31(6):467–469, 1995.

[22] Takaaki Ishigure, Eisuke Nihei, and Yasuhiro Koike. Graded-index polymer optical fiber for high-speed data communication. *Applied Optics*, 33(19):4261–4266, 1994.

[23] K. O. Hill, Y. Fujii, D. C. Johnson, and B.S. Kawasaki. Photosensitivity in optical fiber waveguides: Application to reflection filter fabrication. *Applied Physics Letters*, 32(10):647–649, 1978.

[24] M. Svalgaard, C.V. Poulsen, A. Bjarklev, and O. Poulsen. Direct UV writing of buried singlemode channel waveguides in Ge-doped silica films. *Electronics Letters*, 30(17):1401–1403, 1994.

[25] G. Meltz, W. W. Morey, and W. H. Glenn. Formation of Bragg gratings in optical fibers by a transverse holographic method. *Optics Letters*, 14(15):823–825, 1989.

[26] D. P. Hand and P. St. J. Russell. Photoinduced refractive-index changes in germanosilicate fibers. *Optics Letters*, 15(2):102–104, 1990.

[27] B. Poumellec, P. Guenot, I. Riant, P. Sansonetti, P. Niay, P. Bernage, and J. F. Bayon. UV induced densifitcation during Bragg grating inscription in Ge:SiO2 preforms. *Opctical Materials*, 4:441–449, 1995.

[28] R. M. Atkins, P. J. Lemaire, T. Erdogan, and V. Mizrahi. Mechanisms of Enhanced UV Photosensitivity via Hydrogen Loading in Germanosilicate Glasses. *Electronics Letters*, 29(14):1234–1235, 1993.

[29] P. J. Lemaire, R. M. Atkins, V. Mizrahi, and Reed W. A. High Pressure H_2 Loading as a Technique for Achieving Ultrahigh UV Photosensitivity and Thermal Sensitivity in GeO_2 Doped Optical Fibers. *Electronics Letters*, 29(13):1191–1193, 1993.

[30] G. D. Peng, Z. Xiong, and P. L. Chu. Photosensitivity and Gratings in Dye-Doped Polymer Optical Fibers. *Optical Fiber Technology*, 5(2):242–251, 1999.

[31] Sergey Sarkisov, Zedric Teague, Putcha Venkateswarlu, Hossin Abdeldayem, Donald Frazier, and Grigory Adamovsky. Formation of graded-index waveguide in UV exposed polyimide. *Journal of Applied Physics*, 81(6):2889–2891, 1997.

[32] J. H. Andrews and K. D. Singh. Photoinduced diffraction in polymer waveguides. *Applied Optics*, 32:6703, 1993.

[33] Shaoping Bian, Weiya Zhang, and Mark G. Kuzyk. Erasable holographic recording in photosensitive polymer optical fibers. *Optics Letters*, 28(11):929–931, 2003.

[34] J. M. Moran and I. P. Kaminow. Properties of Holographic Gratings Photoinduced in Polymethyl Methacrylate. *Applied Optics*, 12(8):1964–1970, 1973.

[35] W Driemeier and A Brockmeyer. High resolution photorefractive polymer for optical recording of waveguide gratings. *Applied Optics*, 25:2960, 1986.

[36] Oliver Beyer, Ingo Nee, Frank Havermeyer, and Karsten Buse. Holographic recording of Bragg gratings for wavelength division multiplexing in doped and partially polymerized poly(methyl methacrylate). *Applied Optics*, 42(1):30–37, 2003.

[37] JianMing Yu, XiaoMing Tao, and HwaYaw Tam. Trans-4-stilbenemethanol-doped photosensitive polymer fibers and gratings. *Optics Letters*, 29(2):156–158, 2004.

[38] Z. Xiong, G. D. Peng, B. Wu, and P. L. Chu. Highly Tunable Bragg Gratings in Single-Mode Polymer Optical Fibers. *IEEE Photonics Technology Letters*, 11(3):352–354, 1999.

[39] M. M. Werneck, E. S. Yugue, F. L. Maciel, J. L. Silva-Neto, C. C. Carvalho, M. A. L. Miguel, and R. M. Ribeiro. Application of a POF and ruby florescence based temperature system in an electric power substation. In *Proceedings POF 2007, Turin, Italy*, 2007.

[40] E. Udd, editor. *Fibre-Optic Smart Structures*. New York: Wiley, 1995.

[41] P. D. Foote. Optical fibre Bragg grating sensors for aerospace smart structures. In *Optical Fibre Gratings and Their Applications, IEE Colloquium on*, 1995.

[42] W. W. Morey, Meltz G., and J. M. Welss. Evaluation of a fibre Bragg grating hydrostatic pressure sensor. In *Proc. 8th Int. Conf. on Optical Fibre Sensors, Monterey, USA*, 1992.

[43] D. J. Webb, J. Surowiec, M. Sweeney, D. A. Jackson, J. M. Hand, L. Gavrilow, L. Zhang, and I. Bennion. Miniature fibre optic ultrasonic probe. In *Proc. SPIE 2839*, 1996.

[44] S. Theriault, K. O. Hill, F. Bilodeau, D. C. Johnson, and J. Albert. High-g accelerometer based on in-fibre Bragg grating sensor. In *Proc. 11th Int. Conf. on Optical Fibre Sensors, Sapporo, Japan*, 1996.

[45] R. N. Haward. *The physics of glassy polymers*. Applied science publishers LTD, London, 1973.

[46] S. O'Keeffe, A. Fernandez Fernandez, A. Fitzpatrick, C. Brichard, F. Berhmans, and E. Lewis. Evaluation of PMMA optical fibres as gamma dosimeters for nuclear applications. In *Intl. Plastic Opitcal Fibres Conf., Nuernberg, Germany*, 2005.

[47] J. J. Bayle and J. Mateo. Plastic optical fiber sensor of refractive index based on evanescent field. In *POF '96*, 1996.

[48] G. Garitaonainda, J. Zubia, U. Irusta, J. Arrue, and J. Miskowicz. Passive device based on plastic optical fiber to determine the index of refraction of liquids. In *Intl. Plastic Optical Fiber Conference, Berlin*, 1998.

[49] R. Philip-Chandy, Patricia J. Scully, Piers Eldridge, H. J. Kadim, M. Gérard Grapin, M. Guy Jonca, M. Gérard D'Ambrosio, and Francois Colin. An Optical Fiber Sensor for

Biofilm Measurement Using Intensity Modulation and Image Analysis. *IEEE Journal on selected topics in quantum electronics*, 6(5):764–772, 2000.

[50] K. S. C. Kuang, S. T. Quek, and M Maalej. Assessment of an extrinsic polymer-based optical fibre sensor for structural health monitoring. *Measurement Science and Technology*, 15:2133–2141, 2004.

[51] K. S. C. Kuang, W. J. Cantwell, and P. J. Scully. An evaluation of a novel plastic optical fibre sensor for axial strain and bend measurements. *Measurement Science and Technology*, 13:1523–1534, 2002.

[52] K. S. C. Kuang and W. J. Cantwell. The use of plastic optical fibres and shape memoery alloys for damage assessment and damping control in composite materials. *Measurement Science and Technology*, 14:1305–1313, 2003.

[53] Shinzo Muto, Osamu Suzuki, Takashi Amano, and Masayuki Morisawa. A plastic optical fibre sensor for real-time humidity monitoring. *Measurement Science and Technology*, 14:746–750, 2003.

[54] C. M. Tay, K. M. Tan, S. C. Tjin, C. C. Chan, and H. Rahardjo. Humidity sensing using plastic optical fibers. *Microwave and Optical Technology Letters*, 43(5):387–390, 2004.

[55] Irwan Rawal Husdi, Kentaro Nakamura, and Sadayuki Ueha. Sensing characteristics of plastic optical fibres measured by optical time-domain reflectometry. *Measurement Science and Technology*, 15:1553–1559, 2004.

[56] Philipp Lenke, Sascha Liehr, Katerina Krebber, Frank Weigand, and Elke Thiele. Distributed strain measurement with polymer optical fiber integrated in technical textiles using the optical time domain reflectometry technique. In *Proceedings POF 2007, Turin, Italy*, 2007.

Chapter 2

Polymer optical Fibers

2.1 Introduction and Overview

This chapter gives a brief introduction to optical fibers in general. Special emphasis is on polymer optical fibers. The history of POF is presented and the different polymer materials used for optical fibers are summarized. The optical properties of these materials and the POF are shown and the importance for FBG writing in POF is explained.

2.2 Optical Fibers

An optical fiber is a cylindrical dielectric waveguide. The fiber consists of a core with a refractive index n_{core} and a surrounding cladding layer with a refractive index n_{clad} (Figure 2.1). If the core index is larger than the cladding index, the light will be guided within the core due to total internal reflection at the core cladding interface. The two indices also define the so called numerical aperture NA which is the acceptance angle of the fiber and it is defined as

$$NA = \sqrt{n_{core}^2 - n_{clad}^2} \tag{2.1}$$

Light coupled into the fiber core is guided if the angle of incidence is within the NA. If the angle of incidence is larger, the light ray will leave the fiber core into the cladding.

$$\mathrm{NA} = n \sin \theta \tag{2.2}$$

The boundary between the core and cladding may either be abrupt, in step-index (SI) fiber, or gradual, in graded-index (GI) fiber. As an optical waveguide, the fiber supports one or more confined transverse modes by which light can propagate along the fiber.

The number of bound modes, the mode volume, is related to the normalized frequency, V, which is a measure to determine if the fiber is single mode (V < 2.405) or multimode. The V number is given by [1]
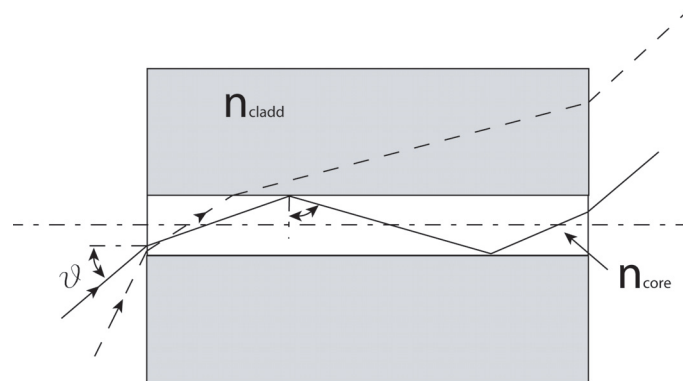
Figure 2.1: *Fiber principle*

$$V = \frac{2\pi r}{\lambda} \sqrt{{n_{core}}^2 - {n_{clad}}^2} \quad = \frac{2\pi r}{\lambda} \mathrm{NA} \tag{2.3}$$

where λ is the wavelength, r is the core radius.

Single mode (SM) fiber

Single mode fibers are composed such as the core radius and the indices allow only the prop-
agation of one mode at a given wavelength and the core diameter has to be small compared
to multimode fibers. For single-mode operation is required that V < 2.405, which is the first
root of the Bessel function J_0 and which is called the cut off condition. Looking at one mode
in a fiber, the light energy is not entirely confined in the core. A significant portion of the light
energy is to be found in the cladding in an evanescent wave. In a single mode fiber the light
basically travels along its axis. This eliminates intermodal dispersion. For data communication
this increases the possible bandwidth as the pulse broadening due to different optical paths does
not occur. The standard single-mode fiber for telecomunication is the SMF-28E.

2.3   Polymer Optical Fiber (POF)

Du Pont was the first company to produce POF in the 1960s [2]. In the 70s mainly Du Pont and
Mitsubishi worked on the production of POF. Mitsubishi filed a patent in 1974 for the melt-
spinning [3] and for continuos bulk polymerization [4] of POF. Du Pont filed patents in 1979 for
low attenuation [5] and deuterated PMMA POF [6]. Interest and research increased in the mid
1980s, when more patents [7–12] on different production methods and different materials for
polymer optical fibers were filed. Work was mainly focussed on the field of data communication
with the aim to lower the losses of POF which were initially as high as $\approx$ 1000 dB/km. With

improved production methods attenuation levels of max. 150 dB/km at 650 nm are reached in current commercial POF [13]. In comparison silica fibers reach attenuation levels below 1 dB/km at telecommunication wavelengths (1300 / 1550 nm). Due to the huge attenuation at the standard telecommunication wavelengths of PMMA (10^4 - 10^5 at $\approx$ 1500 nm [14]), POF were mostly used at their lowest attenuation windows (560 nm and 650 nm). Further effort has gone into still reducing the losses by the introduction of deuterated and fluorinated polymers such as the so called CYTOP ®(Ashai Glass) [15,16], which enables the use of POFs even in the data communications bandwidth range at 850 nm or 1310 nm. These polymers make attenuation levels of 55 dB/km at 567 nm [17] for deuterated and as low as 15dB/km at 1310 nm [18] for CYTOP POF possible. However the short distance data-communication networks over POF are still dominated by solutions at 650 nm where the attenuation levels of PMMA-POF are lowest. Todays cars are already equipped with POF data-bus as standard [19–21].

POF are commonly large core multimode fiber, with core diameter between $250\mu m$ and 1 mm or even larger and are dominantly used in data-communication. One of the main advantages of large core POFs is that the coupling of cheap light sources with high numerical apertures is possible. High tolerance connectors can be used which can be manufactured cheap and in volume as injection molding parts. For this reason the costs for polymer optical links including connectors, fibers and installation are lower than for glass optical fibers (GOF). These reasons drove the industry to mainly produce and research in multi mode (MM) large core diameter POFs. Several papers reported of the production of SM POFs [22–26], however no supplier has a commercial single mode POF in their portfolio. Garvey et al. [27] emphasized the fact that the production of POFs is an empirical task and even using exactly the same parameters did not yield the same results sometimes.

Table 2.1 shows the properties of the SM POF from Paradigm Optics which was used throughout this work. In comparison the specifications of a standard SM silica fiber (SMF-28e from Corning Incorporated [28]) are presented.

2.4 Polymers

The large molecule chains of polymers can either be randomly distributed and oriented, which are amorphous polymers, or they can crystalize or even interconnect and build networks. The commonly used polymers for optical waveguides are transparent amorphous polymers which are also called thermoplastics. At a defined region, the so called glass transition temperature (T_g), thermoplastics show a sudden drop in viscosity which can be compared to a melting behavior in other solid materials. The temperature and deformation history can change the degree of orientation of the molecule chains and with it the mechanical and optical properties [29]. Especially fibers exhibit a certain degree of orientation as the production process promotes a

	Paradigm POF	**SMF 28**
Core Diameter	3.4 μm^a	8.2 μm
Core Material	Copolymer of	SiO$_2$ doped with
	PMMA and PS	$3 \div 4$ mol% of GeO$_2$
Cladding Diameter	125 μm^a	125 μm
Cladding Material	PMMA	SiO$_2$
Numerical Aperture	$<0.27^a$	0.14
N_{eff}	1.4884	1.4682
N_{core}	1.5038^a	1.4508
$N_{cladding}$	1.4794^a 1.4792^b	1.444
λ_c	< 1400nm	≤ 1260nm

[a]Information from Paradigm Optics
[b]Calculated from dispersion data for PMMA

Table 2.1: *Comparison of the SM POF used throughout this work and a standard SM glass fiber*

certain molecule chain orientation in fiber direction [22,30]. Orientation leads in most polymers to birefringence and in some cases to crystallinity. Crystallinity has to be avoided as it is directly affecting the optical transmittance. The polymers used for POF due not easily crystalize, however the birefringence of POF has been addressed in several researches using dopants or copolymerization in order to reduce birefringence [31,32].

To produce polymers, the monomer is mixed with a polymerization initiator and a chain-transfer agent. The purpose of the initiator is the initial start of the polymerization reaction in which the monomers link together to a longer molecule chain, the polymer molecule. The chain-transfer agent has the purpose to control the resulting chain length as different chain lengths can give rise to different macroscopic physical properties [33]. With a suitable initiator and chain transfer agent the polymerization takes place and the desired chain length/chain weight can be influenced. At the same time the residual monomer content can be influenced in order to produce polymer fibers with an increased monomer content [34].

2.4.1 Poly methyl methacrylate, (PMMA)

PMMA Poly methylmethacrylate or also called Plexiglas, Perspex, Acrylate, Lucite and various other trade names exist [35]. It was discovered around 1930 in Germany, Spain and England at approximately the same time. The basic monomer is methylmethacrylate. For the resulting polymer, the glass transition temperature T$_G$ is $95 - 125°C$. The T$_G$ however depends on the Molecular weight and purity of the polymer. The refractive index is 1.49 at 589.2 nm.

PMMA has attenuation levels of $50 - 80$ dB/km at 570 nm and $\sim 100 - 200$ dB/km at 660 nm, [36]. It is the most commonly used POF material. However the attenuation values in
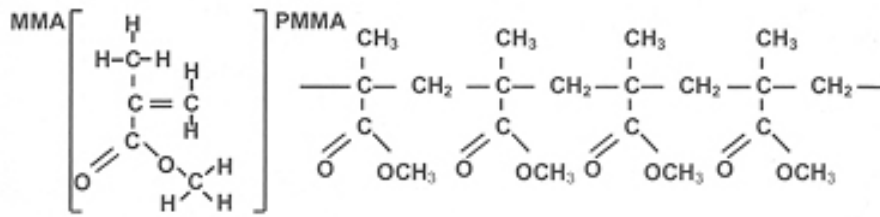
Figure 2.2: PMMA [2]

the data communication wavelength range are very high ($\approx 10^5$ dB/km). Attenuation of an SM POF from Paradigm optics (Table 2.1) was measured using a cut-back technique. The attenuation at 1550 nm is $\approx$ 1dB/cm. For biomedical application PMMA is very well suited due to its good biocompatibility [37, 38].

The properties of PMMA can be found in Table 2.2 in. One major disadvantage of PMMA apart from the relatively high optical attenuation is its high water sorption capabilities [39–41]. PMMA can absorb up to $2wt\%$ of water. The water uptake leads to swelling, i.e. expansion of the PMMA. For parts like PMMA lenses this alters the geometry and in consequence the optical performance. Further depending on the specific PMMA used, water uptake can lead to clustering, largely increasing scattering loss. The detailed mechanisms involved in water sorption will be discussed in section 5.2.

PMMA is the most commonly used material for POF. The optical performance of a POF is influenced by the material and by the quality of the waveguide. In PMMA POF the attenuation is mainly influenced by the absorption of the material and scattering losses due to inclusions and morphology imperfections.

2.4.2 Polystyrene (PS)

The refractive index of PS is n=1.59 , which makes it possible to use either (Polycarbonate) PC n=1.48 or PMMA n=1.49 as cladding. The glass transition temperature is approximately 100°C, which is slightly lower than PMMA. PS is commonly used as copolymer with PMMA. If PS and PMMA are only mixed but not copolymerized, the blend is only transparent for very low content of one of the components ($< 1wt\%$), for blends containing $> 3wt\%$ of the other component, the mixture is opaque. [42] Water sorption in PS was reported to be on the order of $0.1 - 0.2wt\%$ i.e. about one order of magnitude smaller than that of PMMA. Some selected properties of PS can be found in Table 2.2
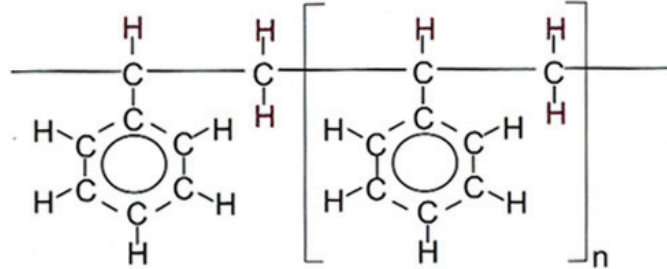
Figure 2.3: *Polystyrene [2]*

	PMMA	**PS**
Tensile strength	$60 - 70 \ \mathrm{N/mm^2}$	$40 - 50 \ \mathrm{N/mm^2}$
Elongation at break	$2,5 - 3,5\%$	$< 3\%$
Tensil modulus	2.9-3.3 GPa	3.3 GPa
Poisson's ratio	0.35 [43]	0.353 [44]
Linear thermal expansion	$7 \times 10^{-5} \ \mathrm{K^{-1}}$	$6 - 8 \times 10^{-5} \ \mathrm{K^{-1}}$
Thermal conductivity	0.18 W/(m K)	0.17 W/(m K)
Specific heat	1.39 J/(g K)	1.2 J/(g K)
Heat of combustion	26.2 kJ/g	42.2 kJ/g
Density	$1.18 \ \mathrm{kg/m^3}$	$1.05 \ \mathrm{kg/m^3}$
Ref. index	1.49 at 589.2 nm	1.59
p_{11}	0.3 [45]	0.32 [44]
p_{12}	0.297 [45]	0.31 [44]
C	$(-2.7 \div -3.8) \times 10^{-12} \mathrm{Pa^{-1}}$ [46,47]	$(6 \div 10) \times 10^{-12} \mathrm{Pa^{-1}}$ [46]

Table 2.2: *Properties of PMMA and PS taken from Saechtling, 'Plastics Handbook ' [35], except where otherwise mentioned.*

2.4.3 PF Polymers, CYTOP $^{®}$

Perfluorinated (PF) polymer based optical fibers have low intrinsic loss in a very wide wavelength range, from visible to near infrared region [2]. Another advantage of PF-GI-POF is its low material dispersion that provides to this fiber a great potential to high-speed transmission link applications. ASAHI Glass Co. in Japan developed this PF polymer in collaboration with Keio University under the name of CYTOP, which has been shown to be suitable for POF manufacturing [15,16]. CYTOP stands for Cyclic Transparent Optical Polymer. The refractive index is n=1.34 (d-line at 589.2 nm) and the glass temperature is given as $108°C$. It can be seen in Figure 2.4 that CYTOP no longer contains any C-H bonds which reduces attenuation at near IR and higher wavelength regions.
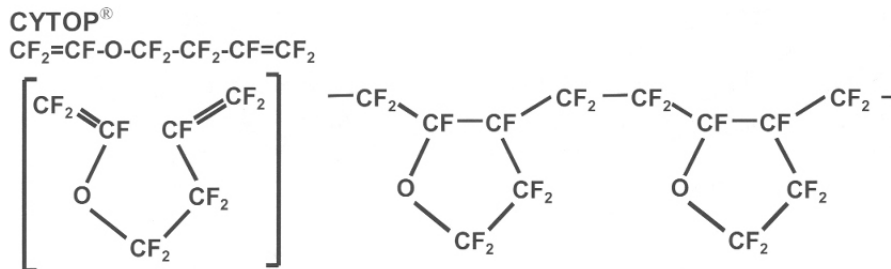
Figure 2.4: CYTOP [2]

2.4.4 Refractive index design

In order to produce waveguides, the refractive index of the cladding and the core material has to be different. For the POF production, either different polymers can be used, or the refractive index can be designed by, a) mixing of polymers, b) addition of dopants, c) co-polymerization of different monomers. The mixing of polymers has the disadvantage, that the miscibility of different polymers can inhibit mixing and lead to opaque blends. In immiscible polymers the chains do not entangle properly; the materials repel each other due to unfavorable enthalpic interactions, making the adhesion between these materials poor. Kaczmarek [42] reported that blends of PMMA and PS were only transparent up to a PS content of <3% and being opaque for higher PS contents.

2.4.5 Dopants

Another way to modify the refractive index is to use a dopant. In that case a compound (dopant) is added to the polymer which does not build a bond to the polymer material but is dispersedly

distributed in the material. Dopants are selected in order to prevent out-diffusion from the fiber with time and therefore changing the optical properties. GI fibers have shown life times of over 10000 hours at 85° C by selecting a large size aromatic dopant [48].In general dopants shouldn't be too small in order not to diffuse out of the polymer at working temperatures. Another important factor is that dopants can alter the glass transition temperature through a change of viscosity and therefore limit the possible service temperature of a POF.

2.4.6 Copolymers

Co-polymerization is the polymerization of two different monomer species together to one polymer chain that is, in general randomly, composed of the two components. The advantage of copolymers is there stability of refractive index. The selection of a co-monomer to be added to the base monomer allows to adjust the refractive index as required. However care must be taken that they form co-polymer chains and not polymer chains of the two species. For this reason the bonding energies between the different monomers should be about the same [2].

2.5 Optical Properties
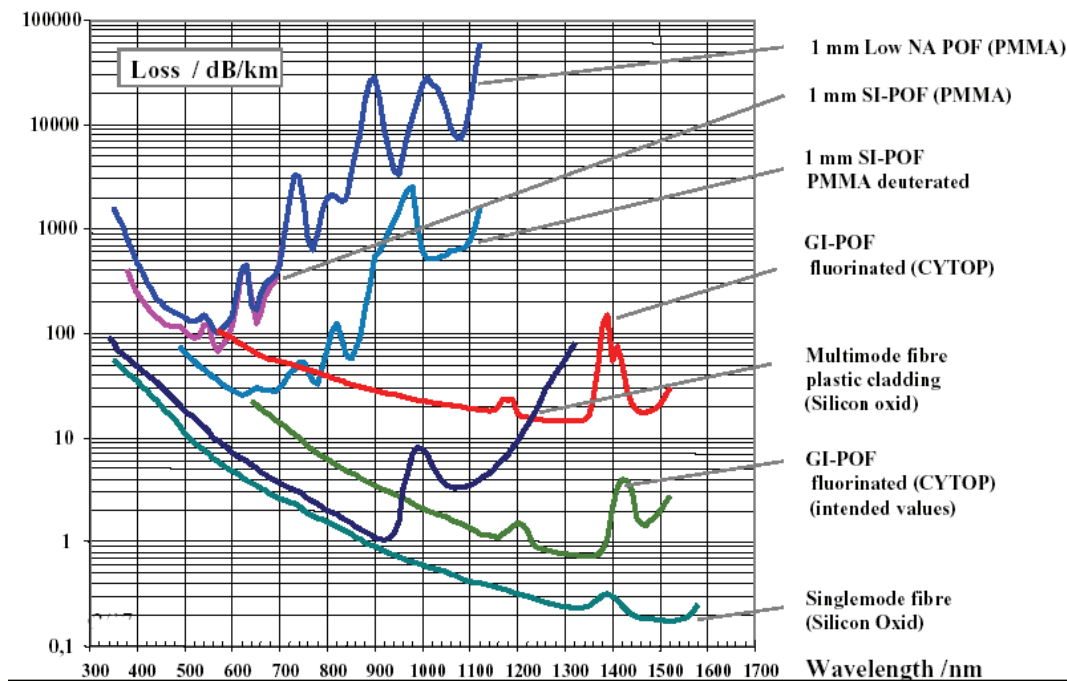
Figure 2.5: Attenuation Spectra of various Optical Fibers [49]

The attenuation spectra for different optical fibers are shown in Figure 2.5. Mainly four separate loss mechanisms define these spectra: Scattering due to imperfections, Rayleigh scattering and absorption in the UV and IR regions. Scattering due to imperfections is wavelength independent and caused by inclusion like dust particles and bubbles. Rayleigh scattering decreases with $1/\lambda^4$ [50] and therefore short wavelengths are scattered more. Total scattering loss for Low-Loss PMMA is between 10 and 400 dB/km at 633 nm depending on the polymerization conditions [51]. Theoretical values are difficult to achieve. The main difficulty is to process the polymer into a fiber as fluorinated polymers, like for example Teflon, tend to crystallize, increasing the scattering losses significantly. The absorption in the UV and IR region is explained in the following two sections.

2.5.1 UV absorption

The UV absorption of solid materials is defined by the transition between electronic energy levels of the bonds. Figures 2.6 and 2.7 show the UV transmission spectra for PMMA and PS [52]. It can be seen that the absorption at 308 nm of PS is substantially higher than for PMMA. This and the fact that irradiation of PMMA with 308 nm did not show an index change [53] suggests, that selective photo-writing in a polymer fiber core containing PS could be possible, leaving the PMMA cladding unchanged.
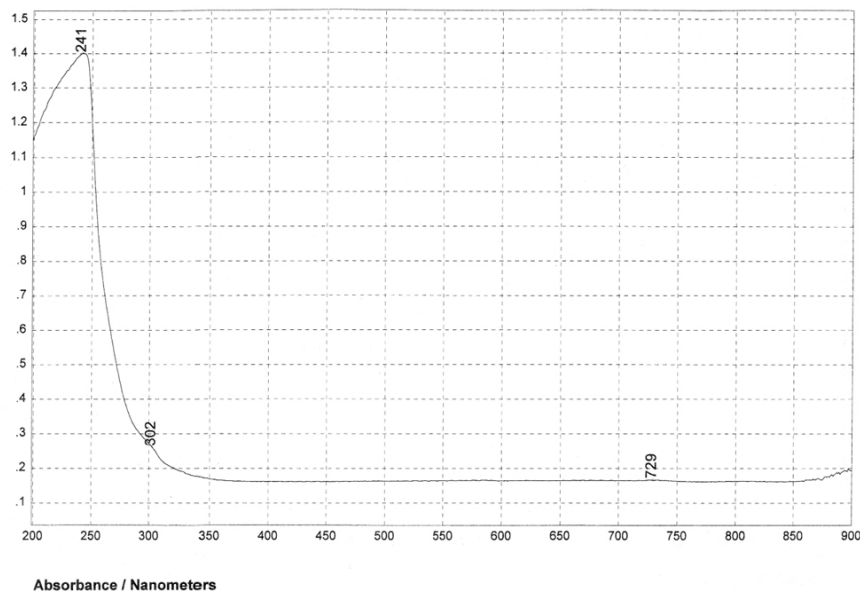
Figure 2.6: *UV transmission spectrum of PMMA [52]*
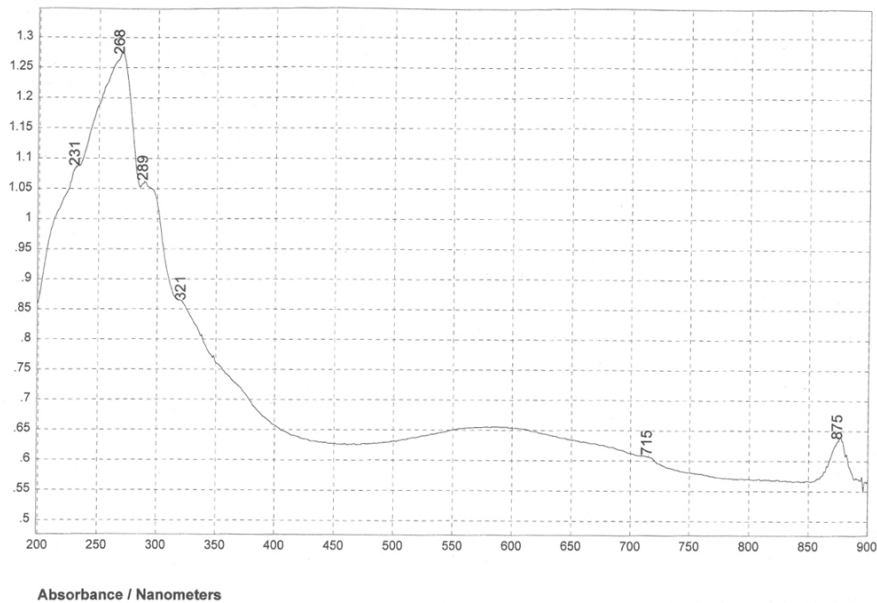
Figure 2.7: *UV transmission spectrum of PS [52]*

2.5.2   IR absorption

Most transparent polymers show high attenuation levels especially towards the near IR region. The main reason for these high absorption losses are C-H bond absorption due to stretching (ν) and bending vibrations (Fig. 2.6 [17]). The high harmonics of the oscillations add also to the attenuation in the visible range. The main problem concerning PMMA for optical fibers is the high attenuation at data communication wavelengths (i.e. 1300 - 1500 nm). The main difference between the IR absorption spectrum of PMMA compared to PS (Figrue 2.9) is the much higher absorption in the IR region due to the ester group in PMMA. Given that PMMA has eight C-H bonds there is some potential in replacing the hydrogen with atoms from the 7th main group. The attenuation values for deuterated PMMA (C-D bonds) are about one order of magnitude smaller then the values for normal PMMA. A heavier core will result in a lower vibration frequency, thus moving the attenuation bands to a larger wavelength. In CYTOP for example, a fluorinated polymer, no more hydrogen is in the monomer or in the polymer, i.e. all bonds are C-C or C-F bonds. Therefore the attenuation due to oscillation and its harmonics is shifted further towards the infrared giving this polymer good attenuation values in the 1.3-1.6 μm range.
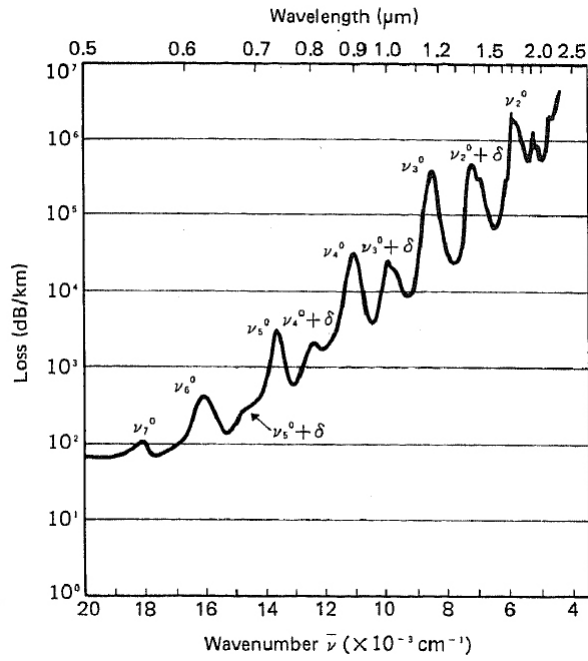
Figure 2.8: *Vibrational and stretching overtones of PMMA [17]*
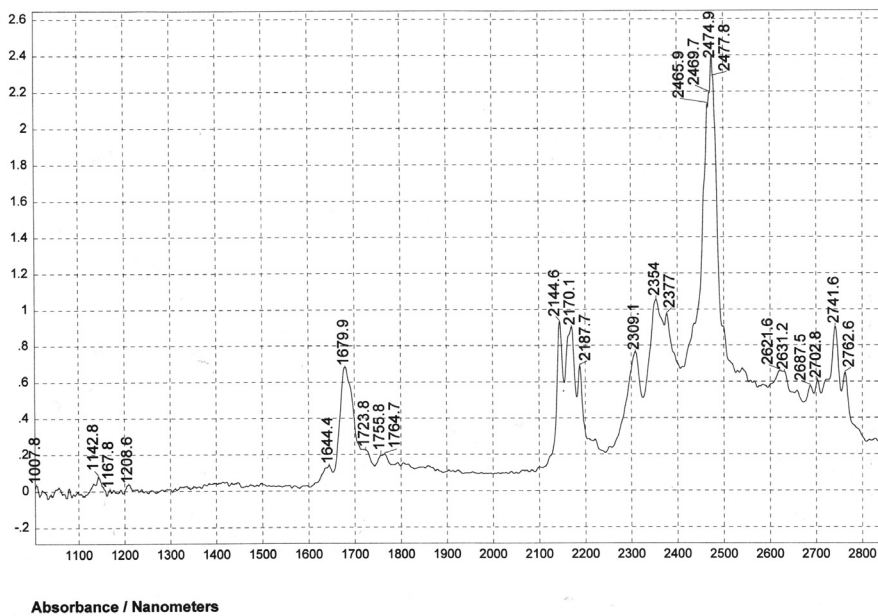
Figure 2.9: *IR absorption spectrum of PS [52]*

Bibliography

[1] D. Marcuse. Loss Analysis of Single-Mode Fiber Splices. *The Bell System Technical Journal*, 56(5):703–718, 1977.

[2] Werner Daum, Jürgen Krauser, Peter E. Zamzow, and Olaf Ziemann. *POF - Polymer Optical Fibers for Data Communication*. Springer, 2002.

[3] Kazuya Chimura, Shunichi Takashima, Ryuichi Nakazono, Masao Kawashima, Hiroyuki Ota, and Kenichi Sakunaga. Light Transmitting Fibers. US Patent No 3930103, also published as GB Patent 1431157, Dec 1975.

[4] Mitsubishi. Light Transmission Filament. GB Patent 1449950, also published as US Patent 3993834, 1974.

[5] DuPont. Low attenuation all-plastic optical fibre. GB Patent 2006790, also published as NL Patent 7810326 and JP Patent 61005206, May 1979.

[6] DuPont. Low attenuation optical fibre of deuterated polymer. GB Patent 2007870, also published as NL Patent 7810327 and JP Patent 54065556, May 1979.

[7] Toshikuni Kaino, Michiya Fujiki, Shigeo Nara, and Shigeru Oikawa. Fabrication of a low-loss plastic optical fiber. US Patent No 4381269, Apr 1983.

[8] Yoshinobu Ueba and Shinichi Miyake. Plastic optical fibers. US Patent No 4505543, also published as JP Patent 58065402, Mar 1985.

[9] Kazuo Ishiwari, Akira Ohmori, Nobuyuki Tomihashi, Sumiko Yuhara, Toshikuni Kaino, Kaname Jinguji, and Shigeo Nara. Plastic optical fibers. US Patent No 4542957, also published as JP Patent 59030502 and EP Patent 0101048, Sep 1985.

[10] Kozi Nishida and Takashi Yamamoto. Plastic optical fibers. US Patent No 4544235, also published as EP Patent 0098578 and IT Patent 1164288, Oct 1985.

[11] Yoshinobu Ueba and Shinichi Miyake. Plastic optical fibers. US Patent No 4681400, also published as JP Patent 58034404, Jul 1987.

[12] Toshio Koishi, Isao Tanaka, Takashi Yasumura, and Yukitoshi Nishikawa. Optical fiber having polymethacrylate core and fluoro-copolymer cladding. US Patent No 4687295, also published as JP Patent 1022305, GB Patent 2161954, FR Patent 2567653, DE Patent 3524369 and IT Patent 1185141, Aug 1987.

[13] Mitsubishi Rayon Co. LTD. ESKA Polymer Optical Fiber SK-80 Specification Sheet. www.pofeska.com, 2001.

[14] Christopher Emslie. Review Polymer optical fibres. *Journal of Materials Science*, 23:2281–2293, 1988.

[15] Manabu Kagami, Hiroshi Ito, Tadashi Ichikawa, Satoru Kato, Morihiro Matsuda, and Nobuaki Takahashi. Fabrication of large fore, high-Δ optical waveguides in polmyers. *Applied Optics*, 43(6):1041, 1995.

[16] Y. Koike. Status of POF in Japan. In *POF Conference Paris*, 1996.

[17] Toshikuni Kaino, Michiya Fujiki, and Kaname Jinguji. Preparation of Plastic Optical Fibers. *Review of the Electrical Communication Laboratories*, 32(3):478–488, 1984.

[18] Y. Koike. Progress in GI-POF - Status of High Speed Plastic Optical Fiber and it's Future Prospect. In *POF 2000, Boston, 2000*, 2000.

[19] Thomas Kibler, Stefan Poferl, Gotthard Böck, Hans-Peter Huber, and Eberhard Zeeb. Optical data buses for automotive application. *Journal of Lightwave Technology*, 22(9):2184–2199, 2004.

[20] D. Seidl, P. Merget, J. Schneider, R. Weniger, and E. Zeeb. Applications of POF's in data links of mobile systems. In *Proc. 7th Int. Polymer Optical Fiber (POF) Conf., Berlin, Germany*, 1998.

[21] Byteflight . Official Homepage, http://www.byteflight.com.

[22] Ladislav Dvoranek, Ludka Machova, Miloslav Sorm, Zdenek Pelzbauer, Jiri Svantner, and Vladimir Kubanek. Effects of Drawing Conditions on the Properties of Optical Fibers Made from Polystyrene and Poly(Methyl Methacrylate). *Die Angewandte Makromolekulare Chemie*, 174:25–39, 1990.

[23] Rebecca J. Bartlett, Rekha Philip-Chandy, Piers Eldridge, David F. Merchant, Roger Morgan, and Patricia J. Scully. Plastic optical fibre sensors and devices. *Transaction of the Institute of Measurement and Control*, 22(5):431–457, 2000.

[24] Edward F. Gurnee. Theory of Orientation and Double Refraction in Polymers. *Journal of Applied Physics*, 25(10):1232–1240, 1954.

[25] Christopher G. Robertson and Garth L. Wilkes. Refractive index: a probe for monitoring volume relaxation during physical aging of glassy polymers. *Polymer*, 39(11):2129–2133, 1998.

[26] Zhiyi Zhang, Gaozhi Xiao, and Chander P. Grover. Volume relaxation in polymers and its effect on waveguide applications. *Applied Optics*, 43(11):2325–2331, 2004.

[27] D. W. Garvey, K. Zimmerman, P. Young, J. Tostenrude, Z. Zhou, M. Lobel, M. Dayton, R. Wittorf, and M. G. Kuzyk. Single-mode nonlinear-optical polymer fibers. *Journal of the Optical Society of America B*, 13(9):2017–2023, 1996.

[28] Corning Incorporated. Corning SMF-28e.

[29] Christin Pellerin, Robert E. Prud'homme, and Michel Pézolet. Effect of thermal history on the molecular orientation in polystyrene/poly/vinyl methyl ether) blends. *Polymer*, 44:3291–3297, 2003.

[30] Jacques Dugas, Isabelle Pierrejean, Jean Farenc, and Jean Philippe Peichot. Birefringence and internal stress in polystyrene optical fibers. *Applied Optics*, 33(16):3545–3548, 1994.

[31] Bernd R. Hahn and Joachim H. Wendorff. Compensation method for zero birefringence in oriented polymers. *Polymer*, 26:1619–1622, 1985.

[32] Rei Furukawa, Akihiro Tagaya, Shuichi Iwata, and Yasuhiro Koike. Design of a polarization maintaining graded index plastic optical fiber by random copolymerization. In *Proceedings POF 2007, Turin, Italy*, 2007.

[33] R. P. Kusy and A. R. Greenberg. Influence of molecular weight on the dynamic mechanical properties of poly(methyl methacrylate). *Journal of Thermal Analysis and Calorimetry*, 18(1):117–126, 1980.

[34] Z. Xiong, G. D. Peng, B. Wu, and P. L. Chu. Highly Tunable Bragg Gratings in Single-Mode Polymer Optical Fibers. *IEEE Photonics Technology Letters*, 11(3):352–354, 1999.

[35] Dr. Hansjürgen Saechtling. *International Plastics Handbook*. Hanser Publishers, 1987.

[36] Lawrence A. Hornak. *Polymers for lightwave and intergrated optics*. Marcel Dekker, Inc., 1992.

[37] Alexandre Dupuis, Ning Guo, Nicolas Godbout, Suzanne Lacroix, Charles Dubois, and Maksim Skorobogatty. Prospective for biodegradable microstructured optical fibers. *Optics Letters*, 32(2):109, 2007.

[38] Theodore L. Parker and G. Robert Collins. Plastic optical fiber for in vivo use having a bio-compatible Polyurethane-siloxane copolymer, or polyurethaneureasiloxane copolymer cladding. US Patent No 4836646, 1989.

[39] Hiromasa Kawai, Fumiaki Kanega, and Hisashi Kohkame. Novel acrylic resion for injection molded precision lenses. In *SPIE Vol. 896 Replication and Molding of Optical Components*, 1988.

[40] J. A. Barrie and D. Machin. Diffusion and Association of Water and Some Polyalkyl-metacrylates. *Transactions of the Faraday Society*, 67:244–256, 1971.

[41] P. P. Roussis. Diffusion of water vapour in polymethyl methacrylate. *Journal of Membrane Science*, 15:141–155, 1983.

[42] Halina Kaczmarek. Changes of polymer morphology caused by u.v. irradiation: 2. Surface destruction of polymer blends. *Polymer*, 37(4):547–553, 1996.

[43] D. Taylor, M. Merlo, R. Pegley, and M. P. Cavatorta. The effect of stress concentrations on the fracture strength of polymethylmethacrylate. *Materials Science and Engineering A*, 382:288–294, 2004.

[44] l. N. Durvasula and Robert W. Gammon. Brillouin scattering from shear waves in amorphous polycarbonate. *Journal of Applied Physics*, 50(6):4339–4344, 1979.

[45] Roy M. Waxler, Deane Horowitz, and Albert Feldman. Optical and physical parameters of Plexiglas 55 and Lexan. *Applied Optics*, 18(1):101–104, 1979.

[46] J. F. Rudd and R. D. Andrews. Photoelastic Properties of Polystyrene in the Glassy State. III. Styrene Derivatives and Copolymers. *Journal of Applied Physics*, 31(5):818–826, 1960.

[47] H Ohkita, K Ishibashi, D. Tsurumoto, A. Tagaya, and Y. Koike. Compensation of the photoelastic birefringence of a polymer by doping with an anisotropic molecule. *Applied Physics*, A 81:617–620, 2005.

[48] Masataka Sato, Takaaki Ishigure, and Yasuhiro Koike. Thermally Stable High-Bandwidth Graded-Index Polymer Optical Fiber. *Journal of Lightwave Technology*, 18(7):952–958, 2000.

[49] Pak L. Chu. Polymer optical fibre challenge. Presentation at City University of Hong Kong, Feb. 2004.

[50] Bahaa E. A. Saleh and Malvin Carl Teich. *Fundamentaly of Photonics*. John Wiley and Sons Inc., 1991.

[51] Yasuhiro Koike, Norihisa Tanio, and Yasuji Ohtsuka. Light Scattering and Heterogeneities in Low-Loss Poly(methyl methacrylate) Glasses. *Macromolecules*, 22:1367–1373, 1989.

[52] Jerry Workman Jr. *Handbook of organic compounds*. Academic Press, 2001.

[53] C. Wochnowski, S. Metev, and G. Sepold. UV-laser-assisted modification of the optical properties of polymethylmethacrylate. *Applied Surface Science*, 154-155:706–711, 1999.

Chapter 3

Photosensitivity

3.1 Introduction

The term photosensitivity in the context of writing waveguides or Bragg gratings in optical materials is used to describe the induced change of the optical properties due to irradiation. In this chapter the photo induced refractive index change will be explained. A very brief explanation of photosensitivty of anorganic glass will be followed by a review of different polymer photosensitivity mechanisms. The importance of the different mechanisms in respect to the polymer fiber used in this work will be emphasized.

3.2 Photosensitivity in inorganic glasses

The UV-induced refractive index change in germano-silicate is related to two different mechanisms. Refractive index change due to the color center model [1] or due to densification [2]. Further hydrogen loading (i.e. diffusion of H_2 into the core of a fiber, often at elevated temperature and pressure) can increase the maximum index change achieved. (e.g. 1.2×10^{-3} for 3% germanium doped fibers [3] and 5.9×10^{-3} for similar core hydrogen loaded fibers [4]). Exposure of hydrogen loaded fibers causes the H_2 to react and therefore increases photosensitivity.

3.3 Photosensitivity in polymers

Photo induced changes in polymers include birefringence and index change which can be caused by different mechanisms like photo-isomerization [5], densification [6] and photo-chemical reactions [7]. This chapter will give an introduction of different photosensitivity mechanisms found in polymers with special attention to PMMA and PS as they are the main components of the fiber core at hand.

3.3.1 Photolysis

Photolysis, also called photo-degradation, is generally considered as a change of the primary structure of a polymer, by oxidative processes and/or chain-scission, due to irradiation. Photo-induced oxidation processes are generally initiated at the surface in oxygen containing environments, which give rise to a gradient of deteriorated material across the specimen thickness. Photo induced chain-scission processes start at specifically radiation sensitive sites (chromophoric groups) in the polymer.
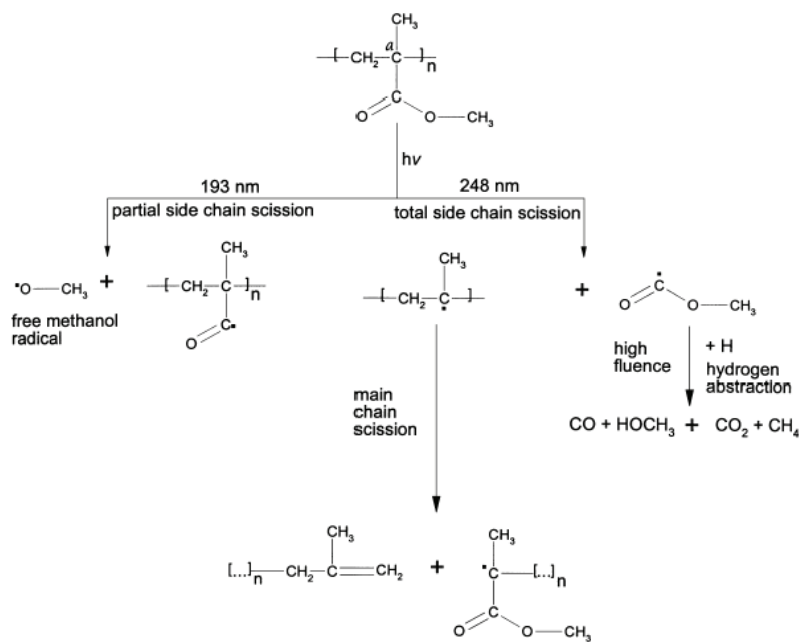
Figure 3.1: Photochemical reactions in PMMA [8]

Photolysis of PMMA

Photolysis of PMMA was investigated by several groups mainly in the context of ablation [9–16] and some investigated on the refractive index change as well [8, 17–21].

Depending on the energy of the irradiation different chemical processes, different amounts of the specific side chain splitting and main chain scission are observed [22]. Figure 3.1 shows the photo-degradation process of PMMA for two different wavelength. Most dominant process for 248 nm irradiation of PMMA is the split-off of an ester group with a subsequent hydrogen abstraction which in turn leads to a C=C double bond or less often to a main chain scission. With 193nm partial side chain scission occurs and therefore slower degradation than with 248

nm as can be seen from Figure 3.1. The main impact of these processes, was reported to be a change in density of the polymer material [17–21, 23] which is responsible for the index change. Index modification was only reported for wavelengths below ≈ 260 nm because of too low photon energies above this wavelength [8]. A general problem regarding PMMA POF and irradiation wavelengths below ~ 350 nm is that the penetration depth is very low (i. e. < 100 μm @ 308 μm) [24, 25]. Depending on the fiber geometry and size, reaching the core with radiation below 260 nm might not be possible.

The temperature at which the net rate of polymer formation is equal to the rate of depolymerization is called the ceiling temperature. Above the ceiling temperature, depolymerization will start, fragmenting the polymer chain into its constituent monomer units through a propagating radical. If a polymer is heated above its ceiling temperature through irradiation one speaks of photo-thermal decomposition. After the irradiation the monomer molecules can polymerize again forming a region of different density or morphology (i.e. less oriented macromolecule chains). It is not clear to which degree direct bond scission due to photons with high enough energies, or photo-thermal effects will dominate in a given irradiation case. [1]

In the case of PMMA PS copolymer irradiated with 308nm excimer laser radiation, it is believed that the PS part acts as absorption centers which then lead to photo-thermal degradation and unzipping of the core. The ceiling temperatures of PS and PMMA are $\approx 230°$ C and $\approx 150°$ C respectively [7].

The advantage of photolysis is that it can be used on undoped polymers and therefore reducing the need of specifically manufactured POF. However adding dopant can be of interest as it enables to shift the irradiation wavelength to more suitable regions and still enable dopant induced photolysis [15, 26].

3.3.2 Photo-polymerization

Polymerization is the process of linking together monomer molecules which leads to long molecule chains or so called macromolecules. A monomer molecule is capable of being linked to two or more other molecules (of the same or a different monomer) by chemical reaction. The polymerization is normally controlled by an initiator agent which creates a radical on a monomer molecule thus starting the polymerization, and a chain transfer agent which is used to control the macromolecule chain lengths. If instead of an initiator irradiation is used to initiate the polymerization, or an initiator is used that can be activated by irradiation the term photo-polymerization is used. In the case of already polymerized materials residual monomers in the polymer matrix can be photo-polymerized or lead cross-links between macromolecules. This is a technique often used in waveguide production or for curing of polymers instead of or in addition to the use of initiator substances. In order to exploit this mechanism in the context of

---

[1]Private communication with P. Hoffmann

photosensitivity, the initial polymerization has to be controlled to the point where the produced polymer still contains a residual amount of monomer. The residual monomer content can be controlled by the amount of initiator and chain transfer agent used [27]. In turn this residual monomer can be locally photo-polymerized which leads to a local density change and a photoinduced refractive index structure. The density change is a result of the bonding of the monomer molecules, because the bonds are much shorter than the initial inter molecular distances held together by Van der Walls interactions. It has been shown that pure PMMA containing residual monomers exhibit photosensitivity [21]. Adding an extra photo-initiator to a not fully polymerized POF allows selecting the wavelength needed to induce photo-polymerization for example a photo-initiation wavelength of 514 nm can be used with titanium-biscyclopentadienylchloride as photo-initiator [21].

Some publications [27, 28] reported on FBGs that were written in residual monomer content fibers. However the mechanism of photo-sensitivity was not investigated in detail so there is not certainty that the reported index change is due to this monomer content. The refractive index modification reached up to 2×10^{-3} using fibers with a core made from a monomer mixture containing MMA[2], EMA and BzMA. To write the grating an irradiation wavelength of 325 nm and a phase mask were used. Peng [29] stated photo-sensitivity of PMMA itself at 325 nm without giving further details on the photo-sensitivity process or residual monomer content. Most recently Kalli et al. [30] presented a work, outlining the photosensitivity of MMA due to photo-polymerization upon irradiation with 325 nm laser light. The UV-induced conversion however is most efficient below 95% of polymerization. Therefore standard PMMA POF with residual monomer contents of a few percent, will probably show little or no photosensitivity due to photo-polymerization. In that work, FBG are written in a MMA-EMA-BzMA-core fiber using 325 nm HeCd laser light.

The main problems with photo-polymerization are longterm stability and inhomogeneity of the resulting polymer. Excess monomer units are extremely detrimental to production process of POF. In fact, manufacturers do everything possible to drive the polymerization reaction to completion [3]. If there are monomer units left in the core, then they will, as a function of ambient temperature, polymerize over time and most probably create bubbles upon polymerization, which in addition is an exothermic process. Bubbles act as scattering centers, which would attenuate the signal in the fiber. Apart from these problems the need for an expensive custom built POF makes this mechanism less attractive to be exploited for photoinduced structures.

3.3.3 Photo-cross-linking

Polymer chains can be cross-linked and the density of the material therefore increased. A prerequisite for such a process is to have a functional side chain which can be activated to

---

[2]Methyl methacrylate (MMA), Ethyl methacrylate (EMA), Benzyl methacrylate (BzMA)

[3]Private conversation with C.D. Breckon from Paradigm Optics Inc., Vancouver, Washington State, USA

induce the cross-linking process. A way of doing this is to oxidize PMMA prior to irradiation. The oxidation leads to peroxide groups in the main chain which serve as cross-linking seeds. These can be activated by irradiation leading to a densification. Already 1970 Tomlinson et al. [19] showed in their work on peroxidized PMMA, that irradiation with 325 nm and 365 nm UV light leads to a refractive index increase of up to 3×10^{-3}. For 488 nm irradiation no photosensitivity was observed with pre-oxydized polymer. This is probably due to too low photon energies to activate the cross-linking seeds. In the view of applications to POFs, this technique has major drawbacks. The oxidation is confined to regions close to the surface and the peroxide groups are very reactive, leading to a low long term stability.

3.3.4   Photo-isomerization

Isomers are molecules that have the same chemical formula but different geometrical arrangement of the atoms within the molecules and that may have different physical and/or chemical properties. The change between such isomer states is called isomerization. Most common are trans-cis isomers (Figure 3.2). If polymers are doped with isomers that exhibit different refractive indices in their different isomer states and isomerization can be done by irradiation, the polymer will exhibit photosensitivity. One example of such an isomer is trans-4-stilbenemethanol where the irradiation with a wavelength of 325 nm initiates isomerization and lowers the refractive index [5]. In the case of azo compounds the isomerization is thermally reversible [31] which could lead to reliability issues. It is also accompanied with induced birefringence.
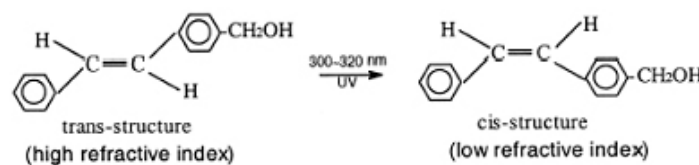
Figure 3.2: *Figure 19 Trans-4-stilbenemethanol isomerization upon UV-irradiation [5]*

The isomerization mechanism was exploited by JianMing Yu et al. [5] to create an FBG in POFs. Isomerization was induced using a laser emitting at 325 nm laser. Depending on the dopant concentration a negative index change between -3×10^{-4} and -9×10^{-4} has been achieved.

Again the disadvantage of this technique is the need of specifically manufactured fibers containing dopants which increases the fiber costs.

3.3.5   Femtosecond laser induced photosensitivity

If a fs-laser is focused into PMMA, the intensity at the focus can be sufficiently high for absorption to occur via multiphoton ionization. Above a material-dependant threshold, permanent structural changes are induced. Work on irradiation of PMMA materials using femtosecond lasers was already done by several groups. Refractive index gratings where written into bulk doped PMMA [32, 33] and in block co-polymers of MMA/EMA [34], relief gratings in bulk undoped PMMA [35] and waveguides in commercially available PMMA [6]. Using a range of femtosecond intensities, gratings were written into different undoped PMMA slabs [36] reaching a maximum refractive index modification of $5 \pm 0.5 \times 10^{-4}$. The experimental threshold fluence was at ~ 30 mJ/cm^{-2}, while above a fluence of ~ 0.8 J/cm^{-2} damage and filament formation takes place. Femtosecond laser irradiation of single mode polymer optical fibers was reported by Baum et al. [37] however the written structure were only investigated with microscope and side diffraction technique.

Different photosensitivity mechanisms were reported leading to different morphologies of material changes. One mechanism is local melting of material in the focal volume after which small density changes occur due to a non-uniform resolidification [38]. Another mechanism is photolysis, explained in section 2.1, which occurs at higher irradiation intensities. The chemical process for fs-laser-induce photolysis in PMMA was investigated by Baum et al. [37] who irradiated PMMA samples with a frequency doubled femtosecond laser. The dominant mechanism was a photolysis process splitting off monomer and dimer fragments. Both cases, densification [6] and photolysis [37], result in a permanent local refractive index modification.

As this method can be employed on pure PMMA it is very attractive to write structures in commercially available POFs. Another important advantage is that the geometry where the refractive index should be altered can be controlled precisely by the spot size of the focusing optics and the movement of this spot relative to the fiber.

3.4   Summary

A comparison of the index changes induced by the different mechanisms can be found in Table 3.1. As commercially available POFs are commonly made from pure PMMA or a simple mixture of two monomers like PS/PMMA, photolysis or fs-laser irradiation are the most promising mechanisms to exploit. An advantage of fs-irradiaton over the photolysis mechanism with UV irradiation is that the change can be induced very locally and the absorption of PMMA @ 400nm is quite low and therefore penetration depth is not a limit.

Mechanism	λ		Material	max $\triangle n$	Sign	Ref.
Photolysis	193 nm 248 nm		pure PMMA	1×10^{-2}	Positive	[8]
	800 nm, fs, 1 kHz		pure PMMA	5×10^{-4}	Positive	[36]
	800 nm, fs, 25 MHz		pure PMMA	2×10^{-4}	Negative	[6]
	387 nm, fs, 1 kHz		pure PMMA	4×10^{-3}	Positive	[39]
Photo-polymerization	325 nm		PMMA core doped with BzMA	2×10^{-3}	Positive	[28]
Poto crosslinking	325 nm 365 nm		pre oxidized PMMA	3×10^{-3}	Positive	[19]
Photo-isomerization	325 nm		trans-4-stilbenemethanol doped MMA-EMA-BzMA	9×10^{-4}	Negative	[5]

Table 3.1: *Comparison of refractive index changes for the different photo-processes.*

Bibliography

[1] D. P. Hand and P. St. J. Russell. Photoinduced refractive-index changes in germanosilicate fibers. *Optics Letters*, 15(2):102–104, 1990.

[2] B. Poumellec, P. Guenot, I. Riant, P. Sansonetti, P. Niay, P. Bernage, and J. F. Bayon. UV induced densifitcation during Bragg grating inscription in Ge:SiO2 preforms. *Opctical Materials*, 4:441–449, 1995.

[3] H. G. Limberger, P. Y. Fonjallaz, and R. P. Salathé. Spectral Characterisation of Photoinduced High Efficient Bragg Gratings in Standard Telecommunication Fibres. *Electronics Letters*, 29(1):47–49, 1993.

[4] P. J. Lemaire, R. M. Atkins, V. Mizrahi, and Reed W. A. High Pressure H_2 Loading as a Technique for Achieving Ultrahigh UV Photosensitivity and Thermal Sensitivity in GeO_2 Doped Optical Fibers. *Electronics Letters*, 29(13):1191–1193, 1993.

[5] JianMing Yu, XiaoMing Tao, and HwaYaw Tam. Trans-4-stilbenemethanol-doped photosensitive polymer fibers and gratings. *Optics Letters*, 29(2):156–158, 2004.

[6] Arnaud Zoubir, Cedric Lopez, Martin Richardson, and Kathleen Richardson. Femtosecond laser fabrication of tubular waveguides in poly(methyl methacrylate). *Optics Letters*, 29(16):1840–1842, 2004.

[7] Thomas Lippert and J. Thomas Dickinson. Chemical and Spectroscopic Aspects of Polymer Ablation: Special Features and Novel Directions. *Chemical Reviews*, 103:453–485, 2003.

[8] C. Wochnowski, S. Metev, and G. Sepold. UV-laser-assisted modification of the optical properties of polymethylmethacrylate. *Applied Surface Science*, 154-155:706–711, 1999.

[9] R. Srinivasan, Emile Sutcliffe, and Bodil Braren. Ablation and etching of polymethylmethacrylate by very short (160 fs) ultraviolet (308 nm) laser pulses. *Applied Physics Letters*, 51(16):1285–1287, 1987.

[10] R. Srinivasan and B. Braren. Ultraviolet Laser Ablation and Etching of Polymethyl Methacrylate Sensitized with an Organic Dopant. *Applied Physics A*, 45:289–292, 1988.

[11] R. Srinivasan. Ablation of polymethyl methacrylate films by pulsed (ns) ultraviolet and infrared (9.17um) lasers: A comparative study by ultrafast imaging. *Journal of Applied Physics*, 73(6):2743–2750, 1993. Ablation of polymethyl methacrylate films by pulsed (ns) ultraviolet and infrared (9.17um) lasers: A comparative study by ultrafast imaging.

[12] Makoto Tsunekawa, Saoru Nishio, and Hiroyasu Sato. Laser ablation of polymethylmetacry-late and polystyrene at 308nm: Demonstration of thermal and photothermal mechanisms by a time-of-flight mass spectroscopic study. *Journal of Applied Physics*, 76(9):5598–5600, 1994.

[13] S. I. Bozhevolnyi and I. V. Potemkin. Dynamics of ablation of polymethyl methacrylate films by near ultraviolet light of an Ar+ laser. *Journal of Physics D: Applied Physics*, 27:19–24, 1994.

[14] N. Bityurin, S. Muraviov, A. Alexandrov, and A. Malyshev. UV laser modifications and etching of polymer films (PMMA) below the ablation threshold. *Applied Surface Science*, 109/110:270–274, 1997.

[15] Hiroshi Masuhara, Hiroyuki Hiraoka, and Kazunami Domen. Dopant-Induced Ablation of Poly(methyl methacrylate) by a 308-nm Excimer Laser. *Macromolecules*, 20:450–452, 1986.

[16] T. Efthimiopoulos, Ch. Kiagias, G. Heliotis, and E. Helidonis. Evidence of volume bubble creation during laser ablation of PMMA organic polymer. *Canadian Journal of Physics*, 78:509–519, 2000.

[17] Takeshi Kada, Takeyoshi Hiramatsu, Kenji Ogino, Chuang Xin Liang, Hideaki Machida, Koichi Kiso, and Seizo Miyata. Fabrication of Refractive Index Profiles in Poly (Methyl Methacrylate) using Ultraviolet Rays Irradiation. *Japanese Journal of Applied Physiscs*, 41:876–880, 2002.

[18] M. J. Bowden, E. A. Chandross, and I. P. Kaminow. Mechanism of the Photoinduced Refractive Index Increase in Polymethyl Methacrylate. *Applied Optics*, 13(1):112–117, 1974.

[19] W. J. Tomlinson, I. P. Kaminow, E. A. Chandross, R. L. Fork, and W. T. Silfvast. Photoinduced Refractive Index Increase in Poly(methylmethacrylate) and its Applications. *Applied Physics Letters*, 16(12):486–489, 1970.

[20] Christopher G. Robertson and Garth L. Wilkes. Refractive index: a probe for monitoring volume relaxation during physical aging of glassy polymers. *Polymer*, 39(11):2129–2133, 1998.

[21] M. Kopietz, M. D. Lechner, D. G. Steinmeier, J. Marotz, H. Franke, and E. Krätzig. Light-induced refractive index changes in polymethyl-methacrylate (PMMA) blocks. *Polymer Photochemistry*, 5(1-6):109–119, 1984.

[22] J. O. Choi, J. A. Moore, J. C. Corelli, J. P. Silverman, and H. Bakhru. Degradation of poly(methylmethacrylate) by deep ultraviolet, x-ray, electron beam, and proton beam irradiations. *Journal of Vacuum Science Technology B*, 6(6):2286–2289, 1988.

[23] R. C. Estler and N. S. Nogar. Mass spectroscopic identification of wavelength dependent UV laser photoablation fragments from polymethylmethacrylate. *Applied Physics Letters*, 49(18):1175–1177, 1986.

[24] T. Lippert. *Polymers and Light.* Springer, 2004.

[25] N. Lekishvili, L. Nadareishvili, G. Zaikov, and L. Khananashvili. *Polymers and Polymeric Materials for Fiber and Gradient Optics.* New concepts in polymer science. VSP, 2002.

[26] T. Lippert, R. L. Webb, S. C. Langford, and J. T. Dickinson. Dopant induced ablation of poly(methyl metacrylate) at 308 nm. *Journal of Applied Physics*, 85(3):1838–1847, 1999.

[27] Z. Xiong, G. D. Peng, B. Wu, and P. L. Chu. Highly Tunable Bragg Gratings in Single-Mode Polymer Optical Fibers. *IEEE Photonics Technology Letters*, 11(3):352–354, 1999.

[28] H. Y. Liu, H. B. Liu, G. D. Peng, and P. L. Chu. Observation of type I and type II gratings behaviour in polymer optical fiber. *Optics Communications*, 220:337–343, 2003.

[29] G. D. Peng, Z. Xiong, and P. L. Chu. Photosensitivity and Gratings in Dye-Doped Polymer Optical Fibers. *Optical Fiber Technology*, 5(2):242–251, 1999.

[30] K. Kalli, H. L. Dobb, D. J. Webb, K. Carroll, C. Themistos, M. Komodromos, G.D. Peng, Q. Fang, and I.W. Boyd. Development of an electrically tuneable Bragg grating filter in polymer optical fibre operating at 1.55 μm. *Measurement Science and Technology*, 18:3155–3164, 2007.

[31] James Guillet. *Polymer Photophysics and Photochemistry.* Cambridge University Press, 1987.

[32] J. Si, J. Qiu, J. Zhai, Y. Shen, and K. Hirao. Photoinduced permanent gratings inside bulk azodye-doped polymers by the coherent field of a femtosecond laser. *Applied Physics Letters*, 80:359–361, 2002.

[33] J. Zhai, Z. Q. Shen, J. Si, J. Qiu, and K. Hirao. The fabrication of permanent holographic gratings in bulk polymer medium by a femtosecond laser. *Journal of Physics D: Applied Physics*, 24:3466–3469, 2001.

[34] Shigeru Katayama, Mika Horiike, Kazyuki Hirao, and Naoto Tsutsumi. Diffraction Measurement of Grating Structure Induced by Irradiation of Femtosecond Laser Pulse in Acrylate Block Copolymers. *Japanese Journal of Applied Physiscs*, 41(4A):2155–2162, 2002.

[35] Yan Li, Kazuhiro Yamada, Tomohiko Ishizuka, Wataru Watanabe, Kazuyoshi Itoh, and Zhongxiang Zhou. Single femtosecond pulse holography using polymethyl methacrylate. *Optics Express*, 10(21):1173–1178, 2002.

[36] P. J. Scully, D. Jones, and D. A. Jaroszynski. Femtosecond laser irradiation of polymethyl-methacrylate for refractive index gratings. *Journal of Optics A: Pure and Applied Optics*, 5:S92–S96, 2003.

[37] Alexandra Baum, Patricia J. Scully, Maria Basanta, C. L. Paul Thomas, Peter R. Fielden, and Nicholas J. Goddard. Photochemistry of refractive index structures in poly(methyl methacrylate) by femtosecond laser irradiation. *Optics Letters*, 32(2):190, 2007.

[38] Chris B. Schaffer. Interaction of Femtosecond Laser Pulses with Transparent Materials, 2001. Interaction of Femtosecond Laser Pulses with Transparent Materials.

[39] A. Baum, W. Perrie, P. J. Scully, M. Basanta, C. L. P. Thomas, N. J. Goddard, P. R. Fielden, and P. R. Chalker. Refractive Index Structures in Poly(methyl methacrylate) and Polymer Optical Fibre by Femtosecond Laser Irradiation. In *The 18th International Optical Fiber Sensors Conference, Cancun, Mexico*, 2006.

Chapter 4

FBG fabrication in POF

4.1 Introduction

This chapter will present the results of the FBG writing experiments in polymer optical fibers. First the basic FBG theory is explained followed by a review of the history of fiber Bragg gratings in polymer optical fibers. Writing of FBG in POF was the main goal of this work and the setup and procedure used to achieve it will be explained. A detailed presentation and discussion of the written FBG will be given, showing the evolution and particularities of refractive index changes in a PMMA/PS core fiber.

4.2 Fiber Bragg gratings (FBG)

Distributed Bragg reflectors are used as high quality reflectors in waveguides. A distributed Bragg reflector is a multilayered structure composed of a material with alternating refractive index for each layer. At each layer interface the guided wave is partially reflected. The optical thickness of the layers define the wavelength which will experience constructive interference of its many reflections. At that particular wavelength the distributed Bragg reflector acts as a mirror. A special type of a distributed Bragg reflector constructed in an optical fiber is a fiber Bragg grating. If a broadband light spectrum is coupled into a fiber containing an FBG, a portion of the incident spectrum is reflected according to the specifications of the FBG, whereas the other part is transmitted. As the effective index of a waveguide and the periodicity of the refractive index structure are a function of temperature, humidity and strain, the FBG can be used as a sensing element.

4.2.1 History

Hill et al. [1] discovered the photosensitivity of germano-silicate optical fibers in 1978. Two counter propagating waves of a 488 nm laser created an interference pattern in the fiber which induced the fiber Bragg grating structure. The side writing technique further facilitated the

production of FBGs and allowed the creation of FBGs at telecommunication wavelengths. It is often credited to Meltz et al. [2] but was already used in the early 70s by Laming et al. [3] and Moran et al. [4] for holographic grating recording. Ever since FBG in germano-silicate fibers have been used extensively as filters and sensors. Fiber Bragg gratings in POF on the contrary, have been presented for the first time in 1999 [5] and though much research effort has gone into this field, have not reached the maturity to be used in commercial applications yet.

4.2.2   FBG writing and spectra

The most common technique to manufacture FBG is the side writing technique. In this technique the fiber is irradiated transversally from the side with UV light and a phase mask or an interference pattern of two beams is used to create the intensity fringes.
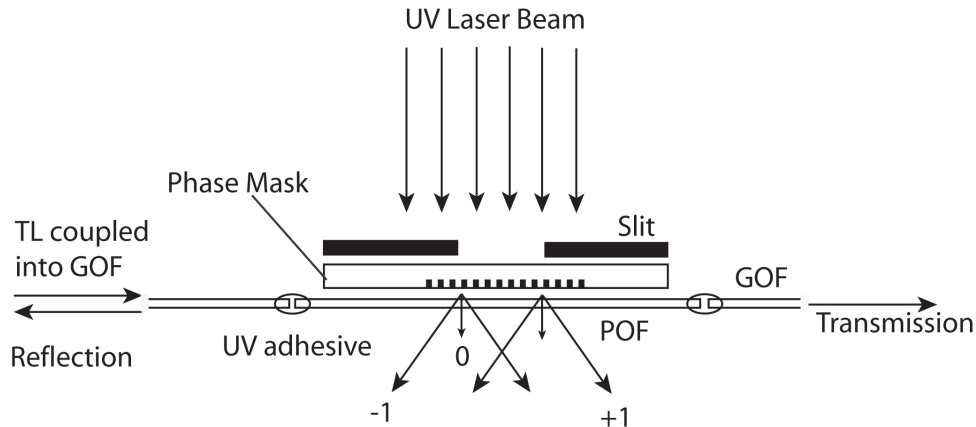
Figure 4.1: *UV-side writing setup. TL: Tunable laser, GOF: Glass optical fiber*

Figure 4.1 shows a UV side-writing setup used for FBG inscription. The basic concept is similar to a setup used to write FBG in silica fibers. Due to the high attenuation levels of the POF at 1550 nm, the POF length has to be kept short. A standard silica fiber is butt-coupled to the polymer fiber. Gluing the two fiber ends together with UV-adhesive allows stable coupling. A slit is used to set the grating length. The phase mask is manufactured to maximize the +1 and -1 diffraction orders and minimize the 0th diffraction order to increase the fringe visibility. The interference fringes than create a permanent refractive index change, the magnitude of which is depending on the photosensitivity of the optical fiber material. The fiber Bragg grating will typically have a sinusoidal refractive index variation Δn_{ac} over a defined length L at a constant period Λ as illustrated in Figure 4.2.2 and it can be represented by Equation 4.1.

$$\Delta n_{core}(z) = \Delta n_{dc}(z) + \Delta n_{ac}(z) cos \left(\frac{2\pi}{\Lambda} z \right)$$

(4.1)
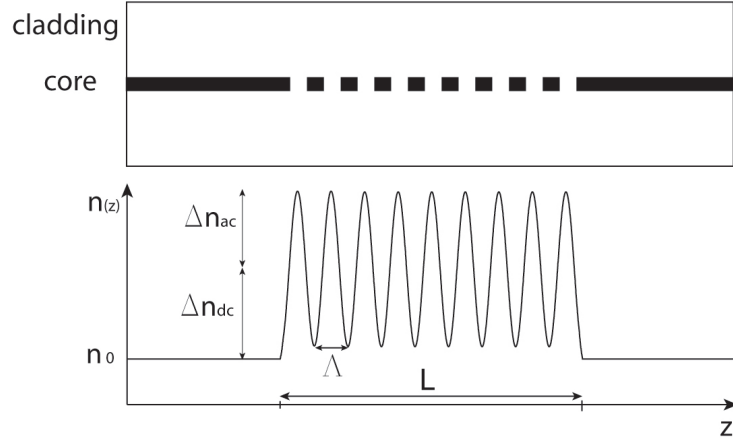
Figure 4.2: *Refractive index modulation in a fiber*

Δn_{core} is the core index change, Δn_{dc} is the average grating index, Δn_{ac} is the grating index amplitude. The forward propagating wave is partially reflected at each index layer interfaces and shows constructive interference at the so called Bragg wavelength which is defined as,

$$\lambda_B = 2n_{eff}\Lambda \tag{4.2}$$

where n_{eff} is the effective refractive index of the core mode which can be approximated by [6]

$$n_{eff}^2 = n_{clad}^2 + \left(\frac{\lambda}{2\pi r_{core}}\right)^2 (1.1428V - 0.996)^2 \tag{4.3}$$

r_{core} being the core radius and V being the V-number as defined in Section 2.2 Equation 2.3.

The coupled mode theory describes the spectral response of a fiber Bragg grating [7,8]. For a grating with an index structure as given in Eq. 4.1 where Δn_{ac} and Δn_{dc} is uniform, the reflectivity can be given by [8]

$$R_{max} = tanh^2(\kappa L) \tag{4.4}$$

where the coupling coefficient κ describes how the forward propagating core mode is coupled to

the reflected, counter propagating mode and is given by [8]

$$\kappa = \frac{\pi \Delta n_{ac} \eta}{\lambda} \tag{4.5}$$

for a power confinement η of the core mode within the core [6].

The comparison of the transmission and reflection spectra of a glass fiber FBG is shown in Figure 4.3. The reflectivity of the reflection spectrum has been normalized with respect to the reflectivity of the transmission spectrum. This is necessary as coupling losses and the 3dB loss from the 50/50 coupler attenuate the reflection peak in the reflection arm.
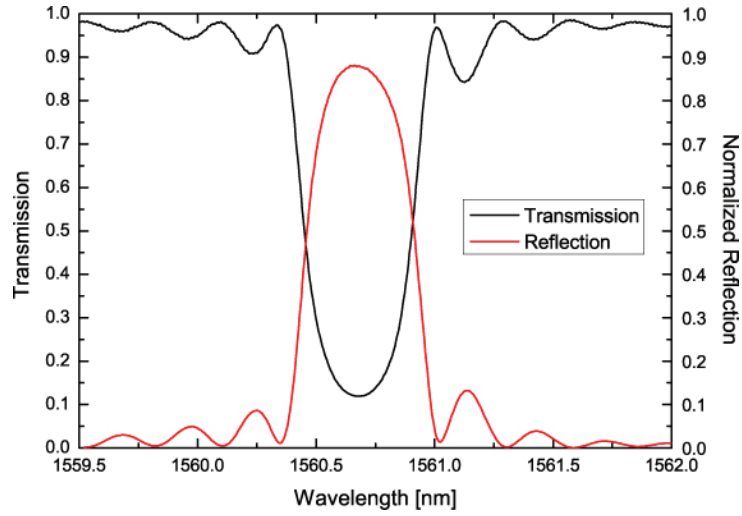
Figure 4.3: *Measured transmission and reflection of a FBG written into a high germanium doped fiber (Ge 18%). L_g=3 mm, Δn_{ac}= 4.5 × 10^{-4}, Λ_{PM}=1075.86 nm, Intensity = 120 mW/cm^2. Taken from the PhD of Y. Tissot [9]*

The induced average grating index changes Δn_{dc} and grating index amplitude Δn_{ac} can be calculated from the measured spectra using the following relations [10],

$$\Delta n_{dc} = \frac{n_{eff} \Delta \lambda_{Bragg}}{\eta \lambda_{Bragg}} \tag{4.6}$$

$$\Delta n_{ac} = \frac{\lambda_{Bragg}}{\eta \pi L} atanh \left(\sqrt{R_{max}} \right) \tag{4.7}$$

The theoretical grating bandwidth $\Delta \lambda_{BW}$ which is defined as the bandwidth between the first zeros on either side of the transmission peak, can be calculated using

$$\Delta \lambda_{BW} = \lambda_B \frac{\Delta n_{ac}}{n_{eff}} \sqrt{\eta^2 + (\frac{\lambda_B}{\Delta n_{ac} L})^2} \tag{4.8}$$

4.3   FBG in POF

4.3.1   History

In recent years research aimed at writing refractive index structures in polymer optical fibers. In the process different routes were taken, such as ablation induced structures [11] or surface refractive index modification accompanied with ablation [12, 13]. First FBGs were written in POF by Peng [5] and Xiong [14]. The single mode POF used by Xiong was produced using lower initiator and chain transfer agent concentrations which would suggest that the monomer content is higher than normal [15]. The photosensitivity mechanism exploited in these first POFBG was not explained but might be due to this residual monomer content. The side writing setup which was used consisted of a modified Sagnac interferometer [16, 17]. Index changes of up to 10^{-3} [18] were achieved without apparent material damage. At prolonged irradiation times and index changes of up to 2×10^{-3} material damage at the core cladding interface could be observed.

JianMing [19] demonstrated POFBG in a fiber with a MMA-EMA-BzMA core doped with trans-4-stilbenemethanol. The fiber was irradiated with 325 nm laser light using a phase mask setup. A maximum index change of -9×10^{-3} was achieved. Xingsheng [20] realized birefringent gratings in azobenzene doped PMMA fibers written with 532 nm laser light.

Photosensitivity has also been demonstrated on CYTOP [21, 22]. However the written gratings were written in MM fibers after removing the cladding and were only characterized by side irradiation with He-Ne laser, measuring the diffraction pattern and efficiency. Photosensitivity was investigated in CYTOP [23] with CW laser at wavelengths of 457, 488 and 514 nm. Refractive index gratings were written with a diffraction efficiency of up to 1.6% and a corresponding index modulation of 3×10^{-4}. These were however only investigations on the photosensitivity, POFBG in CYTOP fibers were not presented.

Scully et al. [24] showed that grating structures can be written into pure PMMA using a femtosecond laser at 800 nm. The structures could be written at a depth of 0.5 mm and a maximum refractive index modification of $5 \pm 0.5 \times 10^{-4}$ which has a positive sign was achieved. The threshold femtosecond fluence was reported to be ≈ 0.03 J/cm^2 for refractive index modification. At fluences higher than ≈ 0.8 J/cm^2 material damage was observed. Baum et al. [25] investigated refractive index structures in PMMA induced by frequency doubled femtosecond laser irradiation at 387 nm. The photoinduced material change was reported to lead to monomer and dimer creation which could lead to an unzipping process. FBG written using femtosecond laser irradiation were however not published up to date.

4.3.2 POFBG fabrication

This work was focused on writing Fiber Bragg gratings in POF containing no dopants using a 308 nm Excimer laser [26]. The polymer fiber used was manufactured by Paradigm Optics, the specifications are presented in Table 2.1. The fiber has a fully polymerized core made of a co-polymer of 22 wt% PS and 78 wt% PMMA which is not sensitized. The cladding is pure PMMA.

Irradiation setup

Figure 4.4 shows the irradiation setup used to write fiber Bragg gratings in the POF. The XeCl Excimer laser emitting at 308 nm (Lambda Physik LPX 315) was operated at frequencies of 2 - 10 Hz, it has a pulse width of 20 ns. The laser beam did not need to be focused in order to reach a fluence per pulse of $F = 100$ mJ/cm^2. For higher fluences a cylindrical lens was used (f=208 mm). Typical fluences were between 70 and 120 mJ/cm^2. A phase mask, diffracting the laser light into the +1 and -1 order, was employed. The phase mask pitch is $\Lambda_{PM} = 1040$ nm and it was designed for use with 308 nm irradiation (0th order diffraction $< 4\%$). This phase mask was placed on top of and in direct contact with the POF. A slit on top of the phase mask was used to define the grating length. Gratings of 5, 7 and 9 mm length were written. Irradiation times were between 30 minutes and one hour, depending on the fluence per pulse and the frequency.
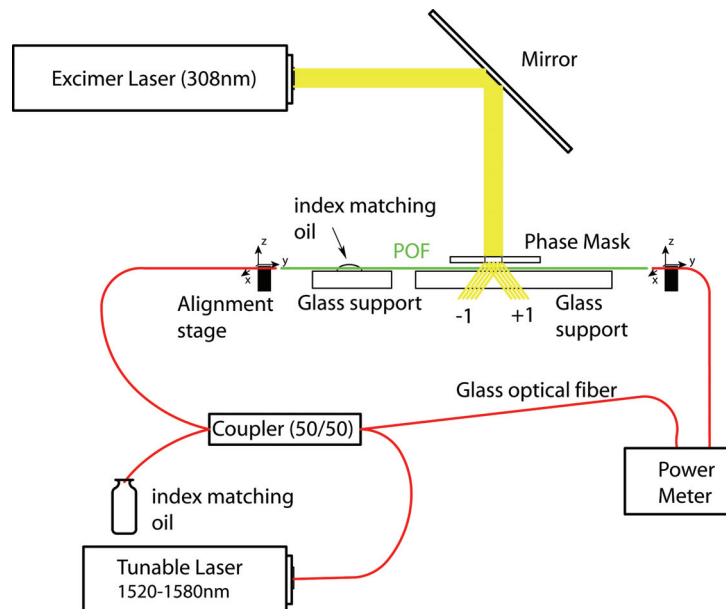
Figure 4.4: *FBG writing setup. Transmission and reflection spectra can be recorded simultaneously during writing process.*

Light coupling to the POF

In order to characterize POFBG during and after irradiation, stable light coupling has to be
ensured throughout the whole process. Figure 4.4 shows the irradiation setup including the
necessary coupling components. Stable coupling can only be achieved by using glass support
slides on which the POF is being fixed. Two 3-axes alignment stages are used to align the glass
to polymer fiber ends. A single mode standard glass fiber (Corning SMF-28e) was aligned to
the POF. The near field of the polymer fiber end was imaged onto an infrared camera (Electro
physics, MicroViewer Serie 7290) using a 40× microscope objective.
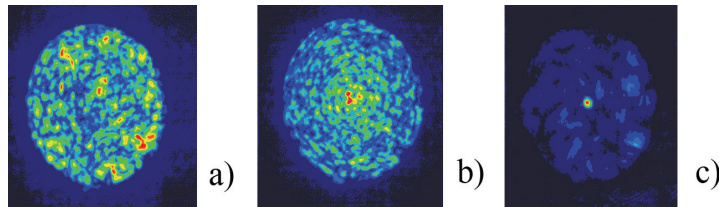
Figure 4.5: *a) coupling to the POF, coarse alignment, b) coupling to the core mode, c) coupling to the
core mode and stripping of the cladding modes*

By monitoring the near field, it could be verified that the light is coupled to the core mode,
shown in Figure 4.5. The near field image on the left (a) is taken while coupling to the POF
on the far end with a coarse alignment. Aligning the glass and the polymer fiber accurately,
coupling to the core mode can be achieved visible in the near field, depicted in the center (b) of
Figure 4.5. The use of index matching gel is necessary to strip the cladding modes which arise
due to two reasons, 1) due to small misalignments and 2) due to a large mode-field mismatches
between the silica and the polymer fiber. The near field image on the right (c) of Fig. 4.5 shows
a typical coupling result where the cladding modes were stripped. (Calculations of the loss due
to mode-field mismatch can be found in Appendix A. Typical glass fiber to POF coupling losses
were between 3 and 10 dB). The butt-coupling connection is subsequently fixed with UV-curable
adhesive[1] which enables stable coupling during UV irradiation and thereafter. The curing takes
approximately 5 minutes.

Using this glass fiber to polymer fiber coupling scheme and a 50/50 coupler, the transmission
and the reflection spectra were simultaneously measured during the irradiation process using
a tunable laser (Photonetics Tunics 3642) and a power meter (Anritsu ML910B). After the
irradiation laser was turned off, the spectra were monitored during several hours in order to
investigate a possible relaxation process.
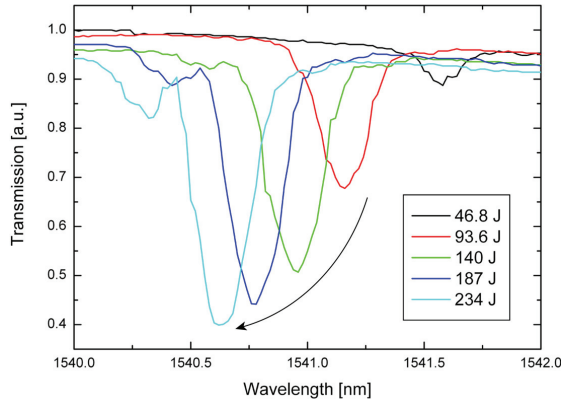
Figure 4.6: *Transmission spectra of a POFBG during the writing process. $L \approx 4.5$ mm, Fluence per pulse $F \approx 75$ mJ/cm^2), $\Lambda_{PM} = 1040$ nm, FBG1*
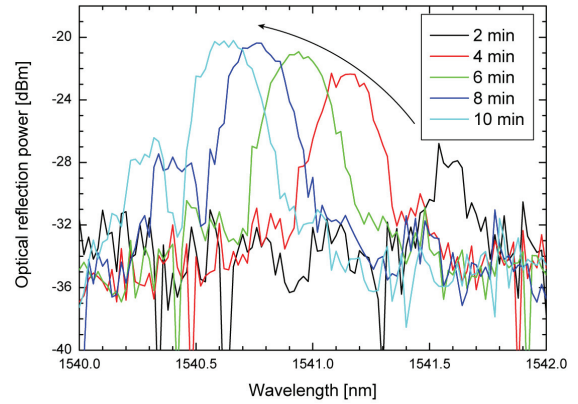
Figure 4.7: *Reflection spectra of the same FBG1 (c.f. Fig. 4.6. The reflectivity is approximately 40% at 234 J total fluence. The irradiation times correspond to the total doses shown in Figure 4.6. FBG1*

Results and Discussion

Figures 4.6 and 4.7 show the transmission and the reflection spectra of a POF Bragg grating during the irradiation process. These spectra show the growth process of the grating during irradiation. The spectrum shifts to shorter wavelength with increasing irradiation. This shift can be explained by three distinct mechanisms. First the Bragg wavelength shifts to lower wavelengths with increasing temperature (contrary to FBGs in glass fibers). This is due to a negative thermo-optic coefficient of the polymer. Second, it shifts due to a reduction of humidity within the fiber. PMMA shows water sorption which is a function of relative humidity. With decreasing water content in the fiber, it contracts changing the grating pitch and the water content changes the mean polarizability, leading to a Bragg peak shift (Detailed description in Chapter 5). And the third influence on the Bragg wavelength is the negative mean refractive index change ($< \Delta n_{eff} >= \eta n_{eff} \Delta \lambda_B / \lambda_B$) or Δn_{dc}. Comparison with Equation 4.6 shows that a negative Δn_{dc} shifts the Bragg wavelength to lower values. The power confinement was estimated to be $\eta = 70\%$ in the core. Only the third of the three mechanisms is permanent. The reflectivity increases with increasing total dose due to an increase in Δn_{ac}. The maximum reflectivity of this grating is 57% (not shown in the Figures) which corresponds to a refractive index change of $\Delta n_{ac} = 1.5 \times 10^{-4}$. With increasing irradiation the double peak structure gets more pronounced in this case. The maximum reflectivity achieved with a $\approx 5 - mm - long$ FBG was 70% corresponding to an index change of $\Delta n_{ac} \approx 1.7 \times 10^{-4}$. A $\approx 7 - mm - long$

---

[1]Norland Optical Adhesive NOA 78

grating showed maximum reflectivity of up to 87%, also corresponding to an index change of $\Delta n_{ac} \approx 1.7 \times 10^{-4}$.

The transmission and reflection spectra of a polymer fiber FBG are shown in Figure 4.8. The reflectivity of the reflection spectrum has been normalized with respect to the reflectivity of the transmission spectrum. This is necessary as high coupling losses and the 3dB loss from the 50/50 coupler attenuate the reflection peak in the reflection arm.
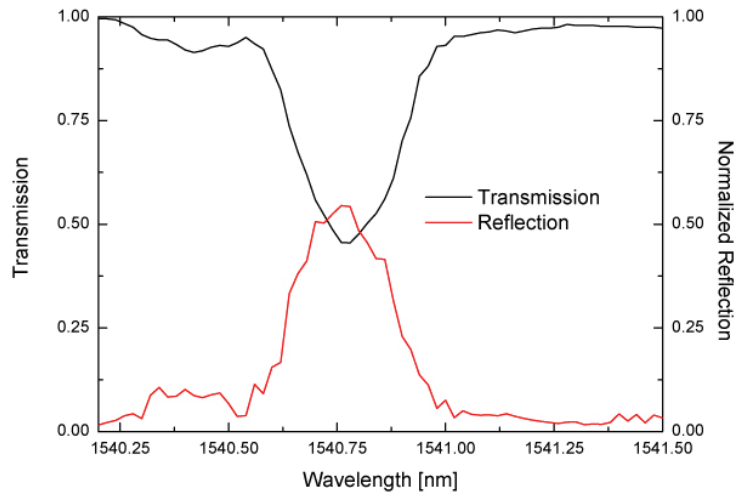
Figure 4.8: *Measured transmission and reflection spectrum of a FBG written in a single mode POF from Paradigm Optics. (Fluence $\approx$ 75 mJ/cm^2, R_{max}=68%, L$\approx$5 mm)*

The POFBG spectrum shown in Figure 4.8 has a $\Delta n_{ac} = 1.4 \times 10^{-4}$. The mean index change Δn_{dc} could not be estimated as the Bragg peak shift during irradiation is in this case a super-position of heating, humidity change and Δn_{dc}. The bandwidth $\Delta\lambda_{BW}$ as defined in Equation 4.8, calculated for the grating shown in Figure 4.8 is 337 pm, compared to a measured value of 418 pm. An index chirp [10] of the FBG can explain this difference which might be introduced by a non uniform laser intensity distribution or a non constant photosensitivity along the fiber which will be addressed in Section 4.4.2. The asymmetry of the POFBG spectrum is probably due to the same effect.

4.3.3 Induced refractive index amplitude change

During the writing process of an FBG different mechanisms influence the growth of the FBG. The refractive index amplitude increases with increasing irradiation dose and thus the reflectivity increases. The irradiation laser leads to heating within the fiber which shifts the Bragg wavelength reversibly. Heating is dependent on the laser frequency used. At the same time, the mean refractive index is changed which leads to a permanent Bragg wavelength shift during

the irradiation. In this section, the change of refractive index amplitude is presented. Mean refractive index change due to 308 nm irradiation will be presented in the following section.

These reflectivity evolution curves for the written gratings can be used to compare the refractive index change induced by the different irradiation conditions. The Bragg grating reflectivity is used to calculated the amplitude index change Δn_{ac} (Eq. 4.7).

Irradiation of untreated POF from the spool showed significant variation in the evolution of the induced index change and in the success of writing FBG. For this reason the initial conditions of the POF at the start of irradiation were changed in a controlled way. FBG written in untreated POF were compared to FBG written in POF that were dried, stored in water and hydrogen loaded prior to FBG inscription. As was later discovered, and which is explained in detail in Section 5, the water content within the fiber changes with ambient conditions and is of influence on the FBG and writing process.

Experiment

FBG were written following the procedure explained in a preceding section. Three different preparation methods were used for the POF to be irradiated. The first preparation method was to dry the fiber at 60°C during at least 12 hours. After the fiber is removed from the oven, handling of the fiber took approximately 10-20 minutes until irradiation started. The second method was to store the fiber submerged in water for at least 24 hours prior to irradiation. The time after removal from the water and irradiation is again approximately 10-20 minutes. Comparable to silica fibers, POF were hydrogen loaded at 160 bar pressure and ambient temperature during 10 days as third conditioning method. Some of the specimen were used directly after removal from the H_2-loading reactor. Pieces of the hydrogen loaded fiber that were not used immediately were submerged in liquid nitrogen until they were used. The results of POFBG written in fibers prepared in such ways were compared to POFBG written in the untreated fiber, stored at ambient humidity and temperature conditions on the fiber spool. The POFBG were written using continuous irradiation for the given irradiation times and frequencies. Irradiation details of the POFBG which will be presented in the following subsection can be found in Appendix G.

POF dried prior to FBG writing

Figure 4.9 shows the evolution of the refractive index change Δn_{ac} for fibers that were dried prior to irradiation. The irradiation conditions for the presented FBG are given in Table 4.1.

The curves show the increase of refractive index amplitude of FBGs with time, during irradiation. For irradiation fluences of $\approx 90 - 100$ mJ/cm^2, the refractive index change is faster than for fluences of ≈ 70 mJ/cm^2. For certain FBG a saturation limit was reached at which the refractive
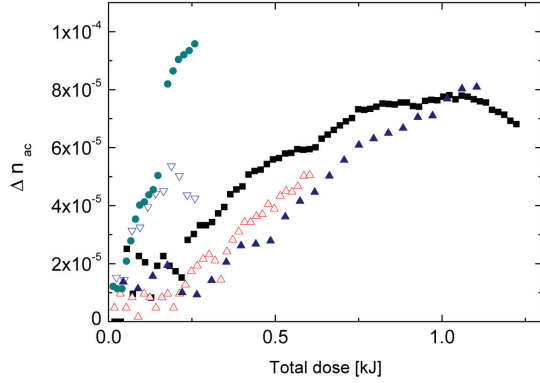
Figure 4.9: Δn_{ac} *evolution during the irradiation for different fibers which were dried previous to FBG writing. Irradiation times:*
● *19 min (FBG9),* ▲ *25 min (FBG8),*
■ *57 min (FBG2),* △ *29 min (FBG3),*
▽ *9 min (FBG19).*
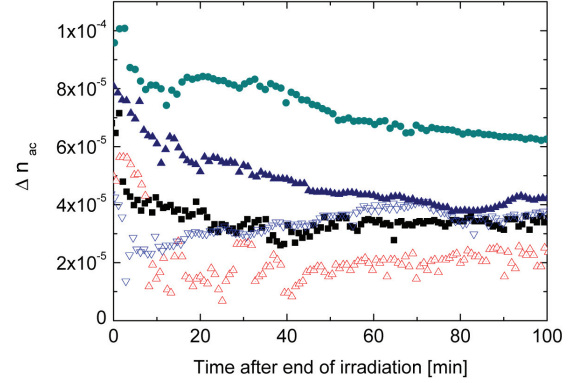
Figure 4.10: Δn_{ac} *evolution after the irradiation for different fibers which were dried previous to FBG writing.*

●	19 min	2 Hz	112 mJ/cm^2	FBG9
▲	25 min	8 Hz	92 mJ/cm^2	FBG8
■	57 min	5 Hz	72 mJ/cm^2	FBG2
△	29 min	5 Hz	70 mJ/cm^2	FBG3
▽	9 min	5 Hz	93 mJ/cm^2	FBG19

Table 4.1: *Irradiation specifications for Figures 4.9 and 4.10*

index amplitude did not change further or even decreased (FBG2 ■). With the exception of FBG8, higher fluence show a faster index change. After the laser is turned off, as shown in Figure 4.10, the refractive index modulation is decreasing again, showing a relaxation process which is evident in almost all written gratings. These curves shown in Figure 4.10 are for dried fibers corresponding to the FBG shown in Figure 4.9. For fiber specimen prepared in the same way and conditions, these Δn_{ac} evolution curves show significant differences. Some FBGs exhibited Δn_{ac} index amplitude increased after the end of irradiation like for example FBG19 (▽) in Figure 4.10. This is comparable to the behavior reported by Liu et al. [27].

As will be shown in Chapter 5, the humidity and the temperature have a large influence on the POF. Due to heating of the fiber and the surrounding support, phase mask and slit, the relative humidity around the fiber decreases and an out diffusion of water from the fiber to the surrounding air takes place. In the case of dried fiber, the fiber starts to absorb water from

the air when removed from the oven. Once the irradiation and therefore heating starts, the humidity equilibrium between the air and the fiber is attained faster than for the fiber stored in ambient conditions or the one removed from the water. This would indicate that FBG writing should be more successful in dried fibers than in the water and untreated fibers which can be seen from Figures 4.9 and 4.15. The maximum water sorption change during irradiation is in the dried experiment probably lower than in the ambient or the water soaked fiber case.

POF stored in water prior to FBG writing

POF that were stored in water prior to irradiation have an increased water content within the fiber. Later experiments showed, that if the fiber is removed from the water, it will lose part of its water content through out diffusion until reaching an equilibrium state with the ambient temperature. This process takes approximately one hour (c.f. Chapter 5). As the irradiation times were generally less than one hour, the water content within the fiber is changing during the whole irradiation process. For the fibers that were stored in water prior to grating inscription the evolution curves of the reflectivity are shown in Figure 4.11. Irradiation conditions for FBG10 and FBG11 are identical. FBG12 was irradiated with slightly lower fluence per pulse and grating growth in two phases can be observed. A quantitative comparison of induced amplitude index change versus total dose shows significant differences even for identical irradiation conditions. After the end of the irradiation (Figure 4.12), the reflectivity drops. For FBG 12 for examples, the reflectivity after irradiation decreases to approximately half its maximum value during irradiation. Measurements of FBG12 after 6 month showed a reflectivity of 68% corresponding to a $\Delta n_{ac} = 8.5 \times 10^{-5}$. Comparing this value with the curve for FBG12 in Figure 4.12, it can be seen that this value corresponds to the maximum measured reflectivity during writing of FBG12.

The apparat large differences between written FBG supports the assumption, that the larger water sorption change of the fiber during the irradiation has a negative effect of grating formation.

FBG in hydrogen loaded POF

The evolution curves for fibers which were hydrogen loaded prior to irradiation are shown in Figure 4.13 and 4.14. Irradiation conditions for FBG15 and FBG16 are identical. FBG17 was irradiated with a slightly higher fluence per pulse. Grating relaxation after the end of the irradiation which are shown in Figure 4.14 exhibit comparable behavior for all gratings. Again measurements 6 month after the irradiation show different final reflectivities compared to the values several minutes or hours after irradiation. A reflectivity of 75% was observed for FBG15 and only 20% for FBG16 6 month after irradiation, even though they were irradiated at exactly identical conditions.
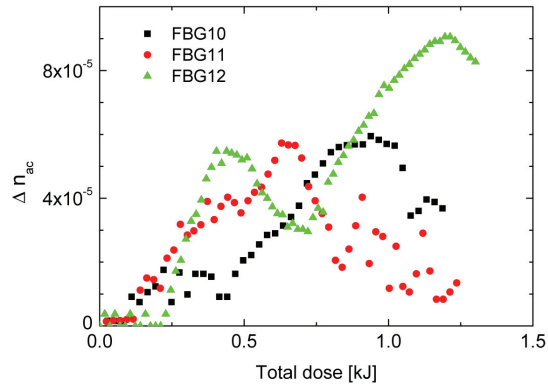
Figure 4.11: Δn_{ac} evolution during writing process for different fibers which were stored in water prior to irradiation.
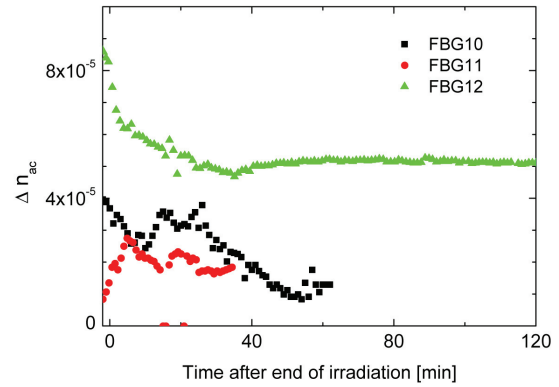
Figure 4.12: Δn_{ac} evolution after the end of irradiation for different fibers which were stored in water prior to irradiation.
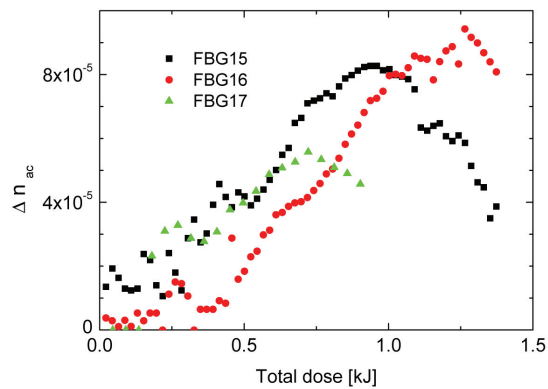
Figure 4.13: Δn_{ac} evolution for different fibers which were hydrogen loaded prior to irradiation.
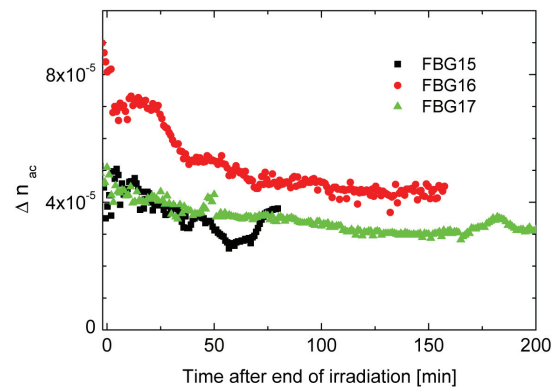
Figure 4.14: Δn_{ac} evolution for different fibers which were hydrogen loaded prior to irradiation.

Hydrogen loading was undertaken to investigate if it has a positive influence on grating growth as is the case for silica fibers. Comparing these results to the Figures 4.9 and 4.15 shows, that the maximum achieved index change is lower than in the case of dried fiber or fiber stored in ambient conditions.

POFBG in untreated POF

Figure 4.15 shows the evolution curves for untreated fibers stored in ambient conditions. The reflectivity of FBG6 is continuously rising with irradiation, whereas FBG7, after an initial reflectivity growths, shows a phase of constant or even declining reflectivity, before it rises again continuously up to a saturation level. Identical irradiation conditions were used for FBG13 and FBG6 as well as for FBG7 and FBG14, only varying the total dose. It is clearly visible that these pairs show little similarities. After the irradiation laser is turned off the refractive index amplitude decreases slowly (Figure 4.16). FBG14 has a maximum reflectivity after 6 month of 75% compared to a maximum reflectivity of 65% during irradiation. The other gratings loose approximately half the reflectivity after 6 month.
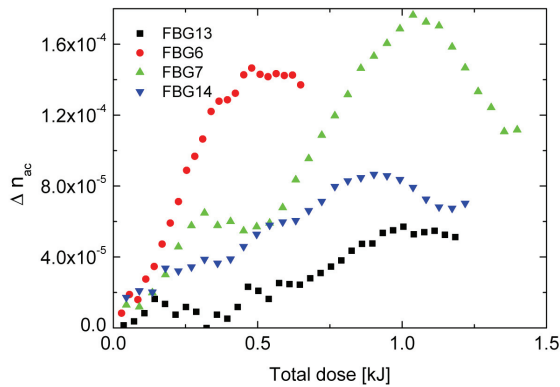
Figure 4.15: Δn_{ac} evolution for different untreated fibers.
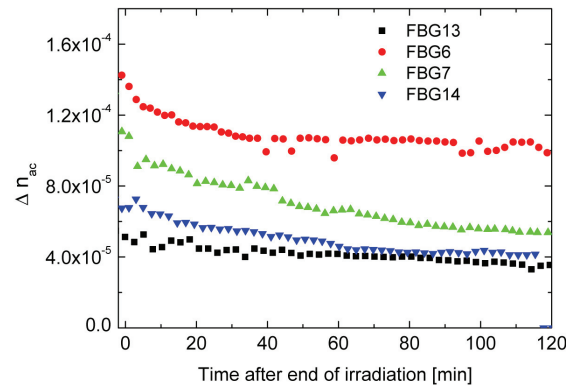
Figure 4.16: Δn_{ac} evolution for different untreated fibers.

Summary and Conclusion

These examples show, that the reproducibility of the irradiation process induced index change is poor. However it can be seen that the induced material alteration gives rise to a time dependent change of the polymer material. Observations of the reflectivity change over up to two weeks after irradiation showed continuing changes. Fibers that were measured after 6 month of irradiation showed stable reflectivities thereafter. This indicates that the induced changes take

several month to reach stability. The evolution of the grating after the writing laser was turned off differ even for fibers exposed under identical irradiation conditions. Results from OLCR (Section 4.4) and birefringence measurements (Section 4.5 will show, that the photosensitivity is a function of fiber position, most probably due to material inhomogeneity of the fiber. This is believed to be of large influence on the photosensitivity observed through FBG writing. A further influence on varying FBG production success could be the changing humidity within the fiber during irradiation. Heating of the setup and the fiber during irradiation leads to a decreased relative humidity in air and a decreased water content within the fiber. For fibers stored in water prior to irradiation, this water content change is larger than for fibers stored in ambient conditions. This is because the difference between the equilibrium water content before irradiation and during irradiation is smaller for the fiber stored in ambient conditions. For dried fibers, this water content change can be even smaller than in the other two cases, depending on the time between removal of a dried fiber from the oven and start of irradiation. In the case of the dried fiber, it will take up water during the irradiation process till it reaches an equilibrium state opposed to the 'wet' and 'ambient' fiber which loose water. Figure 4.9 indicates slightly better reproducibility of FBG writing in dried fibers than for the cases of ambient (Fig. 4.15) and wet (Fig. 4.11) fibers. Within the work conducted, no irradiation parameters for optimum grating writing could be identified. Further work should focus on FBG writing under dry conditions in order to eliminate that parameter form the possible influences on FBG production success. It would enable to ascertain if material inhomogeneity is the major influence on the different FBG reflectivities and reproducibility.

4.3.4   Induced mean refractive index change

Employing Equation 4.6 the mean index change can be calculated from the Bragg peak shift during irradiation. As the Bragg peak position is a function of temperature and humidity (Chapter 5), the irradiation induced temperature and humidity changes have either to be known or the measurement has to allow for elimination of these influences. If a written grating is exposed to uniform irradiation across the whole grating region, the mean index Δn_{dc} can be changed. In order to exclude the humidity influence, the FBG was placed in a controlled, dry environment. The only factor changing the peak wavelength is the temperature and the mean refractive index.

Experiment

A written FBG was irradiated uniformly with 308 nm excimer laser light at a fluence per pulse of $70\,\mathrm{mJ/cm^2}$ and a frequency of 5 Hz. Total irradiation dose was 273 J for this experiment. The FBG was placed in a hermetic chamber (see Section 5.2.2 for details) under dry conditions (at a constant relative humidity of $2.2 \pm 1\%$ RH). The temperature in the chamber was $23.6 \pm 0.2°C$

through out the whole irradiation experiment. The Bragg grating was measured in reflection using a Micron Optics interrogator 125-500 (a tunable laser based interrogation system).

Results

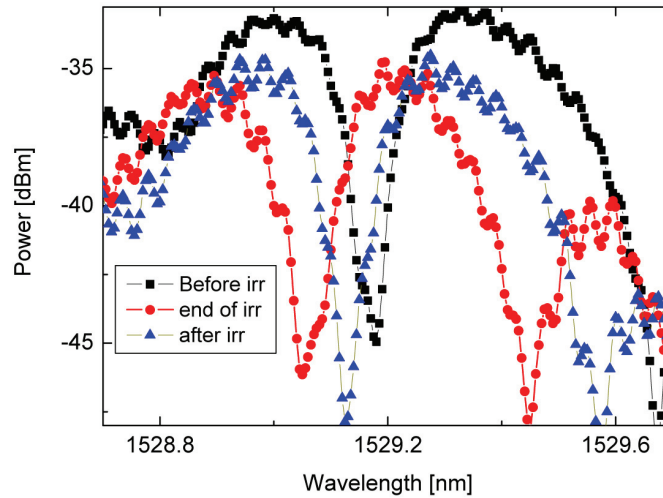Three reflection spectra of FBG4 are shown in Figure 4.17. This grating shows a double reflection

Figure 4.17: *Uniform irradiation of an FBG. 70 mJ, 5 Hz, 2.2 ± 1.2% RH, 23.6 ± 0.2° C. FBG4,* ■ *before irradiation,* ● *end of irradiation,* ▲ *after irradiation.*

peak structure probably due a superposition of two grating structures. Such a superposition could be induced by temperature and water content change in the fiber leading to expansion or contraction of the fiber material during irradiation. The first spectrum (■) shows the grating before irradiation in dry environment. During irradiation, the reflection spectrum shifts to lower wavelengths (●). This shift is due to a temperature increase and a change of mean refractive index. After the irradiation was stopped, the reflection spectrum shifts back to longer wavelengths due to cooling ($\approx -7.5°$C) of the irradiated POF (▲), but the final grating position is still to the left of the initial Bragg position, i.e. at a lower wavelength. The difference between the Bragg position before and after irradiation is $\Delta\lambda_B = -55$ pm. Using Equation 4.6 the corresponding mean index shift Δn_{dc} is - 7.6 $\times 10^{-5}$. This experiment shows that the photosensitivity of PMMA/PS irradiated by 308 nm excimer laser light leads to a negative index change. The reflectivity of the FBG decreases slightly during irradiation. This can be due to increased insertion loss or a change in reflectivity of the grating. After the end of irradiation, the reflectivity stays constant again.

Our result of negative index change is in contrast to the work by Kada et al. [28] on UV induced photolysis. Kada et al. [28] reported that chain scission of PMMA due to UV irradiation at 254

nm leads to a positive index change which they explained by smaller specific volume of polymer chains after ester-group abstraction. However ester-group abstraction accounts only for side chain scission upon irradiation, whereas main chain scission would lead to shorter molecule chains and therefore higher degree of freedom and consequently lower density, i.e. decreased refractive index. In our work, the irradiation of PMMA/PS copolymer at 308 nm is not directly comparable to the irradiation of PMMA at 254 nm, however it shows, that the side chain scission observed by Kada et al. [28] can not explain our results.

Another major difference between the work presented by Kada et al. and the irradiated POF in our work is a difference in birefringence of the irradiated samples. Fibers exhibit large birefringence which is introduced in the production process and undergoes change due to irradiation. Birefringence of the POF will be discussed in a following Section.

4.3.5 Induced insertion loss

The reflectivity of an FBG during the writing process is presented in Figure 4.18. It was irradiated at 8 Hz with a fluence per pulse of 94 mJ/cm^2. The grating length is $\approx$ 9 mm and the maximum reflectivity during irradiation was 96%. The induced index change shows
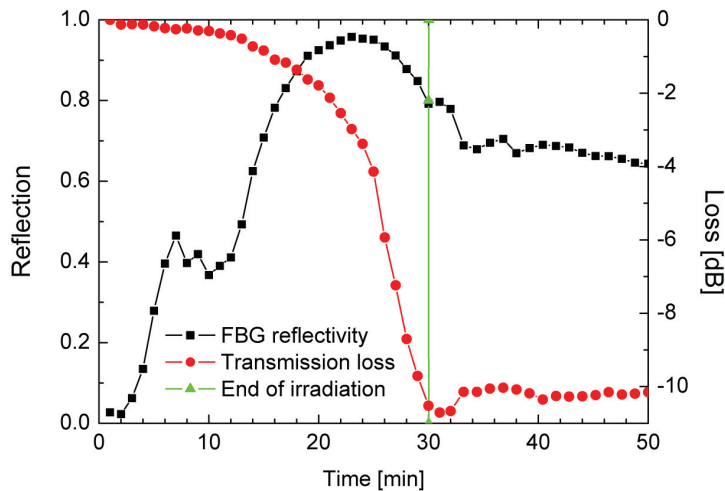
Figure 4.18: *Reflectivity and mean transmission power level during and after irradiation. f=8 Hz, Fluence = 94 mJ/cm^2, irradiation time = 30 min, total dose = 1.35 kJ, FBG7*

a maximum after 25 minutes corresponding to 1.13 kJ/cm^2 total dose. The insertion loss is increasing with irradiation up to a maximum of around 10 dB at the end of irradiation. When the irradiation is stopped, the loss shows a slight relaxation before it reaches a stable value. Fiber loss for the POF of $\approx$ 1 dB/cm was measured at 1550 nm using a cut-back technique. Irradiation induced loss for different POFBG showed very large variations between $\approx$ 4 and

$\approx 11 \ dB/cm.$

4.3.6   Induced heating during irradiation

Figure 4.19 shows the Bragg peak shift ($\Delta\lambda_B$) versus time, after the irradiation was stopped. The gratings presented were written at ambient humidity and temperature conditions. A positive shift is visible, i.e. the Bragg peak shifts to longer wavelengths. For gratings written at 2 Hz, the Bragg wavelength changes about 0.3 nm after the irradiation. Irradiation at 3 Hz leads to a post-irradiation shift increasing to 1 nm and at 5 Hz it is as high as 1.75 nm. This shows that the shift after irradiation is dependent on the laser repetition frequency used to write the gratings. The Bragg wavelength of an FBG is dependent on temperature, humidity and strain
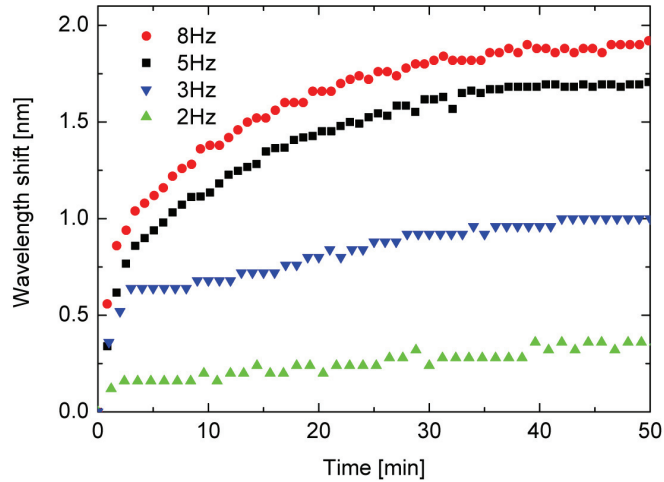
Figure 4.19: *Bragg peak shift after the irradiation laser was turned off for FBG written at different frequencies*

which will be explained in Chapter 5. With increasing temperature the Bragg peak shifts to lower wavelengths and with decreasing water content the Bragg peak shifts to lower wavelengths as well. The positive shift after irradiation therefore indicates a lowering temperature and an increase in water content of the fiber at the same time, because the fiber is in ambient conditions.

During the irradiation, the POF and the glass support was heated by the excimer laser pulses. The main heating is probably due to a part of the laser irradiation being blocked by the aluminum slit used to define the grating length. The temperature of the glass support slide was measured during irradiation, at a position next to the fiber, where it is not exposed directly to irradiation. The maximum temperature increase during irradiation is $\approx 5 \ ^\circ\text{C}$ (5 Hz, 85 mJ/cm^2, 43 min). Therefore the air surrounding the fiber is also heated up and in consequence, the relative humidity decreases during the writing process. This leads to a concentration difference

between the water content within the fiber and the surrounding air and leads to a decrease in water content within the fiber, thus a negative wavelength shift during irradiation, and the opposite effect after irradiation. The shift in Figure 4.19 is a consequence of the temperature and humidity change within the fiber after the irradiation is stopped.

When the excimer laser is turned off, the FBG and the support cool down and the Bragg peak shifts to longer wavelengths. Using a Bragg peak shift dependence of -138 pm/°C for ambient conditions (Accounting for temperature and humidity effects, see Section 5.6), the wavelength shift at an irradiation frequency of 8 Hz can be used to estimate a heating of the POF of $\approx$ 13.9 °C. For a frequency of 2 Hz the heating corresponds only to $\approx$ 2.6 ° C (using the same estimation). Influence on the POFBG through temperature and humidity can thus be minimized by lowering the irradiation frequency.

Frequency	$\Delta\lambda$	ΔT
2 Hz	0.36 nm	2.6°C
3 Hz	1 nm	7°C
5 Hz	1.75 nm	12.6°C
8 Hz	1.92 nm	13.9°C

Table 4.2: *Frequency dependence of induced heating during irradiation*

4.3.7   FBG writing using Femtosecond laser

In the following section preliminary results on fs-laser written FBG are presented. Femtosecond laser light at 400 nm was used for irradiation. The advantage of using the second harmonic is twofold. First the photon energy is increased and the refractive index change can be higher due to enhanced nonlinear absorption [25]. The second advantage is connected to the phase mask used for FBG writing. In order to write gratings at $\approx$ 1550 nm, a phase mask pitch of $\approx$ 1 μm is needed. However as this pitch is close to the wavelength of 800 nm, the 0th order diffraction is increased due to a decrease in diffraction efficiency and in consequence the fringe visibility is reduced. Phase Masks for 800 nm irradiation with a pitch of 1040 nm have a 0th order diffraction of $> 25\%$ [2]. For 400 nm irradiation, phase masks with low 0th order diffraction (e.g. $< 4\%$) are possible and therefore a standard phase mask technique can be employed.

Experiment

The femto second laser system used was a Coherent Mira Rega system with an output wavelength of 800 nm and a peak width of 10 nm. The maximum average output power is $\approx 1\ W$ with a

---

[2]Personal communication with Kristian Buchwald, Ibsen Photonics, (Phase Mask supplier)

pulse length of $\approx 200 \, fs$ at a repetition rate of 200 kHz. The details can be found in Appendix F. The femtosecond laser irradiation setup uses the same phase mask technique as explained in a preceding section. However, as the laser beam width is small, scanning along the fiber axis was performed. Figure 4.20 shows the irradiation setup. The POF is placed on a glass support slide and the phase mask is placed on top. The phase mask was made for femtosecond laser irradiation at 400 nm with a minimized 0th order diffraction of $< 4\%$ and a pitch Λ_{PM} of 1040 nm. A slit defines the grating length. The femtosecond laser is focussed using a cylindrical lens (f= 40 mm). The spot of the laser beam at the position of the fiber was measured using a knife edge technique. The beam size in fiber axis direction is 1.65 mm, perpendicular to the fiber axis the beam size is 36 μm (at $1/e^2$ of maximum power). The fluence per pulse at that position was 0.8 mJ/cm^2. Scanning was performed at a speed of 100 mm/min equaling an exposure duration of 1 second per scan. After each scan the spectrum was measured. The time between scans was approximately 1-2 minutes, therefore the fiber could cool down before each irradiation scan. FBG spectra were only measured in reflection.
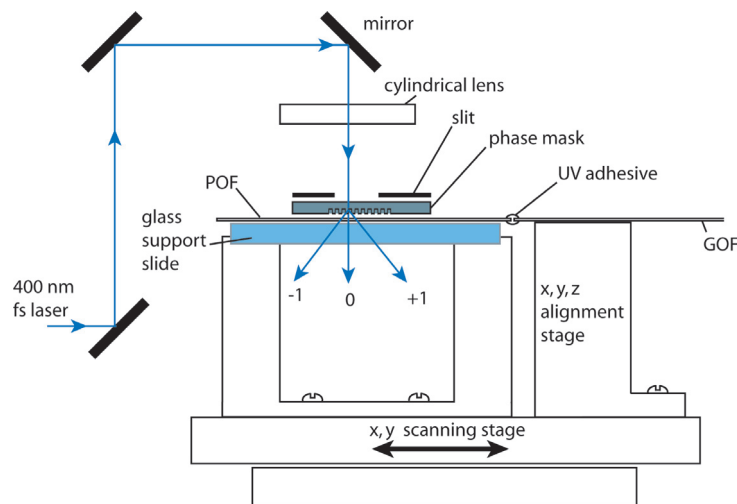
Figure 4.20: *Femtosecond irradiation setup. POF: polymer optical fiber, GOF: glass optical fiber. Cylinder axis of the lens is parallel to the fiber axis.*

Results and Discussion

Figure 4.21 shows the reflection spectra of an FBG after 4 and 45 scans, corresponding to 0.64 and 7.2 kJ total dose respectively. The transmission was not measured for this particular fiber. With the irradiation setup used, the FBG were always written at the same position in the fiber and the fibers to be irradiated were always cut to the same length. From several experiments, a typical transmission power level was known, which was used to estimate the reflectivity for this grating, assuming a grating length of L=5 mm. The slit used was 5 mm, but due to the

small spot size and the scanning scheme, misalignment could lead to a shorter grating. The
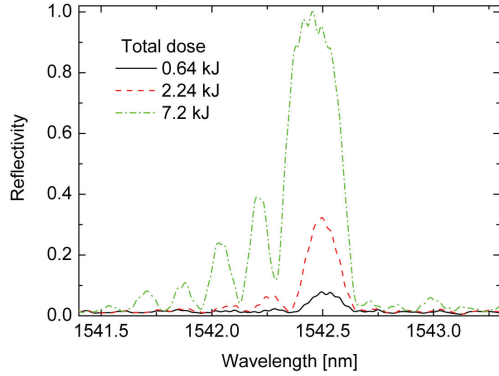
Figure 4.21: *Refractive index change Δn_{ac} spectrum of FBG for different total doses. Scan speed 100 mm/min, Fluence 0.8 mJ/cm^2, Length $\approx$ 5mm.*
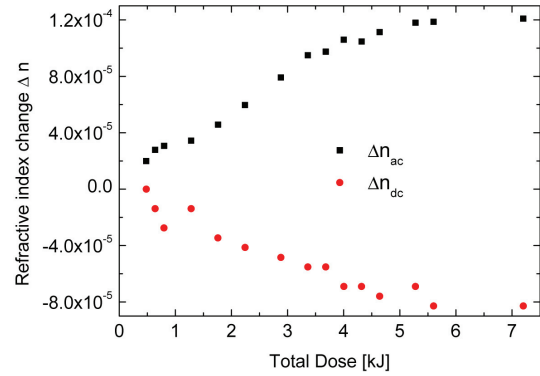
Figure 4.22: *Refractive index change Δn_{ac} and Δn_{dc} for FBG shown in Fig. 4.21.*

induced index amplitude Δn_{ac} was estimated using the same assumption. The bandwidth of the grating $\Delta\lambda_B$ is 385 pm at a total dose of 7.2 kJ. Using equation 4.8, the estimated index change and a grating length of 5 mm, the theoretical bandwidth of 328 pm can be calculated. Given the uncertainty in grating length and index change, the results agrees well to the measured value. Figure 4.22 shows the induced index amplitude Δn_{ac} and the induced mean index change Δn_{dc}. The mean index shift is negative as in the case of irradiation with excimer laser light. Temperature induced wavelength shift has no influence as the fiber can cool down between consecutive scans. Water desorption is slightly faster than sorption, but the scan time, during which desorption occurs, is much shorter than the time for sorption, i.e. between two scans. Therefore humidity is also assumed to be constant within the fiber. The asymmetric Bragg peak spectrum indicates again that either the photosensitivity is not homogenous along the fiber axis or a chirp is induced due to changing effective irradiation intensity in the core, possibly as a result of misalignment. Overall 8 fibers were irradiated, 3 showing FBG formation. Figure 4.23 shows the evolution of the grating after irradiation. The induced index change is not stable, the grating reflectivity decays fast. After 2 month the grating is completely vanished. These experiments show, that reversible index modulation using femtosecond laser light is possible. Irradiation fluences were very low and are a possible reason for this reversibility. Higher fluences however induced fiber damage and melting of the fiber. Increasing the scanning speed might avoid damage at higher fluences. The experimental setup, using a phase mask and a scanning scheme proofed to be a valid solution for FBG writing with femtosecond laser. Further work should focus on the improvement of alignment issues concerning the scanning and enable the identification of the usable fluence ranges and/or scanning speeds for creation of stable fiber

Bragg gratings.
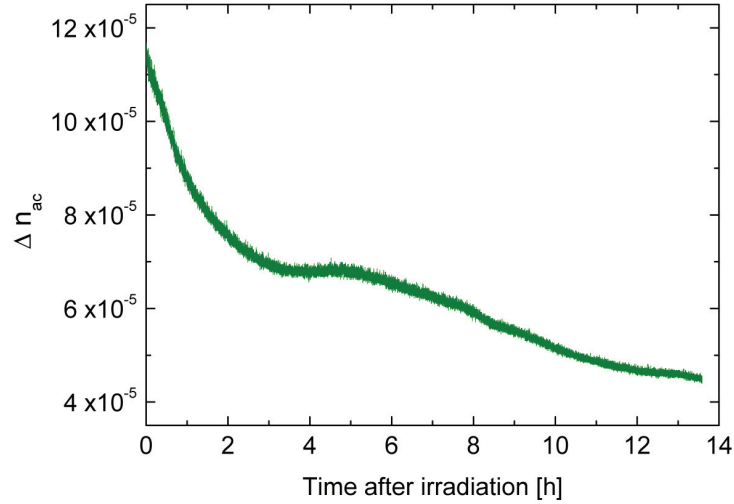
Figure 4.23: *Evolution of the Bragg wavelength and the induced refractive index change after irradiation for FBG shown in Fig. 4.21.*

4.4   FBG characterisation with OLCR

The use of Optical low coherence reflectometry (OLCR) [29] allows the characterization of the local Bragg wavelength of a grating, i.e. the induced amplitude Δn_{ac} and mean refractive index Δn_{dc} along the fiber axis z [30]. The effective spatial resolution is $\approx$ 100 μm. Further the location and the optical length of a grating can be measured.

4.4.1   Experiment

An OLCR setup is basically a Michelson interferometer. Figure 4.24 shows the OLCR setup used (apart from minor modifications the same as presented by Coric et al. [31]). Light which is reflected by the FBG to be characterized will interfere with the light from the reference arm only if the length difference of the two arms is smaller than the coherence length of the light source. The coherence of the light source also defines the resolution achievable with an OLCR system. By scanning the mirror in the reference arm, the FBG can be probed along its length. Measuring the amplitude and phase of the light reflected from the device under test allows to determine the properties of an FBG. A pristine polymer fiber was used to measure the group index n_g using a cut-back method [32]. For this the fiber length is measured with OLCR and with an optical microscope and subsequently the fiber is cut and measured again. From both,
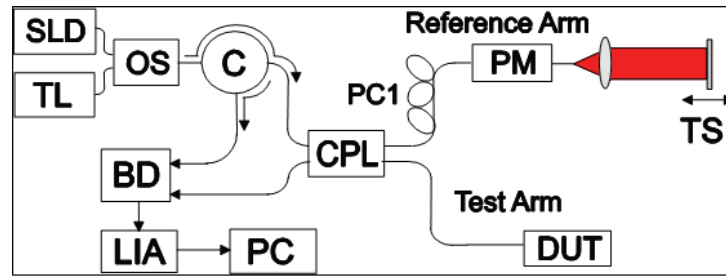
Figure 4.24: *OLCR setup scheme. SLD: superluminescent diode; TL: Tunable laser; C: circulator; PM: piezoelectric modulator; TS: translational stage; DUT: device under test; CPL: 3 dB coupler; BD: balanced detector; PC: computer; LIA: lock-in amplifier.*

amplitude and phase together using an inverse scattering methode, the refractive index change along a written fiber Bragg grating can be characterized

4.4.2   Results and Discussion

Figure 4.25 shows the reconstruction of the OLCR measurement of an FBG in a silica fiber. Comparing this with Figure 4.26 shows, that the index variations in the POFBG are much larger than in the silica FBG. To obtain the geometrical length of the POFBG, a group index of $n_g = 1.467 \pm 0.003$ was measured using a cut-back method. A length of 4.5 mm was obtained, which was slightly smaller than the slit (5 mm) used.
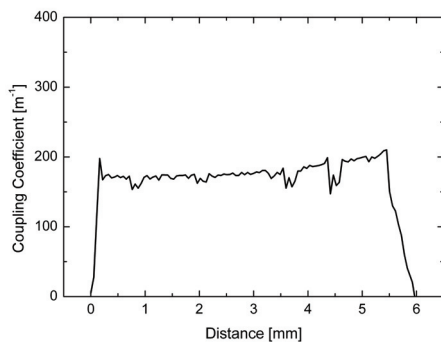
Figure 4.25: *Reconstruction of an OLCR measurement. FBG with 50% reflectivity and 6 mm length in a a silica fiber.*
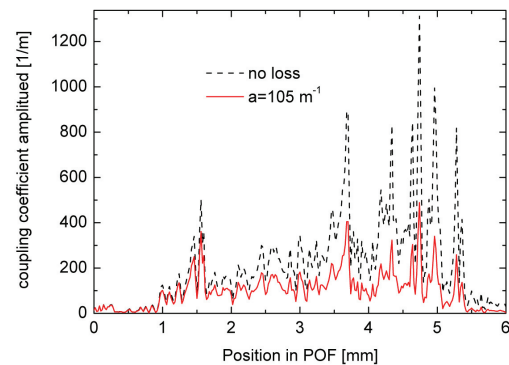
Figure 4.26: *Reconstruction from the OLCR measurement for FBG7. Reconstruction as measured, and reconstruction adjusted for fiber and induced loss.*

The loss of the fiber (≈ 1 dB/cm) and the induced loss of the grating (≈ 3.6 dB/cm) were

taken into account. The total loss of $\alpha \approx 4.6$ dB/cm can be converted to the attenuation in meters^{-1}, a= 105 m^{-1} using the following two relations:

$$P_{out}(L) = P_{in}10^{\frac{-\alpha L}{10}} \tag{4.9}$$

and

$$P_{out}(L) = P_{in}e^{-aL} \tag{4.10}$$

The local coupling coefficient (i.e. induced index change) shows strong variations. Local peaks exhibit index changes of up to 4 times the mean value $< n_{ac}(z) > \approx 0.9 \times 10^{-4}$ (averaged over the length of the grating). The strong variations indicate inhomogeneous photosensitivity due to material inhomogeneities in the fiber. Fourier transforms of the coupling coefficient did not show a dominant frequency in the inhomogeneity pattern. Different FBG show distinct inhomogeneity patterns. The differences in local reflectivities of the written FBGs are therefore influenced by the changing photosensitivity along the fiber.
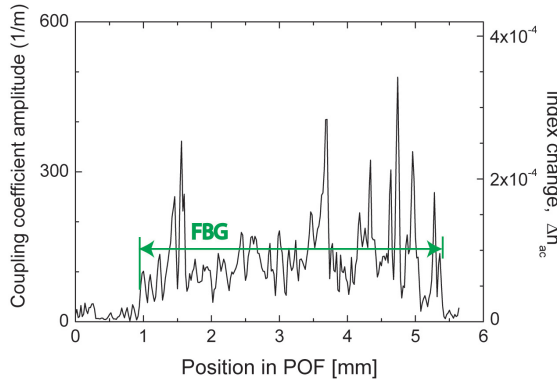
Figure 4.27: *Local grating coupling coefficient reconstructed from OLCR data and inverse scattering for FBG7 with 4.6 dB/cm fiber and grating loss. Measured length $l \approx 4.5$ mm*
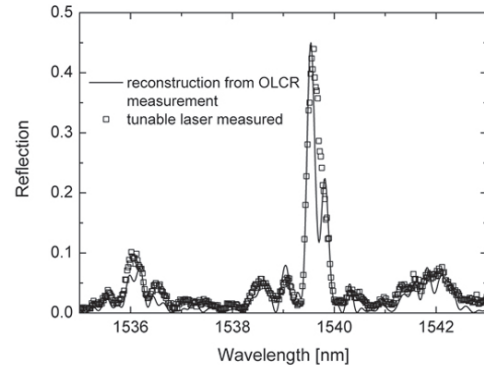
Figure 4.28: *Measured and FBG7 spectrum reconstructed from OLCR measurements.*

Figure 4.28 shows the measured grating spectrum using a tunable laser and the spectrum reconstructed from OLCR measurement (Fourier transformation). The measured wavelength spectrum had to be shifted by 545 pm due to different ambient conditions compared to the OLCR measurement. The reconstruction of the reflection spectrum from the OLCR measurement and the directly measured spectrum show good agreement.

4.5   Irradiation induced birefringence change in POF

Polymer molecule chains usually have anisotropic polarizability in different axis directions. Due to random orientation of these polymer chains however, on the macroscopic scale the material often show isotropic optical characteristics. If a fabrication process induces orientation of the molecules in a preferential direction, the polymer will show birefringence on the macroscopic scale. Such process induced alignment is caused by stresses which arise in fiber drawing or mold filling. Shear stresses due to viscosity gradients in polymer melts close to the T_g lead to partial orientation of the polymer chains. This orientation can be frozen in as the viscosity increases rapidly during the cooling from the melt phase, above the glass transition temperature, to the solid phase at lower temperatures. Dugas et al. [33] showed birefringence measurements and calculations of the temperature and viscosity distribution in fiber drawing processes. The temperature stays higher in the fiber center, the viscosity on the surface of PS fibers can be up to a factor 20-30 higher compared to the center axis during the drawing process. Such gradients influence the degree of molecule orientation and may induce stress in the final fiber. The material thus exhibits anisotropy, in the case of a drawn fiber in general transverse isotropy. Transverse isotropy is when the material is only isotropic in one plane, e.g. perpendicular to the drawing direction, and has different physical properties in the axis perpendicular to that plane, e.g. in the fiber axis. Increasing drawing temperature decreases the chain orientation as relaxation processes are more pronounced and the drawing speed increases the chain orientation by decreasing the relaxation time [34]. Orientation of the polymer chains (inelastic strain) give rise to non-isotropic refractive index [33], observable as birefringence. Such birefringence in polymers is well known and was investigated in several studies [35–41]. However, the orientation is not the only factor influencing the birefringence. Fiber drawing and the different materials used in an optical fiber lead to residual stresses. During fiber drawing, the viscosity of the material influences to which degree the draw tension induces deformation or elastic stess. The highest viscosity material or region bears the major part of the draw stress which can be frozen in after the quenching process. These residual stresses induce birefringence through the photoelastic effect. The induced birefringence due to stress is defined as follows

$$\Delta n = n_z - n_x = C\Delta\sigma \tag{4.11}$$

$$\Delta\sigma = \sigma_z - \sigma_x \tag{4.12}$$

Where Δn is the birefringence, C is the photoelastic coefficient and σ_x and σ_z are normal stresses. In the case of a fiber, z is the direction of the fiber axis and x is perpendicular to the fiber axis. The photoelastic coefficient for PS is $(6 \div 10) \times 10^{-12} Pa^{-1}$ [42] and for PMMA it is $(-2.7 \div -3.8) \times 10^{-12} Pa^{-1}$ [42, 43].

Glassy, amorphous polymers have higher specific volume when cooled below the glass transition temperature compared to the equilibrium state at the given temperature. The relaxation towards thermodynamic equilibrium for glassy materials in general is called structural relaxation [44, 45] for glassy polymers it is referred to as physical aging [46]. The glassy-state structural relaxation results in a time dependence of material properties such as increased modulus and density [47, 48]. The residual stresses and molecular orientation in polymers also relax as a function of time and temperature. Therefore the birefringence is a function of the thermal history of a piece of polymer. For pieces of the same fiber that were stored differently, this leads to different initial birefringence distributions within the fiber pieces when they are irradiated.

Birefringence measurements only show the total refractive index difference in two directions. The birefringence of a polymer is therefore a superposition of polymer chain orientation and residual stresses, both of which show history dependent relaxation processes. These non-isotropies give also rise to anisotropy of mechanical properties like Young's modulus [49], Poisson's ratio [50] and thermal expansion [51].

A third influence on the birefringence within a POF comes from different thermal expansion coefficients of core and cladding. This difference leads to stresses in the POF as a function of its temperature. In contrast to inelastic strain and drawing induced elastic stress, the stress induced through thermal expansion mismatch can not be lowered or removed through annealing.

The distinction between the inelastic and elastic part of birefringence for silica fibers was reported in the work of Duerr [52]. It was assumed that the inelastic contribution is uniform over the fiber cross section. This allows to subtract the inelastic part and get to the residual stress in the fibers.However the assumption which is done for glass fibers, that the inelastic contribution is uniform across the fiber cross section is not valid for the polymer fiber at hand. Intrinsic, inelastic birefringence of PS is much higher than for PMMA [34] which is due to the strong optical anisotropy of the phenyl groups in PS [39]. In consequence the inelastic contribution is higher in the core than in the cladding. For this reason distinguishing between elastic and inelastic birefringence cannot be done following the same procedure as for glass fibers [52].

A method to measure birefringence is to measure the optical retardation, R, between two polarization directions.

$$R = \left(\frac{d}{\lambda}\right)\Delta n \tag{4.13}$$

where d is the sample thickness, λ is the incident wavelength. Birefringence measurements following this principle were employed to visualize the irradiation induced changes in the polymer fiber. In the following section experiments will be shown, that investigate the birefringence in the single mode POF. Differentiation of the three influences on the birefringence where not investigated. In a study on birefringence in polymer optical fibers, Dugas et al. [33] were not able to measure the birefringence of PMMA fibers as the birefringence is too low. They

presented the much higher birefringence of PS optical fibers with values up to -6×10^{-3}. In this work the difference of the birefringence levels for the PS/PMMA core and PMMA cladding could be measured and will be presented. Results will include induced changes due to uniform irradiation and due to FBG writing.

Experiment

Short pieces of SM POF from Paradigm Optics were irradiated uniformly using a XeCl excimer laser (Lambda Physik LPX315iCC). The fiber samples were approximately 4 cm long. Irradiated zones were approximately 1 cm long in the center of the fiber sample leaving the two ends of the fiber un-irradiated. Different irradiation durations (10 - 60 min), frequencies (3 Hz - 8 Hz) and laser fluences (90 - 130 mJ/cm^2) were used which correspond to the irradiation specifications used for FBG writing. The fiber samples were measured using the birefringence measurement setup installed by F. Duerr [52], which is a similar setup to the one of Park et al. [53,54]. In this setup, the fiber is submerged in index matching liquid to minimize refraction. The fiber is then illuminated using a polarization controlled HeNe laser beam using a rotating polarizer. Imaging the fiber with a CCD camera and a microscope objective through an analyzer, the retardation across the fiber can be measured.

Such measurements give the averaged birefringence on a portion of the fiber which is approximately 250 μm long. The measured birefringence is $\Delta n = n_z - n_x$ where n_z is the refractive index in fiber axis direction and n_x the refractive index perpendicular to the fiber axis. Measurements of each fiber sample were taken at 3 locations in the zone of irradiation and at 3 locations on either side of it, i.e. in the not irradiated parts. Measurements on the written FBG followed the same logic. By annealing the fiber, the frozen in stress and strain which are due to drawing tension and viscosity variations can be relaxed. The orientational birefringence due to molecular orientation will probably relax to a ceratin degree but not entirely. The stress which is due to different thermal expansion coefficients of core and cladding can not be altered by annealing. Annealing of the fiber was conducted in an oven at 95°C during 20 hours.

Results and discussion

The retardation as it was measured across a polymer fiber is presented in Figure 4.29. As seen in Equation 4.13, the retardation is the integrated birefringence over the sample thickness, in this case, the fiber section that the light passes through. This and the fact that the birefringence in the cladding does not vary much, is the reason that the retardation has this half-circle like shape. The much higher birefringence in the core is visible as a peak in the retardation profile.

A birefringence tomography of a pristine fiber is shown in Figure 4.30. Cylindrical symmetry of the birefringence within the cladding and the core can be observed. For such a tomography, the fiber is rotated about its axis by angles of 30 degrees. A so called inverse Radon transformation
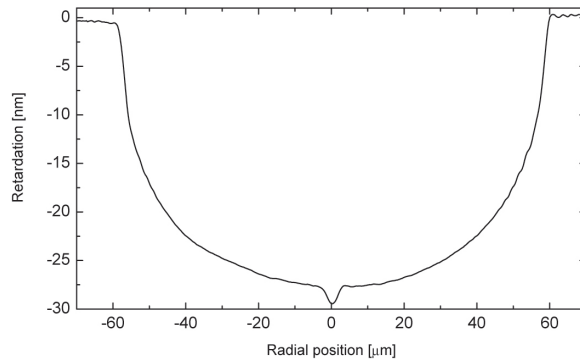
Figure 4.29: *Retardation profile of SM POF.*

than gives the tomography. The fact that the birefringence is axis symmetric enables the use of just one retardation measurement and using the so called Abel transform, the birefringence cross section can be calculated. Such cross sections are shown for a non-treated fiber and an annealed fiber in Figure 4.31. The birefringence in the cladding, i.e. pure PMMA, is approximately -2 × 10^{-4} and the absolute value is slowly decreasing towards the center of the fiber. This shape is probably caused by elastic stress which is due to the temperature and therefore viscosity gradient during the fiber drawing, similar to PS fibers reported in [33]. This PMMA birefringence is relatively small and indicates that the anisotropy of the mechanical properties is also small [49]. The core material with 22 wt% of PS shows much higher birefringence of $\approx -13.6 \times 10^{-4}$. Annealing of drawn polymer fibers show shrinkage at elevated temperatures [55,56] which leads to length reduction and diameter increase. The increase in diameter is visible in Figure 4.31 ($\approx+$ 6 %). The birefringence in the cladding is reduced by approximately 30% ($\approx -0.8 \times 10^{-4}$), the core birefringence is reduce by almost a factor of 3 ($\approx -8.9 \times 10^{-4}$). Two reasons lead to this birefringence change, relaxation of stresses and of the orientation of the molecular chains (strain). The largest residual stresses in the pristine fiber are probably in the region of the core, as the two different materials have different viscosity, thermal expansion, and thermal conductivity properties. Dominant change in the core region after annealing supports this assumption. However, residual stresses are only minimized after annealing, it is likely that a certain amount of residual stresses are still present in the annealed fiber. If stresses are the only birefringence influence in the fiber, the birefringence integration over the cross section surface should be zero. Therefore the integral gives a measure of the molecular orientation, i.e. the inelastic part of the birefringence. For the case of annealing, the integral value drops from -2.42×10^{-4} for the pristine fiber, to -2.12×10^{-4} for the annealed fiber. This shows that a part of the inelastic birefringence is annealed.

Cross sections for pristine and irradiated fibers are shown in Figure 4.32 with the corresponding y-axis on the left. The pristine fiber shows the lower birefringence level in the cladding, i.e. at
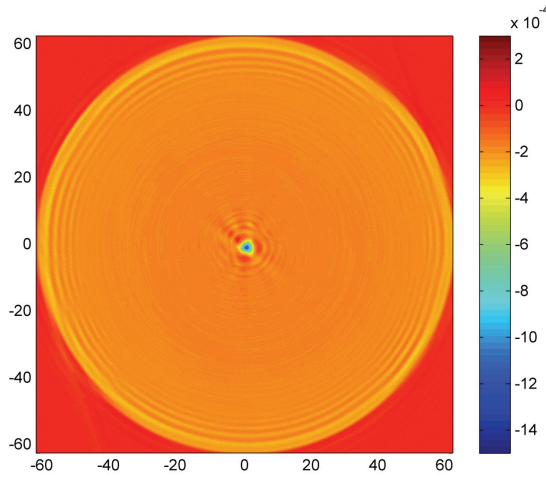
Figure 4.30: *Birefringence tomography of a pristine fiber.*
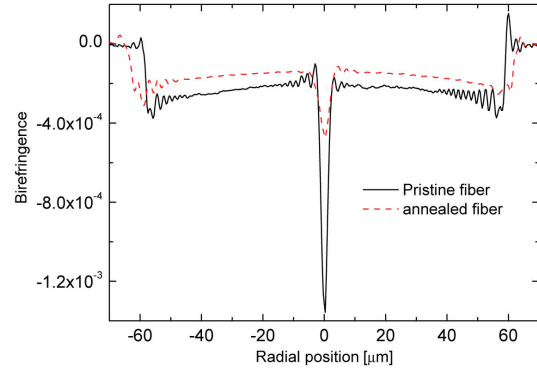
Figure 4.31: *Cross section of a non treated fiber and an annealed fiber (Annealing 20h at $95°C$)*

radial positions between ≈ 2 and $\approx 62\mu m$, compared to the core were the peak birefringence can be observed.
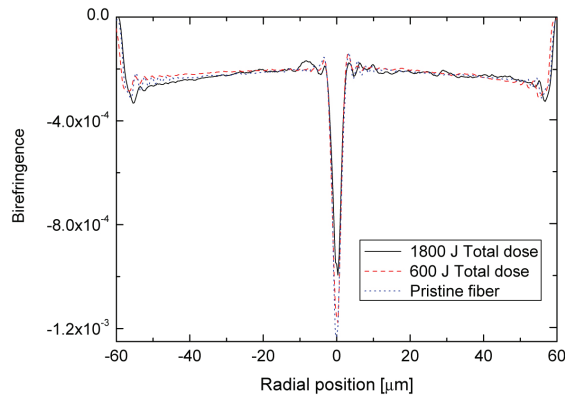
Figure 4.32: *Birefringence cross section of the non irradiated and irradiated POF at different total dose. Fluence per pulse $\approx 100\ mJ/cm^2$, frequency 5 Hz, measured at 6 different locations and averaged.*
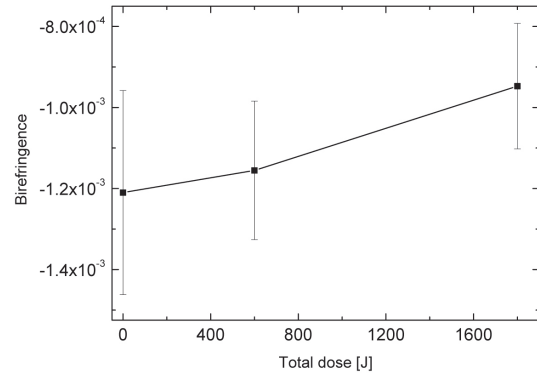
Figure 4.33: *The core values of the birefringence with the standard deviation of the three measurements. Each measurement is an average over 250 μm fiber length.*

The birefringence in the cladding of the irradiated fibers do not show significant changes. However the PS/PMMA core exhibits a decrease in birefringence amplitude upon irradiation. In

the core the birefringence is reduced with increasing irradiation from -12 $\times 10^{-4}$ to -9.5 $\times 10^{-4}$.
Comparing this change with the case of the annealed fiber shows that the irradiation has a much
lower influence on the core birefringence than annealing. The change in the core can be due to
reduction of the elastic birefringence or reorientation of molecular chains after photo-induced
chain scission. The three core values are plotted with the standard deviation of 6 measurements
(at varying locations) for each irradiation step (Fig. 4.33). Variations of the measured core
values are large even in the non-irradiated fiber. Values for all measurements of unirradiated
fibers (including measurements not shown) vary between -7$\times 10^{-4}$ and -30$\times 10^{-4}$ for the core
region. These large variations suggest that the fiber material is not homogeneous or that the
residual stresses vary along the fiber axis. This confirms our results from OLCR measurements,
were large local photosensitivity differences were found.

Figure 4.34 shows the birefringence tomographies of a written FBG and the pristine fiber. The
birefringence in the core decreases. In the cladding small birefringence changes can be observed.
Such features were observed in different FBG in different forms and magnitudes. The direction
of irradiation was from the right in the plane of the image. The locations of the birefringence
changes in the cladding coincide with the region where the laser beam converges due to focussing
of the cylindrical fiber geometry. The core birefringence changes from -12$\times 10^{-4}$ to -10$\times 10^{-4}$ in
this FBG.
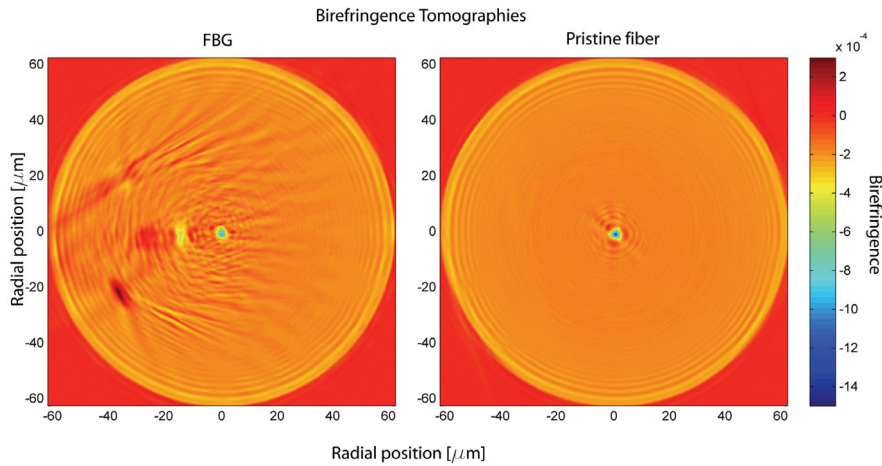
Figure 4.34: *Birefringence tomographies of a written FBG and the pristine fiber. Fluence per pulse $\approx$ 83 mJ/cm^2, frequency 5 Hz, total dose 1.5 kJ. Each tomography is an average of the birefringence on 250 μm. Irradiation direction for the FBG20 was from the right. $\Delta n_{ac} \approx 1.57 \times 10^{-4}$*

Birefringence measurements of pristine and irradiated POF show, that the main impact of the
irradiation is in the core. The cladding region, where the intensity of the irradiation beam
increases due to focusing of the fiber geometry, shows also slight birefringence changes. Uniform

irradiation and FBG writing shows a tendency towards a decrease of the absolute birefringence value in the core. Possible reasons for this, single or in combination, are 1) chain scission leading to a decrease of inelastic strain (chain orientation) and 2) relaxation of drawing induced elastic stress. However large statistical variation of birefringence in the core did not allow quantification of the decrease.

As was explained earlier, Kada et al. [28] reported on a positive refractive index change upon irradiation of PMMA with UV light at 254 nm. This is in contrast with our findings of a negative index change. However the difference in irradiation wavelength and in material (PMMA/PS core in our work) might explain these different findings. Another explanation could be the change in birefringence. It was shown in this section, that the birefringence $\Delta n = n_z - n_x$ is negative. Because n_x is the refractive index seen by the FBG, a negative index change of n_x could be one of the reasons for the measured decrease of absolute birefringence in the irradiated fiber.

Photoinduced refractive index change is therefore due to two different mechanisms, one is the index change due to main- or side-chain scission and the second is the index change due to relaxation of birefringence (inelastic strain and elastic stress).

4.6 Summary

It could be shown that FBG can be written in POF using excimer laser radiation at 308 nm wavelength. Maximum reflectivity is in general attained during irradiation. After the irradiation is stopped, the reflectivity decreases slightly. Approximately 40% of written FBG have a reflectivity of $\geq 37\%$ 6 month after irradiation. Several gratings were monitored during 9 month thereafter showing no significant reflectivity change. Within these stable gratings, 5-mm-long gratings had reflectivities up to 70% and 7-mm-long gratings up to 87%. These both correspond to a maximum index change of 1.7×10^{-4}. Accompanied with the refractive index change is an induced insertion loss which can be as high as 11 dB/cm. The mean refractive index change Δn_{dc} was measured to be negative. The growth process of FBG exhibits large variations. Humidity and temperature changes as well as material inhomogeneities are the most important source of influence on these variations. Heating of the fiber during irradiation was estimated to be up to 13°C at an irradiation frequency of 8 Hz.

Preliminary results of femto second laser irradiation at 400 nm showed grating formation and reflectivities similar to excimer laser written gratings. These gratings however, were not stable and vanished within a few days.

Reflection spectrum reconstruction from the OLCR measurements show good agreement if the loss of the fiber and the irradiation induced loss are taken into account. It further shows that the induced refractive index change, and therefore photosensitivity of the POF, has large locale variations.

The measured birefringence shows, that irradiation induced changes with 308 nm excimer laser are mainly induced in the core. The absolute value of the birefringence changes to lower values, however the statistical variations of the core birefringence does not allow quantification of this change. Also the initial birefringence in pristine fibers exhibit large variations indicating low homogeneity of the fiber material. This variation of the POF material along the fiber axis is probably also the reason for the photosensitivity variations observed in the OLCR measurements. The decrease of absolute birefringence can explain a negative index change seen in the FBG, however it is likely that this is not the only factor influencing the index change in the fiber material.

4.7   Conclusion

The used setup and for FBG writing in POF using excimer laser irradiation showed to be suitable for this purpose. Results of differently prepared fibers lead to the conclusion, that the water content within the POF might still be the main influence for varying writing success. Measurements in controlled humidity environments should yield more insight on the importance of the humidity during irradiation. Comparison of the found negative index change with reported positive index change upon UV induced photolysis indicate, that the photolysis process in PMMA/PS is different compared to pure PMMA. Birefringence measurement in combination with the found negative index change further indicate, that this change of inelastic strain and elastic stress (combined in the birefringence) adds to the negative index change measured with the FBG. As the birefringence is largely influenced by its thermal history, as was shown by the annealing experiment, and there are indication that the birefringence is of importance for the index change and possible reliability issues of POFBG have to be investigated.

Bibliography

[1] K. O. Hill, Y. Fujii, D. C. Johnson, and B.S. Kawasaki. Photosensitivity in optical fiber waveguides: Application to reflection filter fabrication. *Applied Physics Letters*, 32(10):647–649, 1978.

[2] G. Meltz, W. W. Morey, and W. H. Glenn. Formation of Bragg gratings in optical fibers by a transverse holographic method. *Optics Letters*, 14(15):823–825, 1989.

[3] F. P. Laming. Holographic Grating Formation in Photopolymers - Polymethylmethacrylate. *Polymer Engineering and Science*, 11(5):421–425, 1971.

[4] J. M. Moran and I. P. Kaminow. Properties of Holographic Gratings Photoinduced in Polymethyl Methacrylate. *Applied Optics*, 12(8):1964–1970, 1973.

[5] G. D. Peng, Z. Xiong, and P. L. Chu. Photosensitivity and Gratings in Dye-Doped Polymer Optical Fibers. *Optical Fiber Technology*, 5(2):242–251, 1999.

[6] L. B. Jeunhomme. *Single-mode fiber optics: principles and applications.* Marcel Dekker, Inc., 1990.

[7] Dietrich Marcuse. *Theory of Dielectric Optical Waveguides.* Academic Press INC., second edition, 1991.

[8] T. Erdogan. Fiber grating spectra. *Journal of Lightwave Technology*, 15(8):1277–1294, 1997.

[9] Yann Tissot. *Design and Realization of Fiber Integrated Grating Taps for Performance Monitoring Applications.* PhD thesis, Ecole Polytechnique Federale de Lausanne, 2007.

[10] Raman Kashyap. *Fiber Bragg Gratings.* Academic Press, 1999.

[11] P. E. Dyer, R. J. Farley, R. Giedl, and D. M. Karnakis. Excimer laser ablation of polymers and glasses for grating fabrication. *Applied Surface Science*, 96-98:537–549, 1996.

[12] A. K. Baker and P. E. Dyer. Refractive-Index Modification of PolyMethylMethAcrylate (PMMA) Thin Films by KrF-Laser Irradiation. *Applied Physics A*, 57:543–544, 1993.

[13] N. F. Schmitt, E. Lewis, and P. Scully. UV photo induced grating structures on plastic optical fibers. In *Fifth International Conference on Plastic Optical Fibers and Applications*, pages 120–127, Paris, 1996.

[14] Z. Xiong, G. D. Peng, B. Wu, and P. L. Chu. Highly Tunable Bragg Gratings in Single-Mode Polymer Optical Fibers. *IEEE Photonics Technology Letters*, 11(3):352–354, 1999.

[15] Gang Ding Peng, Pak L. Chu, Zhengjun Xiong, Trevor W. Whitbread, and Rod P. Chaplin. Dye-Doped Step-Index Polymer Optical Fiber for Broadband Optical Amplification. *Journal of Lightwave Technology*, 14(10):2215–2223, 1996.

[16] F. Oulette. Ring Interferometer Configuration for Writing Gratings. University of Sydney Patent Cooperation, Treaty AL/96/00782.

[17] P.-Y. Cortes, F. Oullette, and S. LaRochelle. Intrinsic apodisation of Bragg gratings written using UV-pulse interferometry. *Electronics Letters*, 34(4):396–397, 1998.

[18] H. Y. Liu, H. B. Liu, G. D. Peng, and P. L. Chu. Observation of type I and type II gratings behaviour in polymer optical fiber. *Optics Communications*, 220:337–343, 2003.

[19] JianMing Yu, XiaoMing Tao, and HwaYaw Tam. Trans-4-stilbenemethanol-doped photosensitive polymer fibers and gratings. *Optics Letters*, 29(2):156–158, 2004.

[20] Xu Xingsheng, Ming Hai, and Zhang Qijin. Properties of polarized laser-induced birefringent gratings in azobenzene-doped poly(mehyl methecrylate) optical fibers. *Optics Communications*, 204(1-6):137–143, 2002.

[21] H. Y. Liu, G. D. Peng, P. L. Chu, Y. Koike, and Y. Watanabe. Photosensitivity in low-loss perfluoropolymer (CYTOP) fiber material. *Electronics Letters*, 37(6):347–348, 2001.

[22] H. Y. Liu, G. D. Peng, and P. L. Chu. Thermal stability of gratings in PMMA and CYTOP polymer fibers. *Optics Communications*, 204:151–156, 2002.

[23] Liliana R. Kawase, R. M. Ribeiro, Josemir C. Santos, Carlos M. Gibo, H. Y. Liu, G. D. Peng, and P. L. Chu. Study of Photosensitivity in Perfluorinated Polymer (CYTOP) Material. In *International Plastic Optical Fibres Conference*, Amsterdam, 2001.

[24] P. J. Scully, S. Caulder, and R. Barlett. Central Laser Facility Annual Report 1999/2000, UV-Laser Photo-induced Refractive Index Changes in Poly Methyl Methacrylate and Plastic Optical Fibers for Application as Sensors and Devices. Technical report, Liverpool John Moores University, 1999-2000.

[25] Alexandra Baum, Patricia J. Scully, Maria Basanta, C. L. Paul Thomas, Peter R. Fielden, and Nicholas J. Goddard. Photochemistry of refractive index structures in poly(methyl methacrylate) by femtosecond laser irradiation. *Optics Letters*, 32(2):190, 2007.

[26] G. N. Harbach, H. G. Limberger, and R. P. Salathe. UV induced fiber Bragg gratings (FBG) written in fully polymerized polymer optical fibers (POF). In *Proceedings POF 2007, Turin, Italy*, 2007.

[27] H. B. Liu, H. Y. Liu, G. D. Peng, and P. L. Chu. Novel Growth Behaviors of Fiber Bragg Gratings in Polymer Optical Fiber Under UV Irradiation With Low Power. *IEEE Photonics Technology Letters*, 16(1):159–161, 2004.

[28] Takeshi Kada, Takeyoshi Hiramatsu, Kenji Ogino, Chuang Xin Liang, Hideaki Machida, Koichi Kiso, and Seizo Miyata. Fabrication of Refractive Index Profiles in Poly (Methyl Methacrylate) using Ultraviolet Rays Irradiation. *Japanese Journal of Applied Physiscs*, 41:876–880, 2002.

[29] Ph. Giaccari, H. G. Limberger, and R. P. Salathĩ. Local coupling-coefficient characterization in fiber Bragg gratings. *Optics Letters*, 28(8):598, 2003.

[30] Philippe Giaccari. Fiber Bragg Grating Characterization By Optical Low Coherence Reflectometry And Sensing Applications, 2003. Fiber Bragg Grating Characterization By Optical Low Coherence Reflectometry And Sensing Applications.

[31] Dragan Coric, Hans G. Limberger, and René P. Salathé. Distributed measurements of fiber birefringence and diametric load using optical low-coherence reflectometry and fiber gratings. *Optics Express*, 14(24):11804–11813, 2006.

[32] Alessandro Iocco. *Tunable fiber Bragg grating gilters*. PhD thesis, École polytechnique fédérale de Lausanne, Suisse, 1999.

[33] Jacques Dugas, Isabelle Pierrejean, Jean Farenc, and Jean Philippe Peichot. Birefringence and internal stress in polystyrene optical fibers. *Applied Optics*, 33(16):3545–3548, 1994.

[34] Ladislav Dvoranek, Ludka Machova, Miloslav Sorm, Zdenek Pelzbauer, Jiri Svantner, and Vladimir Kubanek. Effects of Drawing Conditions on the Properties of Optical Fibers Made from Polystyrene and Poly(Methyl Methacrylate). *Die Angewandte Makromolekulare Chemie*, 174:25–39, 1990.

[35] R. D. Andrews. Retraction of Oriented Polystyrene Monofilaments. *Journal of Applied Physics*, 26(9):1061–1067, 1955.

[36] R. D. Andrews and J. F. Rudd. Birefringence Changes During Retraction of Oriented Polystyrene Monofilaments. I. Changes of Average Birefringence. *Journal of Applied Physics*, 27(9):990–995, 1956.

[37] R. D. Andrews and J. F. Rudd. Photoelastic Properties of Polystyrene in the Glassy State. I. Effect of Molecular Orientation. *Journal of Applied Physics*, 28(10):1091–1095, 1957.

[38] J. H. Andrews and K. D. Singh. Photoinduced diffraction in polymer waveguides. *Applied Optics*, 32:6703, 1993.

[39] Edward F. Gurnee. Theory of Orientation and Double Refraction in Polymers. *Journal of Applied Physics*, 25(10):1232–1240, 1954.

[40] E. F. Gurnee, L. T. Patterson, and R. D. Andrews. Apparatus for Making Simultaneous Stress and Birefringence Measurements on Polymers. *Journal of Applied Physics*, 26(9):1106–1110, 1955.

[41] Debra D. Wright, Eugene P. Lautenschlager, and Jeremy L. Gilbert. Constrained Shrinkage of Highly Oriented Poly(methyl methacrylate) Fibers. *Journal of Applied Polymer Science*, 91:4047 – 4056, 2004.

[42] J. F. Rudd and R. D. Andrews. Photoelastic Properties of Polystyrene in the Glassy State. III. Styrene Derivatives and Copolymers. *Journal of Applied Physics*, 31(5):818–826, 1960.

[43] H Ohkita, K Ishibashi, D. Tsurumoto, A. Tagaya, and Y. Koike. Compensation of the photoelastic birefringence of a polymer by doping with an anisotropic molecule. *Applied Physics*, A 81:617–620, 2005.

[44] C. A. Angell, K.L. Ngai, G. B. McKenna, P.F. McMillan, and S. W. Martin. Relaxation in glassforming liquids and amorphous solids. *Journal of Applied Physics*, 88(6):3113–3157, 2000.

[45] Eric R. Weeks, J. C Crocker, Andrew C. Levitt, Andrew Schofield, and D. A. Weitz. Three-Dimensional Direct Imaging of Structural Relaxation Near the Colloidal Glass Transition. *Science*, 287:627, 2000.

[46] Y. Huang and D. R. Paul. Physical aging of thin glassy polymer films monitored by gas permeability. *Polymer*, 45:8377–8393, 2004.

[47] I. M. Ward, editor. *Structure and Properties of Oriented Polymers*. Chapman & Hall, 1997.

[48] Zhiyi Zhang, Gaozhi Xiao, and Chander P. Grover. Volume relaxation in polymers and its effect on waveguide applications. *Applied Optics*, 43(11):2325–2331, 2004.

[49] H. Wright, C. S. N. Faraday, E. F. T. White, and L.R. G. Treloar. The elastic constants of oriented glassy polymers. *J. Phys. D: Appl. Phys.*, 4:2002–2014, 1971.

[50] H. Krebecek, J. K. Krüger, and M. Pietralla. Poisson Ratios and Upper Bounds of Intrinsic Birefringence from Brillouin Scattering of Oriented Polymers. *Journal of Polymer Science: Part B: Polymer Physics*, 31:1477–1485, 1993.

[51] Li-Hui Wang, C. L. Choy, and Roger S. Porter. Thermal Expansion of Oriented Poly(methyl Methacrylate). *Journal of Polymer Science: Polymer Physics Edition*, 21:657–665, 1983.

[52] F. Duerr. *Laser-induced stress changes in optical fibers*. PhD thesis, EPFL, 2005.

[53] Yongwoo Park, Un-Chul Paek, and Dug Young Kim. Determination of stress-induced intrinsic birefringence in a single-mode fiber by measurement of the teo-dimensional stress profile. *Optics Letters*, 27(15), 2002.

[54] Yongwoo Park, Tae-Jung Ahn, Yune Hyoun Kim, Won-Taek Han, Un-Chul Paek, and Dug Young Kim. Measurement method for profiling the residual stress and the strain-optic coefficient of an optical fiber. *Applied Optics*, 41(1):21–26, 2002.

[55] Yoshinobu Ueba and Norifumi Matsumiya. Plastic optical fiber and production thereof. US Patent No 4568146, 1986.

[56] K. E. Carroll, D. J. Webb, K. Kalli, C. Zhang, A. Argyros, and M. C. J. Large. Extending the working temperature range of bragg gratings in microstructured polymer optical fibre by annealing. In *Proceedings POF 2007, Turin, Italy*, 2007.

Chapter 5

POF Bragg grating sensitivity

5.1   Introduction

Polymer optical fibers like glass optical fibers have the advantage of being immune to electro magnetic interference. This opens fields of sensing applications which are not accessible for standard electronics based sensors. Polymer fiber sensors up to now were mainly based on light intensity encoded sensing schemes. This however can lead to disadvantages as the light intensity in an optical fiber can also be influenced by bending or other interactions with the fiber, which increases the noise of the signal. Fiber Bragg grating sensors in comparison use the change in refractive index and geometry which results in a 'wavelength encoding'. A further advantage is that FBG can be multiplexed within a fiber and the fibers can be embedded in structures which adds to the possible applications. For glass optical fibers strain, pressure and temperature measurements are the main applications.

POFBG can be used for the same applications [1] but show different sensitivity and measurement ranges. Bragg gratings have been used for sensing in numerous applications. The Bragg peak shows sensitivity on temperature and strain variations. POFBG show the similar sensitivities, but the different material properties lead to some differences in the sensing response. Up to date the large thermal response of POFBG was emphasized [1–4], but it was never explained in detail what causes this large sensitivity. This work shows, that the main influence on PMMA based POFBG is a change in ambient relative humidity upon heating and therefore not a direct thermal effect in the fiber. To explain this humidity dependence in detail, the main focus in this chapter will humidity in POFBG. Characterization of the presented FBG from chapter 4 with respect to their sensitivity to different environmental conditions and to strain will be shown. In a first part of this chapter, the Bragg wavelength dependence on humidity at constant temperature is presented. The variation of the Bragg peak over time at a given temperature could be used to show it is a diffusion controlled mechanism and it allowed to calculate the diffusion coefficient of water in PMMA. Further, at constant humidity, the temperature dependence was measured and is shown. The most general case of ambient conditions, where temperature and humidity are not constant, is presented which shows similar thermal response magnitudes as published in the

literature. Presentation of the strain sensitivity is kept brief as it follows the known behavior like for silica fiber FBG.

The Bragg reflection is defined by Equation 4.2. It can be seen that changes in the refractive index or in the grating pitch will shift the reflection and transmission peaks. Temperature variations will introduce a refractive index change described by the thermo-optic coefficient [5,6] and a change in grating pitch, introduced through thermal expansion [7]. The temperature dependence of plastic optical fiber Bragg gratings (POFBG) [1–3] under ambient conditions was already reported and it was found that it is up to one order of magnitude higher than for silica fibers. Using the generally used relation for thermally induced Bragg shift [8] with the thermo-optic and thermal expansion coefficient for PMMA, this high thermal sensitivity could not be explained up to now. In the subsequent section, an explanation is presented, that takes into account the change of the humidity with increasing temperature. A formalism is proposed that relates the Bragg shift to four material properties, a) thermo-optic coefficient [5], b) thermal expansion coefficient [9], c) hygro-optic coefficient [10] and d) humidity induced swelling [11]. This proposed relation can explain the very high Bragg peak shift in ambient conditions and a comparison with measurements in our POFBG show that it is valid for changing humidity at constant temperature and for simultaneous changes of humidity and temperature. The main influence to the large shift could be identified to be the humidity. Glass fibers do not show swelling with increasing humidity and are therefore not sensitive to humidity.

POFBG can further be used for strain measurements [2]. A fiber under mechanical deformation will exhibit a grating pitch change due to strain deformation [12] and lateral contraction following the generalized Hooke's law [13]. At the same time the refractive index will undergo a change due to photoelasticity [14].

This chapter will show the sensitivities of written POFBG on temperature, humidity and strain.

5.2 Humidity sensitivity of POFBG at constant temperature

5.2.1 Introduction

PMMA and many other polymers have the tendency to sorb water [11,15–18]. PMMA exhibits a maximum water content of up to 2 wt% [11,16]. Polystyrene in contrast adsorbs little or no water at all [19, 20]. Many polymers show water sorption processes, where clustering of water occurs within the polymer matrix [18] leading to a sorption increase at higher humidities. This process leads to a non linear relation of fiber water content as a function of relative humidity surrounding the fiber [17]. There are two mechanisms which influence the Bragg reflection with changing water content in the fiber. The first is swelling of the polymer due to water uptake [16,21] which changes the grating pitch. The second is a change of refractive index with increasing water content [10] due to an altered mean polarizability of the fiber material. The water sorption also

alters the mechanical properties as the water molecules act as plasticisers [11, 22, 23]. Different magnitudes of swelling in the core and in the cladding will induce stress within the fiber. These stresses influences the Bragg wavelength through a change in grating pitch and photoelastic refractive index change. Calculations of this induced stress will be presented.

5.2.2   Experiment

To reach very low relative humidity (dry) conditions, the fiber was placed in a sealed plastic box with optical and electrical feedthrough (Figure 5.1). The box was flushed during more than 24 hours with N_2. The relative humidity was monitored inside the chamber. Humidities down to $1.4 \pm 1\%$ RH were reached. Before the measurements at dry conditions were taken a heat ramp was run to get ride of residual humidity within the fiber.
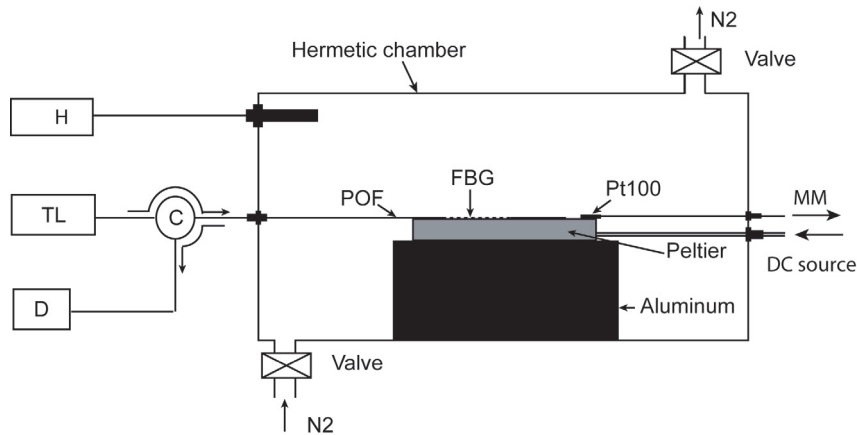
Figure 5.1: *Sketch of the hermetic chamber used for measurement under controlled humidity conditions. TL: tunable laser, C: circulator, D: power detector, Pt100: thermo-resistive element, H: Hygrometer, MM: Multimeter*

For the measurement of the FBG at different relative humidities and constant temperature ($T = 22.4 \pm 0.3°C$), the fiber was left within the hermetic chamber, the N_2 flow was stopped and the valves closed. The humidity in the chamber rose slowly ($< 3\%$ RH/h) to ambient conditions after the N_2 flow was stopped. The time to take one measurement was approximately 3 minutes and the humidity was therefore almost constant during one measurement. The error of the humidity is $\pm 5\%$ RH for this measurement due to the hygrometer that was used.

In order to measure the FBG at maximum sorption conditons, the fiber was removed from the hermetic chamber and was submerged in water at room temperature. Measurements were taken after approximately 10 hours.

5.2.3   Results and Discussion

Figure 5.2 shows reflection spectra of the POFBG under dry, ambient and wet conditions, with corresponding peak positions at 1535.4 nm, 1538.6 nm and 1543.5 nm. The maximum shift from dry to wet conditions is up to 8.1 nm while the shape of the reflection spectrum stays almost the same. Small differences might be due to clustering of water leading to a non-uniform refractive index change along the grating. For a different FBG in the same POF the change was 7.6 nm. The reflectivities in Figure 5.2 were normalized to each FBG's maximum reflectivity. (FBG in water show a reflectivity decay at elevated temperatures ($\sim > 40°C$). This behavior was not investigated in detail.)
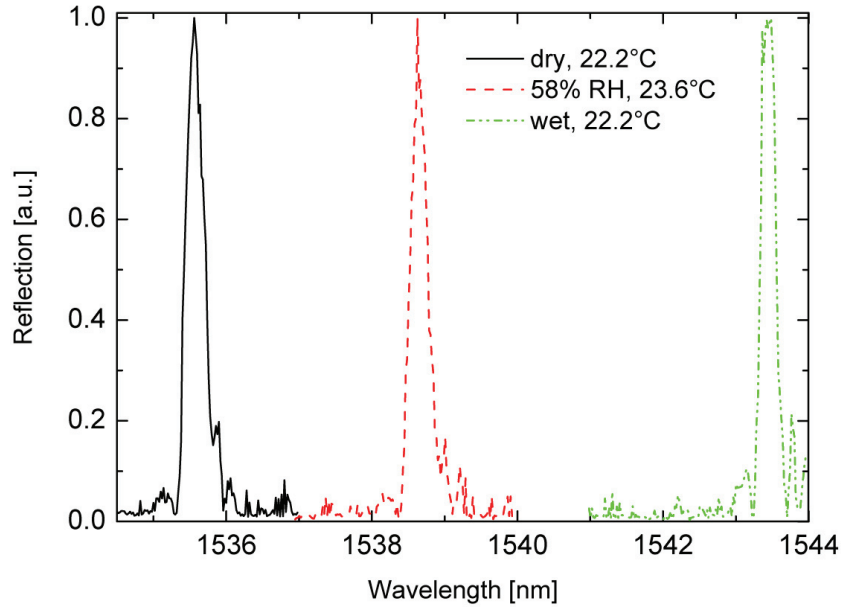
Figure 5.2: *POFBG spectra at low, ambient and 100% RH, grating length L = 5 mm*

The Bragg wavelength depends on the effective core index, n_{eff}, and the grating pitch, Λ which both depend on the temperature T and the water content w:

$$\lambda_{Bragg} = 2n_{eff}(T,w)\,\Lambda(T,w) \tag{5.1}$$

We will first look at the case of constant temperature and rewrite Equation 5.1 for two different relative humidities S_1 and S_2, assuming that the relative Bragg wavelength shift is linear with normalized water content, $w_{ni} = \frac{w_i}{w_{max}}$, for i=1,2, with w_{max} the maximum water sorption, as

$$\lambda_{Bi}(S_i) = \lambda_{Bi}(w_{ni}) = \lambda_{B0} + c_i w_{ni} \tag{5.2}$$

λ_{B0} is the Bragg wavelength at 0% relative humidity, i.e. $w_i = 0$, and the peak wavelength shift due to humidity is an additive term to the 'dry Bragg wavelength'.

Figure 5.3 shows the Bragg wavelength as a function of relative humidity at constant temperature $T = 22.4 \pm 0.3°C$. We observe a non linear dependence of wavelength shift versus relative humidity.
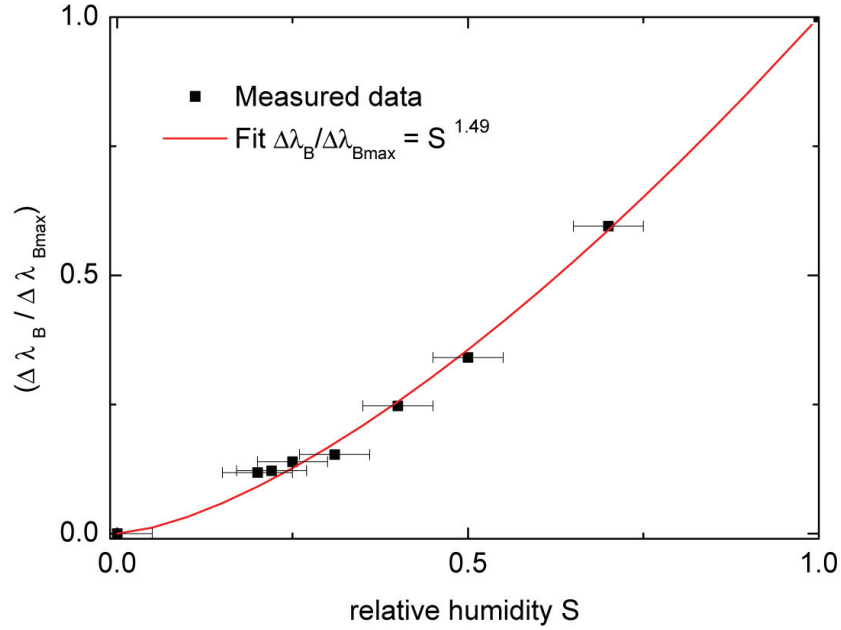
Figure 5.3: *The non-linear relation of normalized Bragg wavelength as function of RH. Similar relation has been shown by Thomas et al. [17], [24]*

The Bragg wavelength change shows a non-linear dependence on the relative humidity. Thomas et al. [17] showed in his work a similar non-linear dependence of the water content in PMMA on relative humidity. Therefore it is assumed that the Bragg wavelength shifts linearly with water content in the fiber, and the water content in the polymer, w, is introducing the non-linearity. The non-linear water content dependence on the relative humidity, S, is

$$\frac{w}{w_{max}} = w_n = S^m \tag{5.3}$$

where w_{max} is the maximum water content (A comparison of this assumption with the model used by Thomas et al. [17] can be found in Appendix E). Equations 5.5 can than be rewritten as

$$\lambda_{B1}(w_{n1} = f(S1)) = \lambda_{B0} + c_1 w_{n1} = \lambda_{B0} + c_1 S_1^m \tag{5.4}$$

$$\lambda_{B2}(w_{n2} = f(S2)) = \lambda_{B0} + c_1 w_{n2} = \lambda_{B0} + c_1 S_2^m \qquad (5.5)$$

The normalized, wavelength shift can be expressed as

$$\frac{\Delta\lambda_{B1\to B2}}{\lambda_{B1}} = \frac{c_1}{\lambda_{B1}}(w_{n2} - w_{n1}) = \frac{c_1}{\lambda_{B1}}\Delta w_n \qquad (5.6)$$

$$\frac{\Delta\lambda_{B1\to B2}}{\lambda_{B1}} = \frac{c_1}{\lambda_{B1}}(S_2^m - S_1^m) \qquad (5.7)$$

corresponding to the non-linearity shown in Figure 5.3 with $m \approx 1.49$. Thomas et al. [17] showed similar non-linear relation between the water content in PMMA and the relative humidity. The m value for his data is $m \approx 1.47$. Therefore the assumption that the non-linearity is only due to the water uptake mechanism is valid in a first approximation. The normalized coefficient c_1/λ_{B1} can be calculated for any two given values from Figure 5.3. The statistical evaluation for all possible combinations of two different relative humidities using Equation 5.7 shows an average value of $(4.6\pm1.2)\times10^{-3}$ for c_1/λ_{B1}. The very large standard deviation is due to the hygrometer measurement uncertainty. The error due to the humidity measurement error is $\pm1.9 \times 10^{-3}$. (For a different FBG $c_1/\lambda_{B1} = (4.1 \pm 1.0) \times 10^{-3}$ was calculated, with a measurement error of $\pm1.5 \times 10^{-3}$.)

The humidity induced Bragg wavelength shift is influenced by the swelling of the polymer and the humidity dependence of the refractive index. Equation 5.7 is therefore rewritten as follows,

$$\frac{\Delta\lambda_{B1\to B2}}{\lambda_B} = (\beta(1 - \chi) + \gamma)\Delta w_n \qquad (5.8)$$

$$\frac{\Delta\lambda_{B1\to B2}}{\lambda_B} = (\beta(1 - \chi) + \gamma)(S_2^m - S_1^m) \qquad (5.9)$$

in which $\beta = L^{-1}\partial L/\partial w_n$ is the swelling coefficient, $\gamma = n^{-1}\partial n/\partial w_n$ the humidity dependence of the refractive index and χ a correction coefficient for the induced stress due to different swelling coefficients of the core and cladding. The theory for this effect will be explained in the subsequent section.

For a change in relative humidity of $\approx 100\%$ RH we have $\Delta w_n = 1$ and obtain $\beta(1 - \chi) + \gamma \approx (4.9 \pm 0.3) \times 10^{-3}$ for FBG1 and $(5.3 \pm 0.3) \times 10^{-3}$ for FBG5. Maximum swelling of PMMA was reported to be $3.9 - 4.4 \times 10^{-3}$ [16, 25] (corresponding to $\Delta w_n = 1$).

Watanabe [10] found $\gamma = 1.3 \times 10^{-3}$ (equivalent to $\Delta w_n = 1$) for d-PMMA. For these values one gets a range of $4.4 - 5.7 \times 10^{-3}$ for the normalized Bragg shift (with stress correction for the minimum and without for the maximum value), showing good agreement with our results for 100% RH change and the statistical calculation for a change between any two measured values.

5.2.4 Differential swelling induced stress theory

In the investigated POF, the core and the cladding material are composed of materials which exhibit different water dependent swelling. Therefore the different dilatations of the core and the cladding lead to an induced strain in the fiber. The induced stress in the core of the fiber and the correction factor χ will be estimated in this section.

Polymer fibers are in general transverse isotropic due to the manufacturing process which induces an orientation of the molecule chains. This orientation can be quantified by the birefringence of the polymer fiber. The birefringence of the fiber used in these experiments indicates, that the orientation induced transverse isotropy is small [26]. Therefore, the calculations were made for the isotropic case. By assuming that the swelling induced by the water uptake is proportional to the water content, χ can be calculated. Shibata et al. [27] reported the equations to calculate stress induced by different thermal expansion coefficients (TEC) for core and cladding in optical fibers. The thermal expansion is linear with temperature. As mentioned before, it is assumed that swelling of PMMA is also linear with water content in the fiber. Therefore the formulas from Shibata et al. can be used used by replacing the TEC with the swelling coefficient β and the ΔT with Δw_n. The swelling induced stress of an axially symmetric fiber with different swelling coefficients for core and cladding can then be written as

$$\sigma_{zz}(r) \;=\; \frac{E}{1-\nu}\left(\frac{2}{R^2}\int_0^R \beta r \mathrm{d}r - \beta\right)\Delta w_n \tag{5.10}$$

$$\sigma_{rr}(r) \;=\; \frac{E}{1-\nu}\left(\frac{1}{R^2}\int_0^R \beta r \mathrm{d}r - \frac{1}{r^2}\int_0^r \beta r \mathrm{d}r\right)\Delta w_n \tag{5.11}$$

$$\sigma_{\vartheta\vartheta}(r) \;=\; \frac{E}{1-\nu}\left(\frac{1}{R^2}\int_0^R \beta r \mathrm{d}r + \frac{1}{r^2}\int_0^r \beta r \mathrm{d}r - \beta\right)\Delta w_n \tag{5.12}$$

The stress distributions can then be derived for a step index fiber with a core radius a and a cladding radius b. The swelling coefficients are β_{core} for $0 \leq r \leq a$ and $\beta_{cladding}$ for $0 \leq r \leq b$. The stresses for the core region, $0 \leq r \leq a$, are then given as

$$\sigma_{zz}^{core}(r) = \frac{E\left(1-\left(\frac{b}{a}\right)^2\right)}{\left(\frac{b}{a}\right)^2(1-\nu)}(\beta_{core}-\beta_{clad})\Delta w_n \tag{5.13}$$

$$\sigma_{\vartheta\vartheta}^{core}(r) = \frac{E\left(1-\left(\frac{b}{a}\right)^2\right)}{2\left(\frac{b}{a}\right)^2(1-\nu)}(\beta_{core}-\beta_{clad})\Delta w_n \tag{5.14}$$

$$\sigma_{rr}^{core}(r) = \frac{E\left(1 - \left(\frac{b}{a}\right)^2\right)}{2\left(\frac{b}{a}\right)^2(1-\nu)}(\beta_{core} - \beta_{clad})\Delta w_n \tag{5.15}$$

It can be seen that the stresses are constant in the core, leading to

$$\sigma_{zz}^{core} = 2\sigma_{rr}^{core} = 2\sigma_{\vartheta\vartheta}^{core} \tag{5.16}$$

where σ is the stress component in the fiber axis direction z, radial direction r, circumferential direction ϑ, E is Young's modulus, ν is Poisson's ratio and R is the fiber radius.

For step index fibers, the swelling induced axial and radial strain can be found following the generalized 3-D Hooke's law [13]:

$$\epsilon_{zz}^{core} = \frac{\sigma_{zz}}{E} - \nu\frac{\sigma_{rr} + \sigma_{\vartheta\vartheta}}{E} = \frac{\sigma_{zz}}{E}(1-\nu) \tag{5.17}$$

$$\epsilon_{rr}^{core} = \frac{\sigma_{rr}}{E} - \nu\frac{\sigma_{zz} + \sigma_{\vartheta\vartheta}}{E} \tag{5.18}$$

$$\epsilon_{\vartheta\vartheta}^{core} = \frac{\sigma_{\vartheta\vartheta}}{E} - \nu\frac{\sigma_{zz} + \sigma_{rr}}{E} \tag{5.19}$$

where $\nu = 0.35$ [28] is the Poisson's ratio for the isotropic case. For ϵ_{zz}^{core} this can be written as

$$\epsilon_{zz}^{core}(r) = \frac{\left(1 - \left(\frac{b}{a}\right)^2\right)}{\left(\frac{b}{a}\right)^2}(\beta_{core} - \beta_{clad})\Delta w_n \tag{5.20}$$

Using Equation 5.1, the change in the Bragg wavelength due to elongation can be given as

$$\Delta\lambda_B = 2\left(\Lambda\frac{\partial n_{eff}}{\partial L} + n_{eff}\frac{\partial\Lambda}{\partial L}\right)\Delta L \tag{5.21}$$

where $\epsilon = \Delta L/L$. If $\frac{\partial\Lambda}{\partial L} = \frac{\Lambda}{L}$ and

$$\Delta\left[\frac{1}{(n_{eff})^2}\right] = -\frac{2\Delta n_{eff}}{(n_{eff})^3} \tag{5.22}$$

Equation 5.21 can be written as

$$\Delta\lambda_B = 2\Lambda\left(-\frac{(n_{eff})^3}{2}\Delta\left[\frac{1}{(n_{eff})^2}\right]\right) + 2n_{eff}\Delta L\frac{\partial\Lambda}{\partial L} \tag{5.23}$$

The change in refractive index under strain is described by the strain-optic theory [14], i.e. a proportional relation between the strain optic tensor, p_{ij}, and the strain tensor, ϵ_j, is given by

$$\Delta \left(\frac{1}{n_{eff}^2} \right)_i = \sum_{j=1}^{6} p_{ij}\epsilon_j \tag{5.24}$$

For a medium that is isotropic, which is under normal strain loading, where the shear strain is zero, ϵ_j, for $j = 4, 5, 6$ is equal to zero.

The orthotropic strain-optic tensor thus reduces to [29]

$$p_{ij} = \begin{pmatrix} p_{11} & p_{12} & p_{12} \\ p_{12} & p_{11} & p_{12} \\ p_{12} & p_{12} & p_{11} \end{pmatrix} \tag{5.25}$$

Inserting Equations 5.17 to 5.19 into 5.24 and combining it with 5.23 yields

$$\frac{\Delta\lambda_B^\sigma}{\lambda_B} = \epsilon_{zz} \left(1 - \frac{n_{eff}^2}{4(1-\nu)} \left[p_{12}(3 - 5\nu) + p_{11}(1 - 3\nu) \right] \right) \tag{5.26}$$

Which can be expressed as

$$\frac{\Delta\lambda_B^\sigma}{\lambda_B} = (1 - \widehat{p}_e)\epsilon_{zz}^{core} \tag{5.27}$$

with

$$\widehat{p}_e = \frac{n_{eff}^2}{4(1-\nu)} \left[p_{11}(1 - 3\nu) + p_{12}(3 - 5\nu) \right] \tag{5.28}$$

where $p_{11} = 0.3$, $p_{12} = 0.297$ [5] and $n_{eff} = 1.4884$. In this case $\widehat{p}_e = 0.16$ is not the same as p_e reported in [30], $\widehat{p}_e$ accounts for simultaneous longitudinal, circumferential and radial stress, whereas p_e is only for the case of applied longitudinal stress.

The core material is composed of $x_{PS} = 22$wt% PS and $x_{PMMA} = 78$wt% PMMA. The volume fractions, y_{PS} and y_{PMMA}, of the two constituent materials can be calculated as,

$$
\begin{aligned}
v_{PMMA} &= \frac{x_{PMMA}}{\rho_{PMMA}} \\
v_{PS} &= \frac{x_{PS}}{\rho_{PS}}
\end{aligned}
$$

$$v_{tot} = v_{PS} + v_{PMMA}$$

$$y_{PMMA} = \frac{v_{PMMA}}{v_{tot}} = 0.76$$

$$y_{PS} = \frac{v_{PS}}{v_{tot}} = 0.24$$

where ρ_{PMMA} and ρ_{PS} are the densities of PMMA and PS, respectively and v_{PS}, v_{PMMA} the specific volumes. The swelling coefficient of the core is then calculated using the volume weighted average of the swelling coefficients for PS and PMMA.

$$\beta_{core} = y_{PS}\ \beta_{PS} + (1 - y_{PS})\ \beta_{PMMA} \tag{5.29}$$

For this POF the swelling coefficient for the cladding is the one from PMMA ($\beta_{clad} = \beta_{PMMA}$). The swelling coefficient of PS is expressed as $\beta_{PS} = q\beta_{PMMA}$ and $\beta_{core} - \beta_{cladd}$ can than be written as

$$\beta_{core} - \beta_{cladd} = y_{PS}\ \beta_{PMMA}\ (q - 1) \tag{5.30}$$

As no values for the swelling of PS were found in the literature (PS sorbs only little or no water [19, 31], PS monofilaments were measured under dry (4% RH) and wet (submerged in water) conditions. The swelling is 0.092 ± 0.04 %, however the systematic measurement error is 0.14%. This result indicates that the PS swelling is significantly smaller than the one of PMMA and q can be set to a positive small value ($\approx < 0.5$).

The swelling induced Bragg shift can then be corrected for the differential-swelling induced stress. Following Equation 5.9, the swelling and the induced stress part can be written as,

$$\frac{\Delta\lambda_{Bswelling}}{\lambda_B} + \frac{\Delta\lambda_{Binducedstress}}{\lambda_B} = (\beta_{core}(1 - \chi))\,\Delta w_n \tag{5.31}$$

using 5.27 and 5.28

$$\beta\Delta w_n + \epsilon_{zz}(1 - \widehat{p_e}) = (\beta(1 - \chi))\,\Delta w_n \tag{5.32}$$

$$\beta + (1 - \widehat{p_e})\ \epsilon_{zz}\ \frac{1}{\Delta w_n} = \beta(1 - \chi) \tag{5.33}$$

$$\tag{5.34}$$

and with Equation 5.20, the correction coefficient χ is

$$\chi = (1 - \widehat{p_e})A\ y_{PS}\ (1 - q) \tag{5.35}$$

where

$$A = \frac{1 - \left(\frac{b}{a}\right)^2}{\left(\frac{b}{a}\right)^2} \approx -1 \tag{5.36}$$

Birefringence measurements compared with results from Wright et al. [26] showed that the non-isotropy of the POF is small. However the minimum and maximum Poisson's ratio were calculated for a PMMA birefringence of $\Delta n = 2 \times 10^{-4}$ and are $\nu_{min} = 0.28$ and $\nu_{max} = 0.43$, respectively. Using these values in combination with the isotropic formulation for the induced stress and taking q=0 to evaluate for maximum possible induced stress, the correction coefficient takes a maximum of -0.2.

It could be shown that the Bragg wavelength shift is largely influenced by the water content of the POF. The derived formalism can be used to predict the Bragg wavelength at a given humidity, provided that the system is in equilibrium. The non-linearity is mainly defined by the water sorption mechanism in PMMA. This humidity dependence has to be taken into account when looking at the temperature dependence which will be explained in a following section. The different water sorption magnitudes of the core and the cladding material will lead to induced stress in the core, which has to be accounted for using a correction factor. This correction factor has been estimated to be as large as 20% of the water induced swelling.

5.3   Diffusion coefficient estimation from Bragg peak shift

The sensitivity to humidity of the POFBG is defined by the water content in the fiber, the fiber refractive index and the grating pitch. The Bragg peak shift during the water sorption process was compared to the analytical model of water diffusion into and out of a long cylinder and is presented in this section.

Experiment

The POFBG was placed on a Peltier element. Next to the fiber a Pt-100 thermo-resistance was placed which was connected by a 4-wire scheme in order to increase the measurement accuracy. After the FBG was set to a given temperature, the wavelength shift evolution was measured during approximately one hour. The dynamic of this shift is influenced by the out-diffusion (in the case of heating) of water from the POF. Using the heat diffusion coefficient for PMMA the time for the fiber to reach the set temperature was estimated to be on the order of seconds (Appendix B). Compared to the time to scan the transmission and reflection spectrum of the fiber (4 minutes using 15 pm steps and a range of 2 nm) this is sufficiently fast for the fiber to be at uniform temperature.

Results and Discussion

The diffusion equation in cylindrical coordinates for a fiber that is long relative to its diameter, can be written as follows [32]

$$\frac{\partial C}{\partial t} = D\frac{\partial^2 C}{\partial r^2} + \frac{D}{r}\frac{\partial C}{\partial r} \tag{5.37}$$

where D is the diffusion coefficient (c.f. 5.43) and C(t,r) is the concentration depending on time t and radial position r. In the analytical model a homogene cylindrical rod was taken as the fiber and the core cladding structure was neglected. The radial diffusion through the cladding (radial distance for diffusion 60.8 μm) is dominant compared to the radial diffuison through the core (radial distance for diffusion 1.7 μm) and therefore the model of a solid rod was assumed to be a good approximation.

Out-diffusion

For the out diffusion we assume that the concentration distribution of water in the fiber is uniform. The mass transfer from the fiber surface into the surrounding air was assumed to be proportional to the concentration difference and much faster than the diffusion of water within the fiber. For this reason, the process is so called diffusion controlled and therefore the Sherwood number Sh is $Sh >> 1$. Another result from this assumption is, that the water concentration in air, at the surface of the fiber is assumed to be constant. This problem is similar to the heat loss of a fiber with radiation at the surface [33] or convection at the surface [34]. Therefore the initial concentration in the fiber center is $C(0,0) = C_0$ and the boundary condition is mass transfer at the surface.

The concentration within the fiber is given by the following equations:

$$w = w_{max}S^m$$

$$\frac{w}{V} = \frac{w_{max}}{V}S^m$$

$$C_{fiber} = C_{fibermax}S^m$$

introducing the normalized concentration c=C/C$_0$, the solution can be written as [34]:

$$c(\tau,\rho) = \sum_{n=1}^{\infty} B_n \mathrm{e}^{-\zeta_n^2 \tau} J_0(\zeta_n \rho) \tag{5.38}$$

where $\tau = Dt/a^2$, $\rho = r/a$, a the fiber radius, J_0 and J_1 are the Bessel functions of the first kind of order 0 and 1 respectively,

$$B_n = \frac{2}{\zeta_n} \frac{J_1(\zeta_n)}{J_0^2(\zeta_n) + J_1^2(\zeta_n)} \qquad (5.39)$$

and the values of ζ_n for $n = 1, 2, 3...$ are the roots of

$$\zeta_n \frac{J_1(\zeta_n)}{J_0(\zeta_n)} = Sh \qquad (5.40)$$

and Sh being the Sherwood number $Sh = kl/D$ [32] (which is the analogous to the Biot number in heat diffusion [34]). With k the gas-phase mass-transfer coefficient and l the characteristic length which can be set to $l = a$ [34].
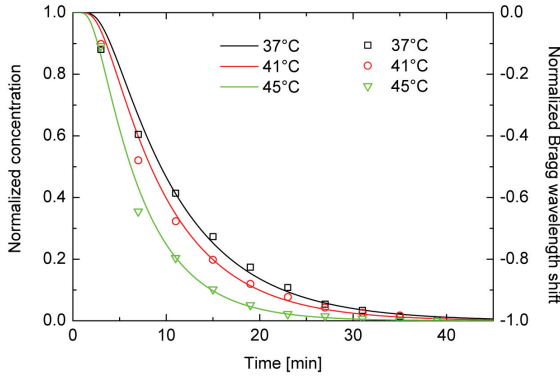
Figure 5.4: *Measured and calculated time evolution of out diffusion (desorption) of water from the fiber.*
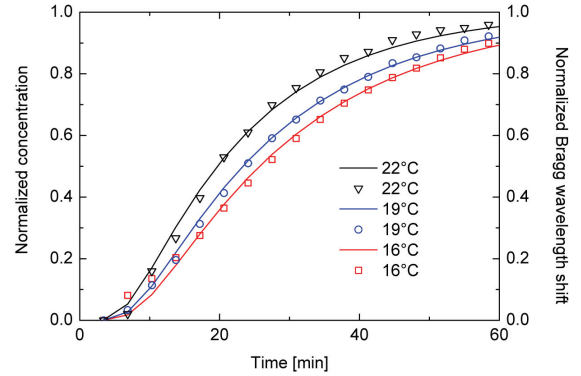
Figure 5.5: *Measured and calculated time evolution of water diffusion into the POF (sorption)*

In-diffusion

Initial conditions for in-diffusion is a constant water concentration within the whole fiber at t=0, $C(0,r) = C_0$ (for $0 < r < a$). The boundary condition is the concentration of water at the fiber surface, r=a, which is constant $C(t,a) = C_a$ for all times t$\geqslant$ 0. This is again due to the assumption that the mass transfer of water in air is much faster than the diffusion in PMMA. In the case the solution can be found as [35]: (using the same notation as for out-diffusion)

$$c(\tau, \rho) = \frac{C(\tau, \rho) - C_0}{C_a - C_0} \qquad (5.41)$$

$$c(\tau, \rho) = 1 - 2 \sum_{n=1}^{\infty} e^{-\psi_n^2 \tau} \left(\frac{J_0(\psi_n \rho)}{\psi_n J_1(\psi_n)} \right) \tag{5.42}$$

were ψ_n, for $n = 1, 2, 3...$ are the roots of $J_0(\psi_n) = 0$.

The temporal evolution of the water desorption from the fiber is shown in Figure 5.4. The discrete data points are the measurements. The FBG was heated to a given temperature and the temporal Bragg peak evolution was monitored. The Bragg wavelength was normalized with respect to maximum wavelength shift for a given temperature. The fiber and the surrounding air reaches the set temperature within seconds. In the case of heating, the relative humidity of the air surrounding the fiber reduces down to approximately 18%RH at 45°C. Cooling increases the local relative humidity of air to approximately 84%RH at 16°C (c.f. Section 5.6.1). Measurements show that the desorption process from the fiber to the surrounding air takes on the order of 40 minutes. The calculation of the normalized water concentration within the fiber using Equation 5.38 is shown as solid lines. The diffusion coefficient was used as fitting parameter. ζ_n was calculated for $n = 0, ..., 10$. The change for the values of c, calculated with $n > 6$ was $< 6 \times 10^{-3}\%$.

Sorption behavior is shown in Figure 5.5 where again the data points are measurements and solid lines are the calculation using Equation 5.42 and the diffusion coefficient as fitting parameter.

As the diffusion coefficient follows the Arrhenius type relationship [32], it can be written as

$$D = D_0 e^{\left(\frac{-Q_D}{RT} \right)} \tag{5.43}$$

where the universal gas constant $R = 8.314$ J/mole and Q_D is the activation energy.

Rewriting Equation 5.43 as

$$lnD = lnD_0 - \left(\frac{Q_D}{R} \right) \frac{1}{T} \tag{5.44}$$

and plotting lnD versus 1/T (Fig. 5.6), Q_D and D_0 can be calculated. Red dots in Figure 5.6 show the desorption corresponding to the calculations of the diffusion coefficient from Figure 5.4. The coefficients for Equation 5.43 can be calculated to be $Q_D = 2.5 \times 10^4$ and $D_0 = 17 \times 10^{-5}$ for the case of desorption. The black squares show the sorption values obtained from the fit shown in Figure 5.5. A linear fit yields the values $Q_D = 3.8 \times 10^4$ and $D_0 = 50 \times 10^{-3}$. The difference between the values for Q_D and D_0 reflect the fact that the desorption process is faster than the sorption process.

The calculated diffusion coefficients at 23.5 °C using Q_D and D_0 from Fig. 5.6 for sorption and desorption are 6.7×10^{-9} cm^2/s and $10 \times 10^{-9} cm^2/s$ respectively. These values are in good
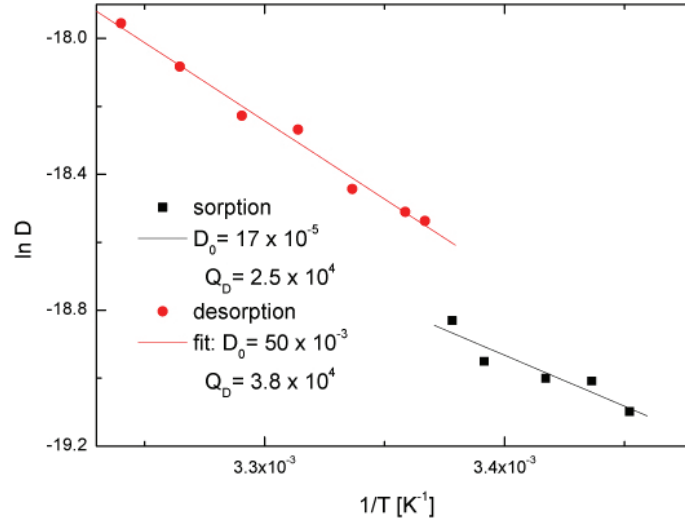
Figure 5.6: *The fitted diffusion values for sorption and desorption as a function of the temperature are plotted. The slope of the fit is used to calculate the activation energy Q_D and the intercept gives D_0.*

agreement with values for PMMA published by Turner et al. [36] ($6.4 \times 10^{-9} cm^2/s$ for sorption and $9 \times 10^{-9} cm^2/s$ for desorption at $23.5°C$).

The time response of the Bragg wavelength shift was used to measure the diffusion coefficient of water in PMMA for sorption and desorption. Analytical calculations of the water content within the fiber at a given time show excellent agreement with the measured Bragg wavelength at that time. It shows that the Bragg wavelength shift is proportional to the water content within the fiber. Good agreement was also found for diffusion coefficient values from the literature for sorption as well as desorption.

These results show that the time dependent Bragg wavelength shift after humidity change is mainly influenced by the water diffusion into or out of the fiber.

5.4 Improved time response of humidity sensing

The time response to humidity changes of the POFBG is relatively slow, on the order of one hour. The main influence on this time response comes from the diffusion coefficient and the fiber geometry.

Figure 5.7 shows calculations using the Equations from the preceding section. The calculated time response shows, that for a fiber diameter of 25 μm the response time can be improved to a couple of minutes.
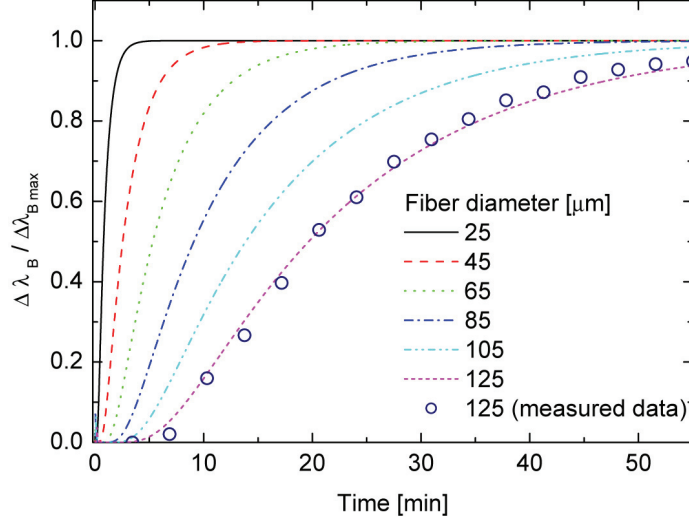
Figure 5.7: *Calculated data for the sorption behavior of POFBG with different diameters. (T=22° C)*

5.5 Temperature sensitivity of POFBG at constant humidity

For silica FBG in general and for POFBG at constant humidity, the temperature dependence
of the wavelength shift is defined as [8]:

$$\frac{\Delta\lambda_{Bragg}}{\lambda_{Bragg}} = (\alpha + \xi)\Delta T \tag{5.45}$$

where $\xi = n_{eff}^{-1}\partial n_{eff}/\partial T$ is the normalized thermo-optic coefficient. In the case of polymer
fibers, the thermal expansion coefficient $\alpha = L^{-1}\partial L/\partial T$ is a function of temperature and water
content in the fiber [9, 11],

$$\alpha = \alpha_0 + \alpha_1 T + \alpha_2 w_n + \alpha_3 w_n T \tag{5.46}$$

Reported thermal expansion coefficients (TEC) for PS and PMMA do not differ significantly
(PMMA $62 - 80 \times 10^{-6}$ [K^{-1}] at 20 °C [9], PS $60 - 80 \times 10^{-6}$ [K^{-1}] [20]). For the following
calculations the TEC of PMMA was taken.

In analogy, it is assumed that the thermo-optic coefficient follows the same relation,

$$\xi = \xi_0 + \xi_1 T + \xi_2 w_n + \xi_3 w_n T \tag{5.47}$$

For PMMA, the temperature dependence is small, $\xi_1 << \xi_0$, for a temperature range between
-20 and 90°C, which can be seen from the work of Cariou et al. [6].

This section will show, that the thermal non-linearity of TEC has to be taken into account for POF. The water content in the fiber on the other hand influences both thermal expansion and thermo-optic coefficient.

5.5.1 Temperature dependence of dry fiber

Experiment

For the temperature dependence at very low humidity the sealed box was permanently flushed with N_2 during the measurements, keeping the humidity constant. The minimum humidity within the box was measured to be $\approx 1.5 \pm 1\%$ RH. The fiber spectrum was recorded $3 - 5$ times for each temperature. The time to record one spectrum was approximately 3 minutes. No significant changes in the peak position were observed at a given temperature. A peltier element with a DC power supply was used to heat the fiber. The temperature was measured using a Pt100 temperature resistance in combination with a multimeter. The peltier element was fixed on an aluminium support with the POF on top and the temperature sensor next to it. Measurements were undertaken with and without heat conduction paste between the heating element and the POF. The measurement showed no significant differences. Using the heat diffusion coefficient for PMMA the time for the fiber to reach the set temperature was estimated to be less than a second. Compared to the heating time of the peltier and the time to scan the transmission and reflection spectra of the fiber this is sufficiently fast for the fiber to be at uniform temperature. (See Appendix B for details.)

Results and Discussion

Figure 5.8 shows the measurement of the Bragg wavelength shift versus the fiber temperature change under dry conditions (RH $\approx 1.5 \pm 1\%$) for heating and cooling. In the range of $25°C$ and $40°C$, no significant difference between heating and cooling could be observed. Using a linear fit, the relative peak wavelength shift has a slope of -10 ± 0.5 pm/K for FBG4 (Fig.5.8) and -7.56 ± 0.08 pm/K for FBG5. Equations 5.45, 5.46 and 5.47 lead to the following expression under dry conditions w_n=0.

$$\frac{\Delta \lambda_B}{\lambda_B \Delta T} = \alpha_0 + \xi_0 + (\alpha_1 + \xi_1)T \tag{5.48}$$

Fitting the measurements of FBG5, using Equation 5.48 and $\alpha_0 = 59.6 \times 10^{-6}$ from Drotning et al. [9], showed that $(\alpha_1 + \xi_1) \approx 0.09 \times 10^{-6}$, where ξ_1 is very small and can therefore be taken as $\xi_1 \approx 0$. For these values α_0, α_1 and $\xi_1 = 0$, the maximum difference between measurement and calculation of the Bragg peak for FBG1 in the temperature range of 25 - 48°C is 17 pm for the linear approximation and 6 pm when using $\alpha = \alpha_0 + \alpha_1 T$, corresponding to a maximum

temperature prediction error of $\approx \pm 1.7°$C and $\approx \pm 0.6°$C respectively. The temperature response magnitude of our POFBG is similar to that of a silica FBG but negative.
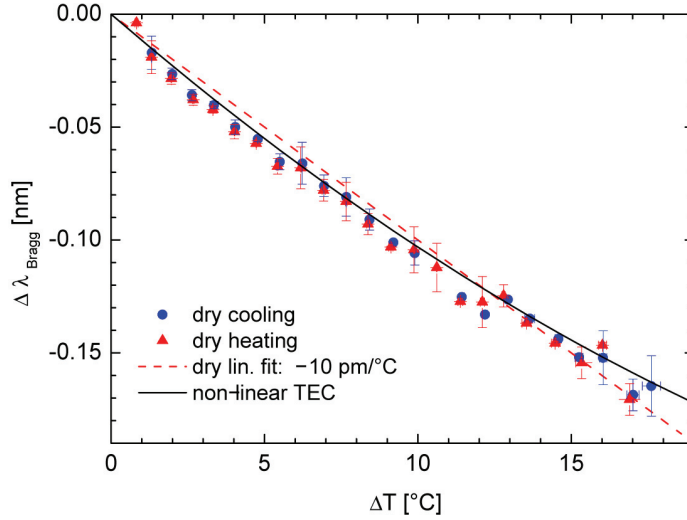
Figure 5.8: *Temperature dependant λ_{Bragg} shift of FBG4 in dry conditions*

Using Equation 5.45 and the thermal expansion coefficient of PMMA under dry conditions at 20°C (Equation 5.46, [9]) of $\alpha = 62 \times 10^{-6}$ [K^{-1}], the thermo-optic coefficient for the core material can be calculated to be -103×10^{-6} [K^{-1}] at 1540 nm. Several investigations have been published on the thermo-optic coefficient of PMMA, ranging from dn/dT of -85×10^{-6} [K^{-1}] [37] to $dn/dT = -120 \times 10^{-6}$ [6]. Waxler [5] reported dn/dT of -105×10^{-6} [K^{-1}] at 633 nm, 20 $°C$ in one of the most comprehensive studies on this topic. The thermo-optic coefficient for PS was only reported by Torbin et al. [37] to be $dn/dT = -120 \times 10^{-6}$ [K^{-1}].

The dn/dT for the core material was calculated using the volume weighted average for PS and PMMA, using the thermo-optic coefficients from Torbin [37](λ not given) and Waxler [5](at 632 nm) respectively. The calculated value is -108×10^{-6} [K^{-1}] compared to a measured value of -103×10^{-6} [K^{-1}] at 1540 nm.

5.5.2   Temperature dependence of wet fiber

Experiment

To obtain wet conditions, the fibers was immersed into water inside a dewar. The water was initially at a temperature of 11°C and 32°C respectively. A Pt100 was submerged next to the FBG. The reflection spectrum of the FBG was measured during about 24 hours. The water temperature within the dewer changed at a maximum rate of 0.3°C/h. For the lower

measurement range the curve corresponds to heating, for the higher measurement the curve corresponds to cooling.

Results and Discussion

The response of the Bragg peak follows again Equation 5.45. Figure 5.9 shows the Bragg wavelength shift of FBG5 submerged in water at two temperature ranges from $11°C$ to $19°C$ and from $25°C$ to $32°C$. From these measurements no significant difference for the two ranges could be found. The same slopes and no nonlinearity within the measurement range were observed ($\alpha_3 << \alpha_0$). The difference between the slopes at dry and at 100 % RH conditions is influenced by the increased thermal expansion coefficient α (Eq. 5.46) in wet conditions as the water molecules within the fiber act as plasizisers [11]. The linearity of measurements in water suggest that $\xi_3 << \xi_0$ (see Figure 5.9). The work of Cariou et al. [6] suggests further that $\xi_1 << \xi_0$.
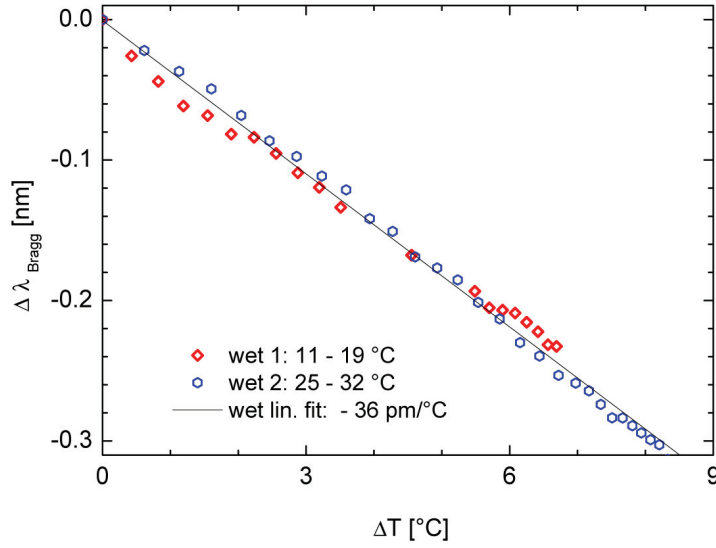
Figure 5.9: *Temperature dependant λ_{Bragg} shift of FBG5 submerged in water*

For the fiber submerged in water the thermo-optic coefficient can be estimated to be $dn/dT = -149 \times 10^{-6}$ using $\alpha = 76 \times 10^{-6}$ (α_2 from Drotning et al. [9]) for a typical water content of 2% [11] in the fiber (corresponding to 100%RH). The equation for the thermo-optic coefficient can be written as [38]

$$\frac{1}{n}\frac{\partial n}{\partial T} = \frac{(n^2 - 1)(n^2 + 2)}{6n^2}(\varphi - 3\alpha) \tag{5.49}$$

where φ is the polarization coefficient. So the thermo-optic effect is composed of the dilatation

part $\sim$(-3α) and the change in polarizability with temperature. Using the thermal expansion coefficients for dry and for wet conditions it can be shown that the polarization coefficient changes its sign from dry to wet conditions. ($\varphi_{dry} = 12 \times 10^{-6}$ compared to $\varphi_{wet} = -22 \times 10^{-6}$). If the thermo-optic coefficient ξ depends linearly on the water content (as suggested in Equation 5.47), then ξ_2 can be calculated to be 44×10^{-6} [K^{-1}].

The thermal Bragg peak shift at constant humidity can be described by Equation 5.45 for POF as well as for silica FBG. In POF however, the temperature dependence is negative compared to silica fibers but has a similar magnitude. The thermal non-linearity and the humidity dependence of the thermal expansion coefficient further influences the Bragg wavelength in POFBG. The thermo-optic coefficient is also a function of humidity and influences the thermal sensitivity, increasing it with increasing humidity.

5.6   Combined temperature and humidity sensitivity

In general, the response of a Bragg grating in the polymer fiber is influenced by the ambient humidity and the temperature at the same time. For the measurements taken at different temperatures, the air surrounding the fiber is heated at the same time as the fiber, thus the relative humidity in this volume of air changes as the temperature changes. This section will explain how the relative humidity was estimated at a given temperature and how this estimation was used to fit the ambient response curve to the measured data.

5.6.1   Saturation pressure of water

The saturation pressure of water depends on the ambient temperature given. As the temperature changes, the saturation pressure increases. If we consider a closed volume of air with a given relative humidity, the total amount of water contained within this volume of air is constant, as the temperature and the saturation pressure rises, the relative humidity will drop as the the water vapor within the volume is constant. Goff and Gratch introduced the *Goff-Gratch* formula [39] (Eq. 5.50 which can be used to calculate the saturation pressure P$_s$ at any given temperature in a range from $-50^\circ C$ and $100^\circ C$ for liquid water.

$$\log P_s = a_1(1 - T_{01}/T) + a_2 \log(T/T_{01}) + a_3\Big(1 - 10^{(a_4(T/T_{01})-1)}\Big) + a_5\Big(10^{(a_6(1-T_{01}/T)-1)}\Big) + a_7 \tag{5.50}$$

where $T_{01} = 273.16$ and p is in standard atmospheres. The values for a_1 through a_7 can be found in Table 5.1. The relative humidity S is given as

$$S = \frac{P_s}{P} \tag{5.51}$$

	Value
a_1	10.79574
a_2	-5.02800
a_3	1.50475×10^{-4}
a_4	-8.2969
a_5	0.42873×10^{-3}
a_6	4.76955
a_7	-2.2195768

Table 5.1: *Values for Equation 5.50 [39]*

where P is the atmospheric pressure.

Figure 5.10 shows the dependence of the relative humidity and temperature. For each curve the initial relative humidity was set to the value shown in the Figure at $25°C$. The relative humidities for all other temperatures were then calculated using Equation 5.50.
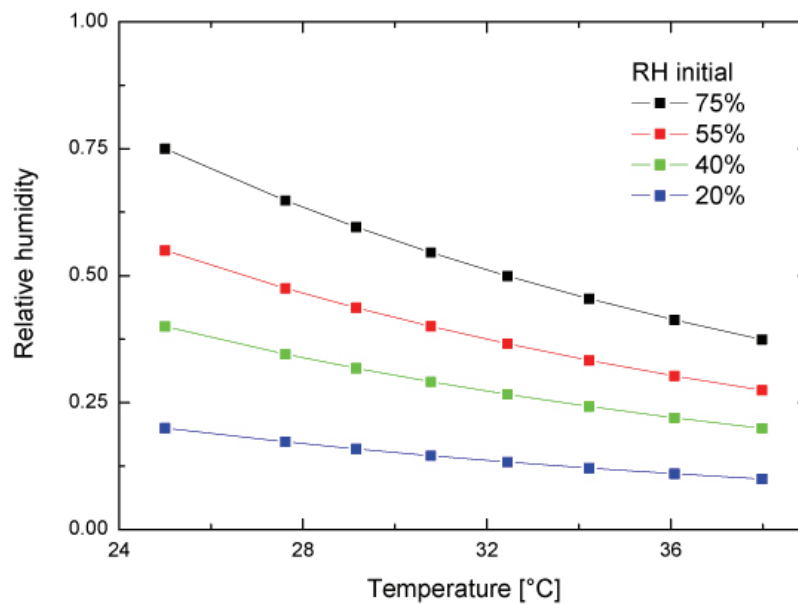
Figure 5.10: *Calculations of the relative humidity (Eq. 5.50) as a function of temperature for different initial values.*

Experiment

Measurements under ambient conditions were taken after one hour for each temperature step. The temperature was varied using a Peltier element and was measured utilizing a PT100 thermal resistance based temperature sensor. The sensor was connected using a 4-point scheme to get more accurate measurements. The absolute temperature measurement had an accuracy of 0.3 K, and a relative measurement error of 0.1 K. The Peltier element was fixed on an aluminum support with the POF on top and the temperature sensor next to it. The temperature sensitivity was measured following the same procedure as in Section 5.5 but outside the hermetic box. The temperature was kept constant for 1 hour during which data points were recorded. The Bragg shift evolution can be seen in Figure 5.4 in Section 5.3.

Results and Discussion

In Fig. 5.11 the relative Bragg peak shift in ambient conditions is shown. The initial relative humidity (at $\Delta T = 0$) was $\approx 50 - 55\% RH$. The wavelength shifts to smaller values in contrast to silica fibers. The slope of the linear fit is $-138 \pm 3\ pm/°C$. This value corresponds to values published by Liu et al. ($-149\ pm/°C$ [2,40]) for the thermal grating response. Liu et al. [1,41] measured a value of $\backsim -150\ pm/°C$ for the thermal tuning for CYTOP fibers and a value of $\backsim -360\ pm/°C$ for MMA-EMA-BzMA core fibers (at 1550 nm). Webb et al. presented FBG in microstructured PMMA POF with a thermal sensitivity between -77 and -95 pm/ °C [4] and Zhang et al. showed FBG in TOPAS® COC [1] fibers with a positive temperature sensitivity of 0.81nm/°C [42].

The response of the POF can be explained by the direct thermal effects and the change in relative humidity due to the temperature change. As mentioned, with increasing temperature the water saturation pressure increases in air, thus the relative humidity is decreasing. This leads to a decrease of the water content in the POF and thus the swelling is reduced. A reduced swelling decreases the grating pitch and changes the refractive index at the same time.

Taking Equations 5.45 and 5.9, the Bragg peak dependence at ambient conditions can be written as:

$$\frac{\Delta \lambda_B}{\lambda_B} = (\alpha + \xi)\Delta T + (\beta(1 - \chi) + \gamma)\Delta w_n \tag{5.52}$$

The relative humidity was calculated for each temperature step using the Goff-Gratch formula (Eq. 5.50) for water vapor pressure [39]. From the initial relative humidity in combination with the calculated water saturation pressure for a given temperature, the relative humidity for that temperature can be calculated. The known temperature, the calculated relative humidity and

---

[1]TOPAS cyclic olefin copolymer
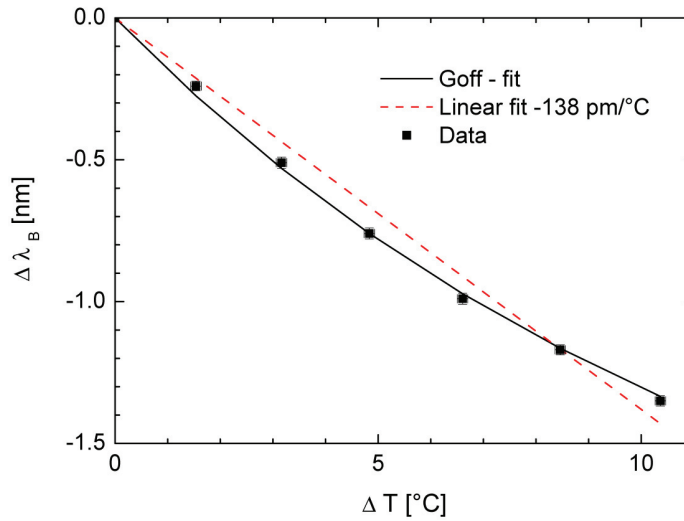
Figure 5.11: *Bragg wavelength shift in ambient conditions as a function of temperature. Shown are a linear fit and a non-linear fit accounting for the change of ambient humidity with changing temperature (using the water vapor pressure formula from Goff and Gratch [39]). FBG4*

Eq. (5.52) were then used to fit the measured data in Fig. 5.11. We obtained an excellent fit of the experimental data were $(\beta(1 - \chi) + \gamma)$ is 4.32×10^{-3} $[RH^{-1}]$ with an R^2 value of 0.9978. However the measurement points after 1 hour at a given temperature correspond only to approximately 90% of the water sorption equilibrium (compare Fig. 5.4).

5.6.2 Summary

The temperature dependence of the Bragg peak shift of a POFBG is influenced by the relative humidity. Using the initial relative humidity at ambient temperature, the humidity at different temperatures can be calculated. Like this the combined effect of temperature and humidity can be predicted for the Bragg wavelength shift upon heating in ambient conditions. Figure 5.12 shows the response in dry and in ambient conditions. The humidity change accounts for the major part of the peak shift. The non-linearity of the thermal expansion coefficient was also included in the calculations for the ambient case. It is however much smaller than the one introduced by the relative humidity change. This shows, that at ambient conditions, a reference measurement has to be taken in order to use the POFBG as a sensor. For such reference measurements a water tightened POFBG could be used.
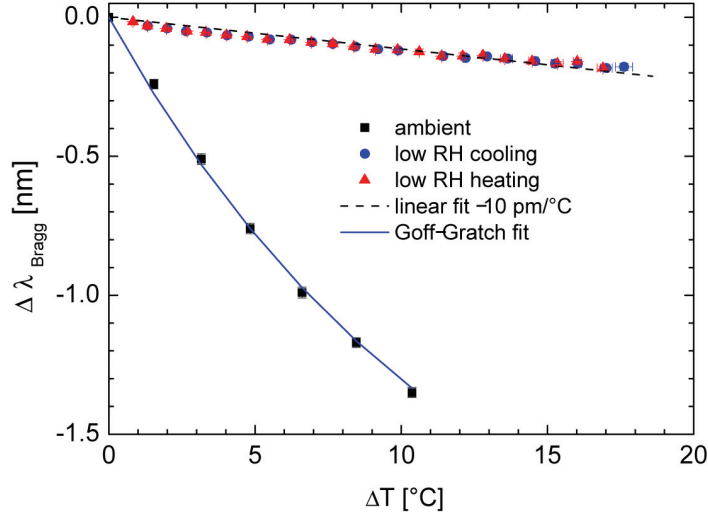
Figure 5.12: *FBG4 wavelength shift during heating and cooling under dry and ambient conditions.*

5.7   Strain sensitivity of FBG in POF

To complete the chapter on sensing, the strain sensitivity characterization of the produced POFBG are presented. The Bragg peak shift for fiber elongation is

$$\Delta\lambda = 2\left(\Lambda\frac{\delta n_{eff}}{\delta L} + n_{eff}\frac{\delta\Lambda}{\delta L}\right)\Delta L \tag{5.53}$$

It is usually rewritten as [30],

$$\Delta\lambda_{Bragg} = \lambda_{Bragg}\left(1 - p_e\right)\epsilon_z \tag{5.54}$$

where ϵ_z is the strain in fiber axis direction. In the case of longitudinal elongation of an isotropic fiber, p_e is defined as [43],

$$p_e = \frac{n_{eff}^2}{2}\left(p_{12} - \nu(p_{11} + p_{12})\right) \tag{5.55}$$

with p_{11} and p_{12} being the components of the strain-optic tensor, ν the isotropic Poisson's ratio. For PMMA these values are $p_{11} = 0.3$, $p_{12} = 0.297$ [5], $\nu = 0.35$ [28]. For PS $p_{11} = 0.32$ was calculated from $p_{12} = 0.31$ [44] and $p_{44} = 0.005$ using $p_{11} - p_{12} = 2p_{44}$ [45]. Poisson's ratio for PS is $\nu = 0.34$ [46]. For pure PMMA Equation 5.55 yields $p_e = 97.5 \times 10^{-3}$ and for PMMA/PS $p_e = 99.5 \times 10^{-3}$ (volume weighted average of p_{11}, p_{12} and ν). For silica fibers these values are $p_{11} = 0.113$, $p_{12} = 0.252$, $\nu = 0.16$. [8]

Experiment

In Figure 5.13 the strain measurement setup is shown. Some specific solutions had to be chosen due to the short fiber lengths and small diameter of the POF core. Clamping of the fiber was not possible as indentation induced large transmission losses. For this reason the fiber was glued to a glass support slide and an aluminum cantilever. The cantilever was displaced using a differential micrometer screw with a resolution of 1 ± 0.2 μm. For each strain set point, the FBG spectrum was recorded in the relaxed state, at the given strain point, and again at the relaxed state. The fiber length was measured with a microscope and has a measurement error of ± 1 μm. The length of the fiber under test was ≈ 2.2 cm. The strain measurement error is $\approx \pm$ 0.01%. Measurements were taken approximately 2 minutes after the given strain was applied.
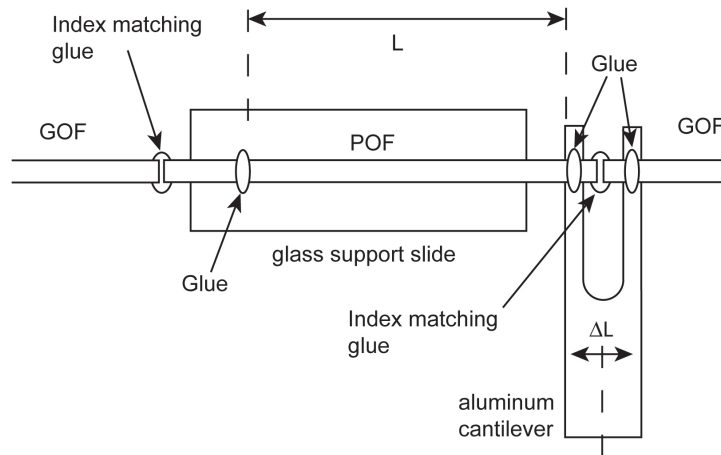
Figure 5.13: *Sketch of the strain measurement setup. L: initial length, ΔL: displacement, GOF: glass optical fiber, POF: polymer optical fiber.*

Results and Discussion

In Figure 5.14 the measured data and the calculated relation using Eq. 5.54 are shown. It can be seen that the measured values agree well with the theory for small strains. The deviation from the predicted linear dependence for higher strains are probably due to relaxation or elasticity of the glue used to fix the fiber ends.

The calculated relation $\Delta\lambda/\lambda_B$ yields 8.9×10^{-7} (1.4 nm / $\mu\epsilon$) for PMMA fibers compared to 7.6×10^{-7} (1.2 nm / $\mu\epsilon$) for silica fibers. It corresponds to a 16% higher strain sensitivity of POFBG than for silica fiber FBG. Using the Young's modulus of 2.9 GPa [20] for PMMA and 69 GPa [47] for silica, the stress sensitivity of POFBG is 0.47 nm/MPa and 0.017 nm/MPa for silica FBG. This is a stress sensitivity improvement of almost factor 30 over silica fibers and
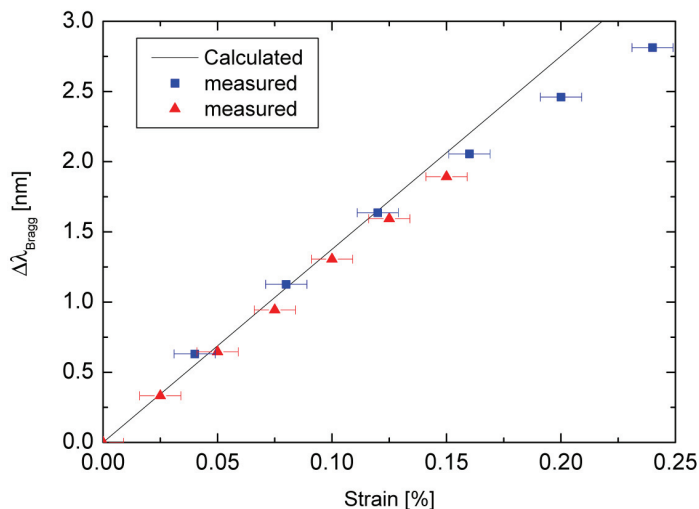
Figure 5.14: *Calculated and measured Strain - $\Delta\lambda_{Bragg}$ relation. FBG7*

can be interesting in applications were small stress or stress variations have to be measured.

5.8   Summary

It could be shown that the POFBG exhibit large humidity sensitivity up to 8 nm for a RH change of $\approx 100\%$. The humidity within the fiber influences the Bragg wavelength through swelling and a change in refractive index. The non-linearity of the Bragg peak shift is induced by the water sorption mechanism in PMMA. The difference in swelling of core and cladding material lead to humidity induced stress. A maximum correction factor for the stress induced Bragg shift was estimated to be -0.2, using an isotropic model.

The comparison of the temporal evolution of Bragg peak shift after changed humidity conditions with diffusion calculations show that the Bragg peak follows closely the humidity concentration in the fiber. The difference in sorption and desorption of water in PMMA is evident in the measurements and comparable to data from literature.

The temperature response of the POFBG at dry and wet conditions can be associated to the thermal expansion coefficient and the thermo-optic coefficient of the POF materials, as is the case in silica fibers. Unlike in glass fibers however, the coefficients for PMMA show dependence of humidity. The temperature sensitivity increases by more than a factor 3 from dry to wet conditions. The temperature dependence of the thermal expansion further introduces a

nonlinearity.

Changing the temperature under ambient conditions leads to a relative humidity change which can be calculated using the *Goff-Gratch* formula. This relative humidity change under ambient conditions introduces a non-lineartiy in the Bragg peak resopnse on temperature change.

In the most general case for strain, temperature and humidity inducing a reflection peak shift in a POFBG, the following Equation can be employed to predict the wavelength shift $\Delta\lambda_B$:

$$\frac{\Delta\lambda_B}{\lambda_B} = (1 - p_e)\epsilon_z + (\alpha + \xi)\Delta T + (\beta_{core}(1 - \chi) + \gamma)(S_2^m - S_1^m) \tag{5.56}$$

The first term on the right hand side of Equation 5.56 represents the strain sensitivity of the POFBG. The strain sensitivity of the POFBG was measured to be 1.4 nm/$\mu\epsilon$ compared to 1.2 nm / $\mu\epsilon$ for silica FBG. The second term on the right hand side corresponds to the thermal Bragg peak shift at constant humidity. Compared to silica fibers, α and ξ are dependent on the temperature and humidity in PMMA based POF. The temperature sensitivity of POFBG under dry conditions is comparable to the one of silica FBG. The third term on right hand side of Equation 5.56 stands for the humidity sensitivity of POFBG. This sensitivity is influenced by the humidity dependent swelling β, the correction factor χ for swelling mismatch induced stress between core and cladding, and γ which is the humidity dependent refractive index change.

5.9   Conclusion

In this chapter it could be shown, that the humidity is of very important influence on the POF Bragg grating sensitivity in ambient conditions. The POFBG is a good candidate as a fiber humidity sensor. In order to use the POFBG as a sensor for temperature or humidity however, a sealed POFBG has to be taken as reference measurement device. Also for tuning applications in communication applications the POFBG has to be sealed.

The diffusion coefficients for sorption and desorption could be evaluated from measured Bragg wavelength shift. Calculations using these results show, that POFBG reaction time can be improved down to minutes by reducing the diameter of the POF. Brittleness of POFBG necessitate that the fiber diameter has to be reduced prior to FBG inscription.

An increased water content in the fiber at elevated temperatures leads to a decay of reflectivity. This behavior will lead to reliability issues if the POFBG are used as sensing devices. Restricting the working temperature range might be necessary in that case.

Bibliography

[1] H. Y. Liu, G. D. Peng, and P. L. Chu. Thermal Tuning of Polymer Optical Fiber Bragg Gratings. *IEEE Photonics Technology Letters*, 13(8):824–826, 2001.

[2] H. B. Liu, H. Y. Liu, G. D. Peng, and P. L. Chu. Strain and temperature sensor using a combination of polymer and silica fiber Bragg gratings. *Optics Communications*, 219:139–142, 2003.

[3] H. Y. Liu, G. D. Peng, and P. L. Chu. Polymer Fiber Bragg Gratings With 28-dB Transmission Rejection. *IEEE Photonics Technology Letters*, 14(7):935–937, 2002.

[4] K. E. Carroll, D. J. Webb, K. Kalli, C. Zhang, A. Argyros, and M. C. J. Large. Extending the working temperature range of bragg gratings in microstructured polymer optical fibre by annealing. In *Proceedings POF 2007, Turin, Italy*, 2007.

[5] Roy M. Waxler, Deane Horowitz, and Albert Feldman. Optical and physical parameters of Plexiglas 55 and Lexan. *Applied Optics*, 18(1):101–104, 1979.

[6] J. M. Cariou, J. Dugas, L. Martin, and P. Michel. Refractive-index variations with temperature of PMMA and polycarbonate. *Applied Optics*, 25(3):334–336, 1986.

[7] H. Y. Liu, G. D. Peng, P. L. Chu, Y. Koike, and Y. Watanabe. Photosensitivity in low-loss perfluoropolymer (CYTOP) fiber material. *Electronics Letters*, 37(6):347–348, 2001.

[8] Andreas Othonos. Fiber Bragg gratings. *Rev. Sci Instrum*, 68(12):4309–4341, 1997.

[9] W. D. Drotning and E. P. Roth. Effects of moisture on the thermal expansion of poly(methylmethacrylate). *Journal of Materials Science*, 24:3137–3140, 1989.

[10] Toshio Watanabe, Naoki Ooba, Shoichi Hayashida, Takashi Kurihara, and Saburo Imamura. Polymeric Optical Waveguide Circuits Formed Using Silicone Resin. *Journal of Lightwave Technology*, 16(6):1049–1055, 1998.

[11] O. V. Startsev, V. P. Rudnev, and B. V. Perov. Reversible moisture effects in the climatic ageing of organic glass. *Polymer Degradation and Stability*, 39:373–379, 1993.

[12] Raman Kashyap. *Fiber Bragg Gratings*. Academic Press, 1999.

[13] Clive L. Dym and Irving H. Shames. *Solid Mechanics*. McGraw-Hill Kogakusha, Ltd., 1973.

[14] F. Pockels. *Lehrbuch der Kristalloptik*. B. G. Teubners Lehrbücher, 1906.

[15] F. Bueche. Diffusion of Water in Polymethyl Methacrylate. *Journal of Polymer Science*, 14(76):414, 1954.

[16] S. H. Goods, R.M. Watson, and M. Yi. Thermal Expansion and Hydration Behavior of PMMA Molding Materials for LIGA Applications. Technical report, Sandia National Laboratories SAND Report SAND2003-8000, 2003.

[17] A. Morris Thomas. Moisture Permeability, Diffusion and Sorption in Organic Film-Forming Materials. *Journal of Applied Chemistry*, 1:141, 1951.

[18] J. A. Barrie and B. Platt. The Diffusion and Clustering of Water Vapour in Polymers. *Polymer*, 4:303, 1963.

[19] H. H. G. Jellinek, M. D. Luh, and V. Nagarajan. Sorbed water on polymers near 0°C. *Kolloid-Zeitschrift und Zeitschrift für Polymere*, 232(2):758–763, 1969.

[20] Dr. Hansjürgen Saechtling. *International Plastics Handbook*. Hanser Publishers, 1987.

[21] Hiromasa Kawai, Fumiaki Kanega, and Hisashi Kohkame. Novel acrylic resion for injection molded precision lenses. In *SPIE Vol. 896 Replication and Molding of Optical Components*, 1988.

[22] C. Ishiyama and Y. Higo. Effects of Humidity on Young's Modulus in Poly(methyl methacrylate). *Journal of Polymer Science: Part B: Polymer Physics*, 40:460–465, 2002.

[23] R. P. Kusy and A. R. Greenberg. Influence of molecular weight on the dynamic mechanical properties of poly(methyl methacrylate). *Journal of Thermal Analysis and Calorimetry*, 18(1):117–126, 1980.

[24] Wan-Lin Chen and Kenneth R. Shull. Equilibrium Swelling of Hydrophilic Polyacrylates in Humid Environments. *Macromolecules*, 32:136–144, 1999.

[25] Dieter Pütz and Georg Menges. The Influence of Liquid Environmental Media on the Mechanical Behaviour of Thermoplastics. *The British Polymer Journal*, 10:69–73, 1978.

[26] H. Wright, C. S. N. Faraday, E. F. T. White, and L.R. G. Treloar. The elastic constants of oriented glassy polymers. *J. Phys. D: Appl. Phys.*, 4:2002–2014, 1971.

[27] Noriyoshi Shibata, Kaname Jinguji, Masao Kawachi, and Takao Edahiro. Nondestructive Structure Measurement of Optical-Fiber Preforms with Photoelastic Effect. *Japanese Journal of Applied Physics*, 18(7):1267–1273, 1979.

[28] D. Taylor, M. Merlo, R. Pegley, and M. P. Cavatorta. The effect of stress concentrations on the fracture strength of polymethylmethacrylate. *Materials Science and Engineering A*, 382:288–294, 2004.

[29] G. B. Hocker. Fiber-optic sensing of pressure and temperature. *Applied Optics*, 18(9):1445–1448, 1979.

[30] Kenneth O. Hill and Gerald Meltz. Fiber Bragg Grating Technology Fundamentals and Overview. *Journal of Lightwave Technology*, 15(8):1263–1276, 1997.

[31] F. A. Long and L. J. Thompson. Water Induced Acceleration of the Diffusion of Organic Vapors in Polymers. *Journal of Polymer Science*, 14:321–327, 1954.

[32] E. L. Cussler. *Diffusion - Mass Transfer in Fluid Systems*. Cambridge University Press, 1997.

[33] H. S. Carslaw and J. C. Jaeger. *Conduction of Heat in Solids*. Carendon Press - Oxford, 2001.

[34] Frank P. Incropera and David P. DeWitt. *Fundamentals of Heat and Mass Transfer*. John Wiley & Sons, 1996.

[35] J. Crank. *The Mathematics of Diffusion*. Clarendon Press - Oxford, 1998.

[36] D. T. Turner. Polymethyl methacrylate plus water: sorption kinetics and volumetric changes. *Polymer*, 23:197–202, 1982.

[37] I. D. Torbin and Yu. F. Daminov. Polymer optical components. *Soviet Journal of Optical Technology*, 41(10):492–499, 1974.

[38] L. Prod'homme. A new approach to the thermal change in the refractive index of glasses. *Physics and Chemistry of Glasses*, 1(4):119–122, 1960.

[39] John A. Goff. Saturation pressure of water on new kelvin temperature scale. *Heating, Piping and Air Conditioning*, 29:151, 1957.

[40] H. Y. Liu, H. B. Liu, G. D. Peng, and P. L. Chu. Observation of type I and type II gratings behaviour in polymer optical fiber. *Optics Communications*, 220:337–343, 2003.

[41] H. Y. Liu, G. D. Peng, and P. L. Chu. Thermal stability of gratings in PMMA and CYTOP polymer fibers. *Optics Communications*, 204:151–156, 2002.

[42] C. Zhang, D. J. Webb, K. Kalli, G. Emiliyanov, O. Bang, and E. Kjaer. Bragg grating inscription in TOPAS microstructured polymer optical fibre. In *POF Torino*, 2007.

[43] G. Meltz, W. W. Morey, and W. H. Glenn. Formation of Bragg gratings in optical fibers by a transverse holographic method. *Optics Letters*, 14(15):823–825, 1989.

[44] l. N. Durvasula and Robert W. Gammon. Brillouin scattering from shear waves in amorphous polycarbonate. *Journal of Applied Physics*, 50(6):4339–4344, 1979.

[45] A. Bertholds and R. Dändliker. Deformation of Single-Mode Optical Fibers Under Static Longitudinal Stress. *Journal of Lightwave Technology*, 5(7):895–900, 1987.

[46] M. E. J. Dekkers and D. Heikens. The effect of interfacial adhesion on the mechanism for craze formation in Polystyrene-glass bead composites. *Journal of Materials Science*, 18:3281–3287, 1983.

[47] Eric Udd, editor. *Fiber Optic Sensors - An Introduction for Engineers and Scientists*. John Wiley & Sons, Inc, 1991.

Chapter 6

<div align="right">

Conclusion

</div>

6.1 Summary and Conclusion

A setup for POFBG writing was installed which could be used to produce stable gratings. The setup consists of a conventional phase-mask, side-writing technique which was paired with the necessary coupling and fiber support needed due to the small core size and the flexibility of the POF. It was shown that permanent FBGs can be written in fully polymerized POF that are not sensitized prior to irradiation using 308 nm excimer light. FBG reflectivity up to 87% could be reached in 7-mm-long gratings corresponding to an index change of 1.7×10^{-4}. Irradiation induces an insertion loss of up to 11 dB/cm. It was found that the refractive index change is negative. Part of the index modification is not stable after FBG inscription, but changes within a time frame of weeks to months after irradiation. Never the less approximately 40% of written gratings exhibited reflectivities $\geq 37\%$ after 6 months. These FBG had a stable reflectivity over a measurement periode between 6 and 15 months after production. A reason for varying success in FBG writing is the humidity and temperature change within the fiber during irradiation. A controlled or minimal heating and a low humidity environment could improve FBG writing repeatability.

OLCR measurements showed that the refractive index change is not homogeneous along the fiber axis but exhibits very large variations (refractive index modification peaks are up to a factor four of the mean value). This indicates that the photosensitivity of the fiber is a function of fiber axis position. OLCR measurements and the reconstruction thereof further show good agreement if the loss of the fiber and the irradiation induced loss are taken into account. The material inhomogeneities are important and may be an additional factor leading to varying success in grating writing.

Photosensitivity was accounted to PS content within the core of the fiber which acts as absorbtion center leading to photo-thermal or/and photo-lytic chain scission and a subsequent chain 'unzipping'. Birefringence measurements show, that irradiation induced changes with 308 nm excimer laser are mainly induced in the core. Observed reduction of absolute birefringence values in conjunction with the measured negative refractive index change indicate, that the refracitve

index change is due to two mechanisms. A change in density and a change in birefringence (which is a combination of inelastic strain and elastic stress). Large variations of initial birefringence in the fiber material, especially in the core, are observed indicating in-homogeneity of the fiber material.

Humidity sensitivity of the POFBG at constant temperature was presented. The humidity influences the Bragg peak through swelling, changing the grating pitch, and through a change in refractive index due to the water content within the fiber. A difference in humidity dependent swelling between core and cladding further leads to induced stress within the fiber influencing the Bragg wavelength. The correction factor, to account for this induced stress, was estimated using an isotropic model. A relative humidity change of $\approx 100\%$ was measured to lead to a non-linear Bragg peak shift of up to 8 nm. The non-linearity is due to the water sorption process in PMMA.

The temporal change of the Bragg wavelength after humidity change was used to calculate the diffusion coefficient for the case of sorption ($6.7 \times 10^{-9} \mathrm{cm}^2/\mathrm{s}$) and desorption ($10 \times 10^{-9} \mathrm{cm}^2/\mathrm{s}$) for water in PMMA at 23.5°C. These values reflect the fact, that the sorption process is slower than the desorption process and are in good agreement with literature.

The temperature dependence under dry conditions (constant relative humidity, 1.5 ± 1 % RH) is -10 ± 0.5 pm/°C and showed that the sensitivity of POFBG is comparable to silica FBG. However under wet conditions (again constant humidity), the temperature sensitivity of POFBG increases by approximately a factor of 3 (-36 ± 2 pm $/^\circ C$) which is due to a change in thermal expansion coefficient and a change in the temperature dependence of the polarizability.

Characterization of the Bragg peak sensitivity under ambient conditions showed that the large sensitivity, is mainly due to a changing humidity content within the fiber and the temperature is of minor influence. The main influence was identified to be due to relative humidity changes within the heated atmosphere surrounding the fiber. The thermal response at ambient conditions is therefore a function of the initial relative humidity conditions. Using the Goff-Gratch formula, the realtive humidity at a given temperature can be calculated. This formula introduces the non-linear temperature-dependence under ambient conditions.

6.2   Future work

This work showed the basic concept and proof that FBG can be written with excimer laser light in these kind of POF. Further experiments on irradiation in dry conditions should be done in order to evaluate if the humidity within the fiber influences the photosensitivity process and reproducibility.

The irradiation induced index change was accounted to photo-lytic processes and to a change in birefringence. As annealing reduced the birefringence, writing of FBG in annealed fibers would

be interesting. It could explain if the photo-lytic or the birefringence is the main influence on the photosensitivty.

In the prospect of further characterization of the humidity and temperature sensitivity, measurements in a climate chamber should be undertaken in order to characterize the temperature dependence at different humidities as well as the humidity dependence at different temperatures.

As no publications on the hygro-optic coefficient of PS was found, and the publication for the value of PMMA leaves some questions unanswered, these values should be measured. The measurement of the swelling coefficient of PS with a better accuracy would enable to find the stress correction factor with better precision.

Humidity sensing response time can be increased by fiber diameter reduction. First test on fiber etching resulted in POFBG destruction due to brittleness of the POF after FBG inscription. Etching of the POF should therefore be performed prior to FBG writing in order to produce fast POFBG humidity sensors. In this respect the water tightening of POF has to be investigated as well to eliminate the cross sensitivity of temperature and humidity.

List of Figures

List of Tables

Appendix A

Glass to polymer fiber coupling

The polymer fiber used is not connectorized which necessitate custom coupling techniques. As Polymer optical fibers cannot be easily spliced to standard telecom glass fibers, there are mainly three possibilities to do the coupling, butt-coupling of the fiber ends, fabrication of connectors or mechanical splices. Fabrication of FC/PC connectors and use of mechanical splices were investigated. The polishing of the POF fiber ends yielded satisfactory end faces. However large coupling losses were still obtained with such connectors which are probably due to insufficient concentricity of the POF core. Mechanical splicing yielded the similar high loss connections. Butt-coupling was therefore selected as the best coupling technique.

Coupling losses

The calculations for the splicing losses used were derived and presented by Marcuse [1]. Only the calculations for step index fibers will be presented. The factors influencing coupling loss which are taken into account are, a) distance between fiber ends, b) transversal offset of the two fibers, c) improper alignment of the fiber axes, d) end face reflection. The factors further increasing coupling loss are, quality of the fiber end faces which is influenced by the cleavage angle and the surface roughness.

For step index fibers the width parameter w of the Gaussian mode field can be calculated as follows

$$\frac{w}{a} = 0.65 + \frac{1.619}{V^{\frac{3}{2}}} + \frac{2.879}{V^6} \tag{A.1}$$

were V is the reduced frequency

$$V^2 = (n_1^2 + n_2^2)ka^2 \tag{A.2}$$

and a is the core radius, n_1 the core refractive index and n_2 the cladding refractive index.

For a longitudinal separation, Markuse showed that the power transmission coefficient T can be calculated as

$$T = \frac{4\left[4Z^2 + \frac{w_1^2}{w_2^2}\right]}{\left[4Z^2 + \frac{w_2^2 + w_1^2}{w_2^2}\right]^2 + 4Z^2 \frac{w_2^2}{w_1^2}} \tag{A.3}$$

where Z is the normalized fiber separation distance defined as

$$Z = \frac{D}{n_3 k w_1 w_2} \tag{A.4}$$

where D is the distance between the fiber ends, n_3 is the refractive index of air and $k = 2\pi/\lambda$. Calculating the transmission coefficient for a distance D=0 gives

$$T = 0.670 \tag{A.5}$$

If a transversal offset between the two fibers of 1 μm is assumed, the power transmission coefficient reduces to T=0.622 by employing equation A.6

$$T = \left(\frac{2w_1 w_2}{w_1^2 + w_2^2}\right)^2 e^{\left(-\frac{2d^2}{w_1^2 + w_2^2}\right)} \tag{A.6}$$

were d is the transversal offset between the fibers.

In a first test the fibers were aligned in air which adds the reflection losses at the end Surfaces. The reflection coefficient can be calculated using equation A.7, however we are interested in the transmission and therefore take t=1-r.

$$r^2 = \left(\frac{n_1 - n_3}{n_1 + n_3}\right)^2 \tag{A.7}$$

If we calculate the reflection losses we find 3.4% loss on the silica air interface and another 4% at the air POF interface with an additional phase shift at the later.

Adding up all the losses we get a transmission coefficient T_{tot} between the SMF 28 and the SM-POF which are transversally offset by 1 μm and where it is assumed that the longitudinal offset D $\to$ 0 but with air in the gap anyway.

$$T_{tot} = 0.577 \tag{A.8}$$

As the POF fiber is not properly cleaved but only cut with a knife, the end surface has an angle different from 90°. In reality the end face will also show roughness but this was not be looked at in this frame.

Taking the equation for end face tilt from Eq. A.9 we get T=0.89 as the power transmission coefficient for a properly cleaved SMF 28 and a POF fiber end face with a tilt angle of 10°.

$$T_{tilt} = \frac{16k^2}{(1+k)^4} \left[1 - \frac{\mid a}{1} \right] \tag{A.9}$$

Again adding up the losses we get a value of

$$T_{tot} = 0.513 \tag{A.10}$$

Appendix B

Polymer fiber heating

For temperature measurements under dry and ambient conditions, a peltier element was used to heat the POF. The peltier was placed on an aluminium support. Heat conduction paste was applied between support and peltier element. Several measurements were undertaken without POF, measuring the temporal temperature change of the peltier element surface, with a POF on the peltier element and the thermo-resistive element next to and on top of the fiber. No significant difference between these measurements were found. In order to assess the temperature of the fiber core the heat diffusion within the fiber was estimated. The heat diffusion coefficient, or also called the heat diffusivity is [2,3]

$$\alpha = \frac{k}{\rho c_p} \tag{B.1}$$

where k is the heat conductivity, ρ the density and c_p the specific heat. Values for PMMA and PS can be found in Table C.1. As the calculations presented in Section 5.3 are derived from the heat diffusion equations, Equations 5.37 through 5.42 hold true for the case of thermal diffusion. Using the thermal diffusivity instead of the water/PMMA diffusion coefficient, the transient response upon heating or cooling of the fiber can be calculated. For a temperature increase of 20°C it takes less than a second for the fiber to reach thermal equilibrium at the higher temperature. In comparison, the temperature increase on the peltier element can be seen in Figure B.1. The initial temperature was 24°C. Heating to ≈ 50°C takes about 1 minute. The limiting factor for temperature measurements is therefore the heating system. Typical measurements were taken using a LabView program controlling the tunable laser, power meter, DC power source and the multi meter. Time between two data points is on the order of 1-2 seconds. The POF can therefore be assumed to exhibit a uniform temperature distribution throughout the fiber at all measurement points. The time it takes for a spectrum to be measured depends on the wavelength range and step size. It was typically on the order of 2-4 minutes. For this reason, a time delay was set between the start of heating and the start of spectral measurement, minimizing the thermal shift during the recording of a spectrum.
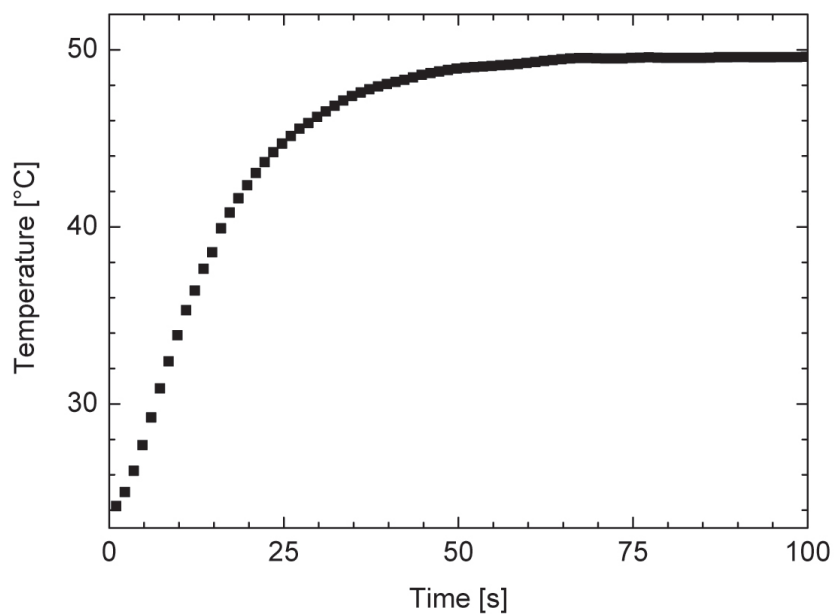
Figure B.1: *Temperature increase of the peltier element upon heating. Heat-resistance sensor Pt100 was placed on top of the peltier element.*

Appendix C

Polymer properties

On the following pages the properties of PMMA and PS will be given in Table 2.2. A summary of known POF manufacturers is given in Table D.1.

	PMMA	**PS**
Tensile strength	$60 - 70$ N/mm^2	$40 - 50$ N/mm^2
Elongation at break	$2, 5 - 3, 5\%$	$< 3\%$
Tensil modulus	2.9-3.3 GPa	3.3 GPa
Poisson's ratio	0.35 [4]	0.353 [5]
Linear thermal expansion	7×10^{-5} K^{-1}	$6 - 8 \times 10^{-5}$ K^{-1}
Thermal conductivity	0.18 W/(m K)	0.17 W/(m K)
Specific heat	1.39 J/(g K)	1.2 J/(g K)
Heat of combustion	26.2 kJ/g	42.2 kJ/g
Density	1.18 kg/m^3	1.05 kg/m^3
Ref. index	1.49 at 589.2 nm	1.59
p_{11}	0.3 [6]	0.32 [5]
p_{12}	0.297 [6]	0.31 [5]
C	$(-2.7 \div -3.8) \times 10^{-12}$Pa^{-1} [7,8]	$(6 \div 10) \times 10^{-12}$Pa^{-1} [7]

Table C.1: *Properties of PMMA and PS taken from Saechtling, 'Plastics Handbook ' [9], except where otherwise mentioned.*

Appendix D

Companies producing POF

Manufacturer	Address
NUVITECH Co. Ltd.	Buk-Gu, Gwangju, Korea
Sojitz Europe plc	Dusseldorf, Germany
Paradigm Optics	Vancouver, WA, USA
Toray	Overseas Branch, Toray Deutschland, Dusseldorf
Fujifilm	
Digital Optronics	Alachua, FL, USA
Nanoptics Inc	Gainesville, FL, USA
Corning	
Hitachi Cable Ltd	Japan
NTT	Japan
Mitsubishi Rayon, Brandname ESKA	Japan
ASAHI Glass	Japan

Table D.1: *POF Manufacturers*

Appendix E

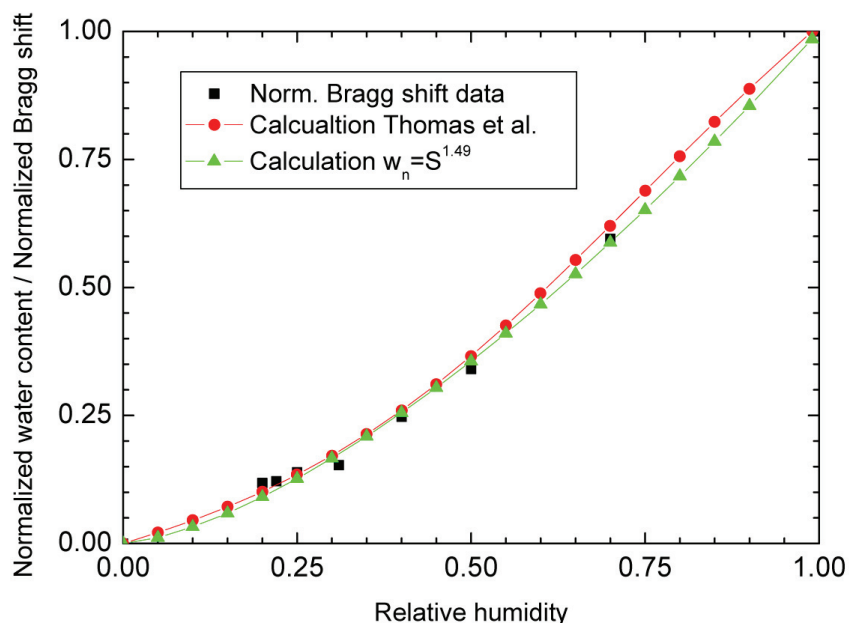## Water sorption comparison with Thomas et al.

Figure E.1: *Normalized Bragg wavelength shift compared to the water sorption model by Thomas et al. [10] and the simplified model used in this work.*

The water sorption mechanisms in PMMA were reported to be non-linear with relative humidity [10–12]. Thomas et al. [10] used a multilayer adsorption BET (Brunauer-Emmett-Teller) model [13, 14] to fit his experimental data using the following formula (for PMMA):

$$w = \frac{6.25S(1 - 6S^5 + 5S^6)}{(S - 1)(S^6 - 1)} \tag{E.1}$$

where w is the water sorption in mg/g and S the relative humidity. In this work a simplified relation was taken:

$$w = w_{max}S^m \tag{E.2}$$

As the maximum water sorption in our case is not known, the normalized water sorption w_n is taken instead. In Figure E.1, our experimental data of the normalized wavelength shift is shown along with the calculations using Equation E.1 which was also normalized and calculations using Equation E.2. Using the later, m can be fitted for our experimental data to be 1.49. Fitting m for the calculations of Thomas, m=1.47 can be found. The result shows clearly, that our assumption agrees well with the BET model from Thomas.

Appendix F

Femtosecond laser

Argon	Wavelength	515 nm
	Power	18 W cw
MIRA	Wavelength	799.8 nm
		10 nm peak width
		tunable 760 nm - 930 nm
	Power	1.4 W continuos
		1 W mode locked
	Pulse length	$< 200\ fs$
	Repetition rate	76 MHz
REGA	Wavelength	Idem MIRA
	Power	1.25 W
	Pulse length	206 fs
	Repetition rate	10 kHz - 300 kHz
OPA	Wavelength	Signal $480 - 700\ nm$
		Idler $930 - 2300\ nm$
	Power	$\approx 15\ mW$ Signal
		55 mW Idler
Second harmonic	Wavelength	400 nm
	Power	220 mW

Appendix G

Written POFBG

On the following page, a table of the written gratings that were presented in this work is shown. Not all of the POFBG could be measured 6 month after irradiation which is why some of these values are missing.

Different FBG have been created. Overall approximately 110 pieces of fiber were irradiated using the phase mask setup to create FBGs. Out of 78 FBG irradiations only 53 showed the formation of an FBG in the transmission or reflection spectrum. Most of the FBGs written decayed very fast (within minutes to hours) after the irradiation was stopped. Only 16 are stable after 6 months i.e. still have a reflectivity of the grating larger than $\geq 37\%$. Table G.1 shows the number of fibers irradiated under different conditions and the number of positive results.

	Total irradiated	showed FBG growth	Stable after 6 month
Untreated fiber	30	24	7
Dried fiber	20	14	5
Fiber stored in water	15	7	3
H_2 loaded	13	7	1

Table G.1: *The number of different irradiated fiber specimens with respect to their behavior under irradiation.*

	Name	frequency	length	irradiaton duration	fluence per pulse	specimen	maximum reflectivity	
		Hz	mm	min	mJ/cm^2		during	after irradiation
spool	FBG1	5	5	24	75	06-02-21	57%	
dried	FBG2	5	7	57	72	06-06-07	42%	
dried	FBG3	5	7	29	70	06-06-09	26%	
water	FBG4	5	7	57	70	06-06-13	54%	87.40%
dried	FBG5	5	7	50	93	06-06-14	55%	75%
spool	FBG6	5	9	23	94	06-07-25	90%	42.40%
spool	FBG7	8	9	31	94	06-08-01	96%	37%
dried	FBG8	8	9	25	92	06-08-24	60%	28%
dried	FBG9	2	9	19	112	06-09-08	73%	50%
water	FBG10	5	9	43	92	06-07-18	38%	1%
water	FBG11	5	9	45	92	06-07-17	38%	
water	FBG12	5	9	52	84	06-07-12	68%	68%
spool	FBG13	5	9	43	92	06-07-18-02	40%	
spool	FBG14	5	9	27	94	06-08-02	65%	75%
H$_2$	FBG15	5	9	53	86	06-07-13	68%	75%
H$_2$	FBG16	5	9	53	86	06-07-13-02	61%	20%
H$_2$	FBG17	5	9	22	94	06-08-05	37%	1%
spool	FBG18	5	7	46	75	06-06-02	84%	60%
dried	FBG19	5	7	9	93	06-06-14-02	22%	30%
dried	FBG20	5	7	60	83	06-06-08	58%	84%
spool	FBG21	3	7	28	115	06-09-12	41%	71%

Bibliography

[1] D. Marcuse. Loss Analysis of Single-Mode Fiber Splices. *The Bell System Technical Journal*, May-June(1977):703–718, 1976. Loss Analysis of Single-Mode Fiber Splices.

[2] Frank P. Incropera and David P. DeWitt. *Fundamentals of Heat and Mass Transfer*. John Wiley & Sons, 1996.

[3] Stefan Bäumer, editor. *Handbook of Plastic Optics*. Wiley-VCH, 2005.

[4] D. Taylor, M. Merlo, R. Pegley, and M. P. Cavatorta. The effect of stress concentrations on the fracture strength of polymethylmethacrylate. *Materials Science and Engineering A*, 382:288–294, 2004.

[5] l. N. Durvasula and Robert W. Gammon. Brillouin scattering from shear waves in amorphous polycarbonate. *Journal of Applied Physics*, 50(6):4339–4344, 1979.

[6] Roy M. Waxler, Deane Horowitz, and Albert Feldman. Optical and physical parameters of Plexiglas 55 and Lexan. *Applied Optics*, 18(1):101–104, 1979.

[7] J. F. Rudd and R. D. Andrews. Photoelastic Properties of Polystyrene in the Glassy State. III. Styrene Derivatives and Copolymers. *Journal of Applied Physics*, 31(5):818–826, 1960.

[8] H Ohkita, K Ishibashi, D. Tsurumoto, A. Tagaya, and Y. Koike. Compensation of the photoelastic birefringence of a polymer by doping with an anisotropic molecule. *Applied Physics*, A 81:617–620, 2005.

[9] Dr. Hansjürgen Saechtling. *International Plastics Handbook*. Hanser Publishers, 1987.

[10] A. Morris Thomas. Moisture Permeability, Diffusion and Sorption in Organic Film-Forming Materials. *Journal of Applied Chemistry*, 1:141, 1951.

[11] H. H. G. Jellinek, M. D. Luh, and V. Nagarajan. Sorbed water on polymers near $0°C$. *Kolloid-Zeitschrift und Zeitschrift für Polymere*, 232(2):758–763, 1969.

[12] J. A. Barrie and D. Machin. Diffusion and Association of Water and Some Polyalkylmetacrylates. *Transactions of the Faraday Society*, 67:244–256, 1971.

[13] Richard I. Masel. *Principles of Adsorption and Reaction on Solid Surfaces.* Wiley, New York, 1996.

[14] J. Crank and G. S. Park, editors. *Diffusion in Polymers.* Academic Press London and New York, 1975.

Gérard Nico Harbach

Badenerstrasse 398   gerard@harbach.ch

8004 Zürich   Swiss citizen

Switzerland   Date of birth: 15.12.1976

Education

2004 – 2007	**PhD student** in Applied Optics
	EPFL, Lausanne, Switzerland
2004	**Diploma in Mechanical Engineering**
	Dipl. Masch.-Ing. ETHZ
	Swiss Federal Institute of Technology, Zurich, Switzerland
1996	**Matura Type C**, Gymnasium Raemibuehl, Zurich

Work experience

2004 – 2007	**Research assistant / PhD student**
	Institute of Applied Optics, EPF, Lausanne
Oct 03 – Feb 04	**Diploma thesis**, Contraves Space AG
Jul 02 – Sept 02	**Trainee**, Holcim Lanka Ltd., Sri Lanka
Jan 01 – Jun 01	**Trainee**, Nortel Networks, Zurich, (R&D Optical Components)
Aug 98 – Oct 00	**Project leader**, **Customer consultant**, UBS, Zurich
Feb 98 – Mar 98	**Trainee**, ABB, Zurich
Jan 97 – Oct 97	**Trainee**, UBS, Zurich

Language

German	mother tongue
English	fluent
French	fluent

IT Literacy

Linux:	SuSe, Debian , Ubuntu, Slackware
Windows:	9x / NT / 2000 / XP
Software Packages	OpenOffice, MS-Office, Latex2e, Adobe FrameMaker, Illustrator
	Photoshop, Unigraphics (CAD), AUTOCAD 2000, ProEngineer
	ANSYS, ESAComp, I-DEAS, MSC/Nastran
Programming	MatLab, Lab View, C++, Shell programming